WATER MONOGRAPHS

#WaterMonographs

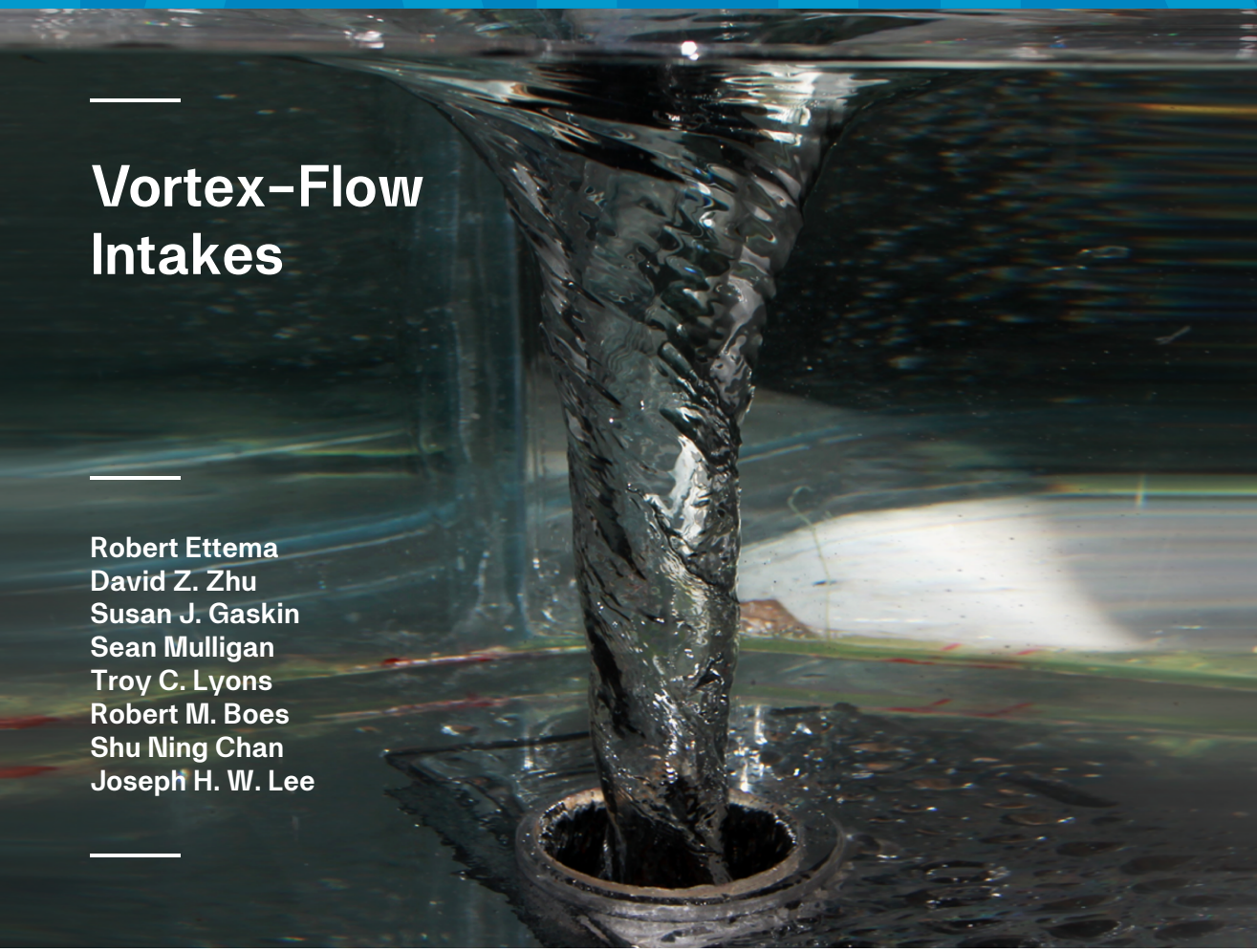

Vortex-Flow Intakes

Robert Ettema
David Z. Zhu
Susan J. Gaskin
Sean Mulligan
Troy C. Lyons
Robert M. Boes
Shu Ning Chan
Joseph H. W. Lee

Supported by

nhc northwest hydraulic consultants

VorTech WATER SOLUTIONS

OPEN ACCESS

IAHR AIRH International Association for Hydro-Environment Engineering and Research

Hosted by Spain Water and IWHR, China

IAHR.org

Vortex-Flow Intakes

Robert Ettema, David Z. Zhu, Susan J. Gaskin, Troy C. Lyons,
Robert M. Boes, Shu Ning Chan, and Joseph H. W. Lee

Vortex-Flow Intakes

Robert Ettema
David Z. Zhu
Susan J. Gaskin
Sean Mulligan
Troy C. Lyons
Robert M. Boes
Shu Ning Chan
Joseph H. W. Lee

IAHR WATER MONOGRAPH SERIES

Series Editor

Damien Violeau
LNHE, EDF R&D, France.
Saint-Venant Hydraulics Laboratory, Ecole des Ponts ParisTech, France.
E-mail: damien.violeau@edf.fr

Cover information:
"Laboratory physical model of a free-surface vortex in a scroll type vortex drop structure at the Atlantic Technological University, Sligo, Ireland". Photo by Sean Mulligan"

ISBN (electronic version): 978-90-833476-0-8

ISBN (printed version): 978-90-833476-1-5

ISSN 2959-7978

doi: 10.3850/978-90-833476-0-8_IAHR_Watermonograph_002

Typeset by Research Publishing, Singapore
Cover by Tres Estudio Creativo, Spain

Published by:
IAHR — International Association for Hydro-Environment Engineering and Research

Madrid Office

Paseo Bajo Virgen del Puerto 3, 28005, Madrid, SPAIN
Tel: +34 913357908; Fax: +34 913357935

Beijing Office

A-1 Fuxing Road, Haidian District, 100038, Beijing, CHINA
Tel: +86 1068781128; Fax: +86 1068781890

The International Association for Hydro-Environment Engineering and Research (IAHR), founded in 1935, is a worldwide independent organisation of engineers and water specialists working in fields related to the hydro-environmental sciences and their practical application. Activities range from river and maritime hydraulics to water resources development and eco-hydraulics, through to ice engineering, hydro-informatics and continuing education and training. IAHR stimulates and promotes both research and it's application, and by so doing strives to contribute to sustainable development, the optimisation of the world's water resources management and industrial flow processes. IAHR accomplishes its goals by a wide variety of member activities including: working groups, research agenda, congresses, specialty conferences, workshops and short courses; Journals, Monographs and Proceedings; by involvement in international programmes such as UNESCO, WMO, IDNDR, GWP, ICSU, and by co-operation with other water-related (inter)national organisations.

IAHR publications follow the Ethical Guidelines and Codes of Conduct provided by the Committee of Publication Ethics (COPE).

About the IAHR Water Monograph Series

The Water Monograph Series joins IAHR's portfolio of publications, which includes journals, magazines, conference proceedings, whitepapers, and books. Since its start in 1935, IAHR has been dedicated to supporting the development and dissemination of knowledge that aids hydro-environment engineering and research.

The Water Monographs are mid-sized publications (about 50-150 pages long) that bridge knowledge gaps, summarize existing knowledge, and publicize recent advances in technologies and methods. More narrowly focused than a book, the Water Monographs occupy the publication space between a journal paper and a book. They concisely present information on physical processes, measurement techniques, theoretical material, numerical modeling techniques, engineering applications, and historical and cultural matters in an appealing readable and well-illustrated manner.

IAHR intends that the Water Monograph Series helps people understand specific longstanding, current, or emerging topics in hydro-environment engineering and research.

Damien Violeau
Chair of IAHR Water Monograph Series

Table of Contents

Summary

Vortex-flow intakes are being increasingly used in water supply, storm sewer and combined-sewer-overflow systems with the purpose of conveying relatively large flow rates of water over significant elevation differences. The main function of such intakes is to swirl flow into the dropshaft of a vortex drop-structure, which then safely and efficiently discharges water from a higher elevation to a lower elevation. Several forms of vortex-flow intake exist — tangential, scroll, and spiral. The first two forms are most used, though the tangential form generally is more compact, which is an important consideration along with energy dissipation efficiency when building the above-mentioned systems in urban settings.

A vortex-flow intake establishes a spiraling vortex flow that experiences enhanced energy dissipation, due to friction as the flow adheres to the dropshaft's circular wall. This feature is essential for stable flow and consistent energy dissipation as water is conveyed from a higher to a lower elevation and the flow's energy is not harvested as hydropower. The consequent substantial reduction of pressure at the base of the dropshaft greatly simplifies dropshaft design. Additionally, a well-designed vortex-flow intake creates a stable air core within a dropshaft. As water flow swirls down a dropshaft, the swirling flow significantly reduces the rate at which water entrains air into the dropshaft; compared to the case where the flow plunges vertically into the dropshaft. Entrained air bulks water flow and increases the sizes of the system's storage and air-venting components. Typically, those components are installed underground in situations where available land for water storage is limited. Therefore, the use of vortex-flow intakes helps in preventing excessive amounts of air entrainment and, in sanitary sewer systems, thereby substantially limits sewer odor problems.

However, when flow energy must be conserved (for example in pump or hydropower intakes), the occurrence of swirl and vortex formation are undesired aspects of flow. They increase energy loss and result in larger conduit designs and may adversely affect turbine or pump performance. Also, when flow distribution is critically important such as on the approach to turbine and pump intakes, flow swirl and vortex formation near the intake harmfully influence flow distribution entering such hydro-machinery. Current design practice is indicated for hydropower and pump intakes.

This monograph shows how designers use swirl and vortex generation to design vortex-flow intakes used to create vortex flows in dropshafts. Special focus is given to tangential vortex intakes, as this form is becoming especially common in urban areas. In addition, this monograph considers when swirl and vortex formation are undesired for intakes, especially submerged intakes such as used for hydropower and pumps. In so doing, this monograph serves as an update of the valuable 1987 IAHR monograph. The use of vortex-flow intakes has grown substantially since IAHR's original monograph and will continue to grow in the foreseeable future.

Robert Ettema and David Z. Zhu (IAHR members)

Nomenclature

Some of the symbols have multiple meanings, as indicated below. Not all symbols are listed here (e.g., geometry of intake, coefficients). Symbols not listed here are defined in the text when the symbols are first used.

Acronyms

CC	Curvature correction (numerical modeling)
CFD	Computational Fluid Dynamics
CSSS	Critical Spherical Sink Surface (numerical modeling)
DES	Detached Eddy Simulation (numerical modeling)
exp	Exponential
FEM	Finite Element Method (numerical modeling)
FSV	Free-surface vortex
FVM	Finite Volume Method (numerical modeling)
GLM	General Linear Model (numerical modeling)
HKWDT	Hong Kong West Drainage Tunnel
LES	Large Eddy Simulation (numerical modeling)
PIV	Particle image velocimetry
PTV	Particle tracking velocimetry
RANS	Reynolds-Averaged Navier Stokes (numerical modeling)
RBNN	Radial Basis Neural Network (numerical modeling)
RSM	Reynolds Stress Models (numerical modeling)
SAS	Scale Adaptive Simulation (numerical modeling)
SPM	Smoothed Particle Method (numerical modeling)
SST	Shear Stress Transport (numerical modeling)
TTT	Thames Tideway Tunnel
VOF	Volume of Fluid Method (numerical modeling)
VT	Vortex type (Hecker scale)
w.r.t.	With respect to (in differential sense)

1D	One dimensional
2D	Two dimensional
3D	Three dimensional
k-ε or k-ω	Eddy viscosity models

Dimensionless numbers

N_Γ	Circulation number, defined as $N_r = \Gamma D/Q$
Fr	Froude number, defined as $Fr_= U_i/\sqrt{gh}$
Fr_D, Fr_s	Froude number, defined as $Fr_D = U_i/\sqrt{gD}$ or $Fr_s = U_i/\sqrt{gS}$
φ	Oseen parameter, constant of O(1) providing a fit to experimental data.
Re	Reynolds number, defined as $Re = Vd/\nu$ or $R_e = VY/\nu$
Ro	Rossby number, defined as $Ro = V/(2\omega L)$
We	Weber number, defined as $We = \rho V^2 L/\sigma$

Coordinates

r, θ, and z	Radial, tangential and vertical directions, respectively

Greek symbols

α	Axial (down vortex) gradient of velocity component, V_z
β	Air-entrainment rate; angle
δ	Radius of curvature of dropshaft entrance; thickness of annular water jet in dropshaft
Δ	Eccentricity between the approach channel and the dropshaft (scroll intake)
∂	Partial differential
γ	Specific weight of water
λ	Air core size ratio
ϕ	Angle of conical coordinates
Γ	Circulation
Γ_∞	Circulation at characteristic radius, r_0
ν	Kinematic viscosity of water
η	Distance from the top of the inlet opening; safety factor
π	Pi (value used, 3,14)
ρ	Water density

σ Surface tension of water in air
θ Angle; tangential component
ω Rotation velocity; Earth's rotational velocity
$\vec{\omega}$ Average rotation velocity
φ Oseen parameter

Roman symbols

a Distance between the top of bellmouth and the chamber wall
a_c Critical air-core diameter
A Cross-sectional area of vortex; power
B Approach-channel width, coefficient
c_1, c_2 'Coefficients
d Diameter of circular intake pipe or shaft
D Diameter of circular intake pipe or shaft
E Specific energy
f Darcy-Weisbach friction factor
g Gravity acceleration
$h, h_0,$ Water depth (sometimes also Y, y)
h_r Water depth at radius r; first derivative of h w.r.t. r
h_{rr} Second derivative of h w.r.t. r
h_∞ Water depth at infinite radius
h, h_0, h_{n0} Depth of free surface depression of vortex
k Distance between the piers flanking the inlet
$K(r)$ Mean local curvature profile
l_σ Characteristic length of water in air
L A length scale
L_r Length scale (of a hydraulic model)
n Manning's roughness coefficient, coefficient
n ratio of tangential to axial velocity at the free surface of an air-core vortex
p Pressure
p_∞ Pressure at infinite radius
P Point
Q Discharge
Q_c Control discharge

Q_f Free discharge (less than Q_c)
r Radius
R Pump radius
R_i Radius of i-th arc (scroll intake geometry)
$\vec{r}$ Radius vector
r_c Radius of forced core region of Rankine vortex
r_0 Characteristic radius
r_∞ Infinite radius
s Offset distance
S Submergence (elevation of intake entrance below free surface)
S_c Critical submergence
$(S/D)_c$ Critical value of submergence normalized with intake diameter
S_0 Slope
t Time
t_0 Start time
$|U|$ Representative magnitude of velocity outside a vortex
U_i Mean velocity of flow entering an intake
V Velocity of flow
V_D Velocity of flow at pump's suction bell
V_r, V_θ, and V_z Components of velocity along coordinate directions mentioned above
Y, y Flow depth (sometimes instead of h)

Subscripts

a air
c Critical condition
m Model
0 Origin
p Prototype
r Radial component
s Submergence
w water
z Vertical component
θ Tangential component

REVIEWERS

Dr Giovanni De Cesare

Plateforme de Constructions Hydrauliques
L'École Polytechnique Fédérale, Lausanne, Switzerland

Dr Stefan Felder

Water Research Laboratory, School of Civil and Environmental Engineering,
University of New South Wales, Sydney, Australia

Dr Gregory Guyot

Geophysical and Industrial Flows Laboratory
Université Grenoble Alpes, Grenoble, France

CHAPTER 1

Introduction

ROBERT ETTEMA
Civil & Environmental Engineering Dept., Colorado State University, USA.
E-mail: *Robert.Ettema@colostate.edu*

DAVID Z. ZHU
Civil & Environmental Engineering Dept., University of Alberta, Canada.
E-mail: *dzhu@ualberta.ca*

1.1 | Scope

Water intakes can be designed to generate or avoid swirling flows. In other words, the features of swirling flows can be desirable or undesirable, depending on the purpose of the intake. Additionally, the rotation in swirling flows can be sufficient to form free-surface vortices. Vortex-flow intakes use the desirable features of swirl and vortex formation.

This monograph extends IAHR's publication *Swirling Flow Problems at Intakes*, coordinated and edited by Dr. Jost Knauss (Knauss 1987). *Swirling Flow Problems at Intakes* was the first publication in the IAHR Hydraulic Structures Design Manual series and remains a widely used reference on vortices and water intakes. Now, thirty-six years later, the present monograph updates and extends Knauss (1987). Engineers' understanding of water intakes and vortices has advanced, and developments in the use of vortex forming water intakes in contemporary civil-engineering structures continue. The advances and developments have prompted the writing of this monograph, which considers the desirable features of vortex formation for water intakes and the undesirable features relating to water-intake performance.

Although this monograph extends Knauss (1987), Dr. Eduard Naudascher's words in the Preface to Knauss (1987) continue to ring true: "There still is intensive research activity today on swirling flows so that it is impossible to present material in final form". To be sure, new insights enable engineers to design better intakes. Yet, certain basic processes and design issues remain inadequately understood and, therefore, formulated. Swirling flows continue to be an active area of research. For example, although engineers have an improved understanding of air entrainment in swift, swirling, free-surface flows, much of that understanding was obtained from studies on hydraulic scale models

in hydraulics laboratories. The translation of air entrainment, air-conveyance, and air rise results to the prototype scale, or the law of similitude remains unclear. This concern is unclear in other hydraulic engineering applications with aerated flows, such as high-speed flows down stepped spillways. In addition, in numerical modeling the accurate simulation of air-entraining or heavily aerated flows is an active area of research. Incomplete understanding of aerated flows is not unique to water intakes.

Fairly recent developments in hydraulic structures entail the design and construction of underground systems for stormwater and combined-sewer-overflow conveyance and collection (sometimes termed “deep tunnel” or “dropshaft” systems). Many large urban centers (e.g., in China, Singapore, United Kingdom and the United States of America) are implementing such systems, which typically use vortex-intakes. Such systems collect storm water to avert urban flooding and treat the collected water before it is released with an environmentally acceptable quality into a river or coastal region. Sometimes too, such systems gather water for subsequent use. Also, vortex intakes are used in sanitary and combined sewer systems to reduce sewer odor complaints and sewer corrosion related to H2S gases. Vortex formation is a design aim, thus leading vortices to be viewed in a somewhat more positive light than in Knauss (1987), which dwelt extensively on the problems created by swirling flows at intakes.

1.2 | Purposes of monograph

This monograph presents the status of insights on and the modeling of vortices at water intakes. The two general topics are:

a) The generation of the desirable features of vortices by means of vortex-flow intakes that form wall jets intended to vertically convey stormwater to a conveyance and collection system located at a much lower elevation than the intake. Such intakes are extensively used for collecting stormwater drainage in deep-tunnel settings.
b) The generation of vortices whose features are deemed undesirable, as they may consume flow energy and reduce the discharge capacity of water intakes for spillways, outlets of dams, pump intakes, and they may result in undesirable vibrational loading and wear of components within intakes.

Much of the research performed on these two types of vortex flow are included here. The topics covered focus on the fundamentals of vortex flows and their flow fields, and the essential aspects of vortex-flow intakes. References are cited that both present the details of the design and operation

of intakes to avoid the formation of vortices and of vortex-intakes, and those that present examples or case-studies. Additionally, this monograph is well-illustrated to aid understanding.

No overall or summary set of recommendations are given by this monograph. Instead, the individual chapters indicate the current suggestions regarding distinct aspects of vortex formation. As mentioned, in some circumstances vortices have desirable flow features (e.g., drainage drop structures), in other circumstances vortices are to be avoided (reservoir and pump intakes). Additionally, certain investigation approaches (e.g., numerical) and aspects of design (e.g., drop structures) entail further work. The present monograph seeks to be a useful update to Knauss (1987).

1.3 | Features of free-surface vortices and swirl

1.3.1 | Main flow-field features

The main flow-field features of free-surface vortices, in the context of vortex-flow intakes and water intakes generally, are

- Swirling flow
- Centrifugal acceleration
- Non-uniform distribution of flow
- Energy loss
- Air entrainment
- Debris entrainment
- Unsteadiness and possible vibration

Some of these features are desirable in certain intake situations and undesirable (or problematic) in other situations. A key characteristic of vortex flow fields is flow swirl, involving centrifugal acceleration, non-uniform distribution of flow, and varying extents of unsteadiness. Swirl often occurs in water flow, which itself responds to instabilities within the flow or between the flow and its boundaries. This characterizing feature potentially influences the other main features of the flow field at a water intake. In consequence, swirl may intensify to form a vortex, which can have desirable or undesirable consequences for intake performance.

Swirl in flows may have other attributes that offer advantages for flows conveying heat or material in addition to the fluid comprising the flow. An ensuing subsection briefly mentions the other advantages.

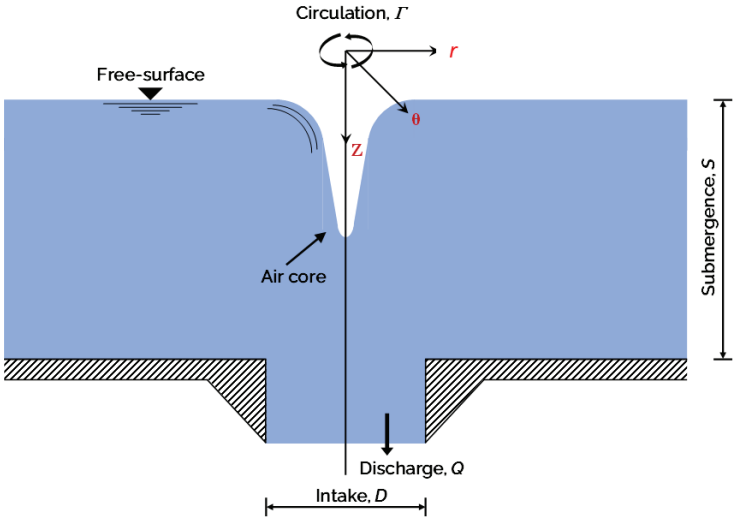

Figure 1.1 | Variables associated with water flow into a vertical, circular intake.

Figure 1.1 illustrates the fundamental variables associated with vortex formation in the flow to an intake formed as a pipe. The present monograph frequently mentions these variables and the non-dimensional parameters stemming from them. The parameters are submergence Froude number ($F_h = V/[gS]^{0.5}$), radial Reynolds number ($R_R = Q/[\upsilon S]$), circulation number ($N_\Gamma = [\Gamma D]/Q$), and relative submergence of intake (S/D). Here, $V = Q/(\pi D^2/4)$. The variables are indicated in Fig. 1.1.

1.3.2 | When swirl at intakes is desirable

Vortex-flow intakes commonly are selected as the intake design used when approach, open-channel flows of water must vertically drop water to elevations substantially lower than that of the intake. Such intakes normally collect surface water and discharge it to underground conveyance and collection systems (e.g., deep tunnels). Typically, the drop requires that flow energy associated with the difference between the two elevations be extensively dissipated in the vertical conduit between the two elevations, though additional energy dissipation may be necessary at the lower elevation. The conduit linking the two elevations is commonly called a dropshaft or drop shaft (e.g., Knauss, 1987; Toda and Inoue, 1999; Mulligan et al., 2019). Intakes to dropshafts deliberately guide flow to swirl like a single vortex within the intake and create a spiraling, wall-jet flow that concentrates angular motion of flow near the dropshaft wall and has an air core. In some respects, vortex-flow intakes could be named spiral-flow intakes or swirling-flow intakes, insofar that they cause flow to spiral or swirl down a vertical dropshaft.

For comparatively long dropshafts whose length exceeds, say, about four or five diameters of the dropshaft's circular cross-section (e.g., Jain and Kennedy, 1983; Toda and Inoue, 1999; Yu and Lee, 2009), having the flow swirl down a dropshaft's perimeter increases energy dissipation and decreases air entrainment (Zhao et al., 2006) by maintaining a stable air core that reduces the ratio of the air flow to the water flow by up to two orders of magnitude compared to air entrained by flow plunging directly down a conduit (Ma et al., 2016; Zhang et al. 2016). Swirl increases flow length and increases flow velocities nearer the sides of the dropshaft, thereby causing flow to expend more energy overcoming resistance exerted by the dropshaft's fixed perimeter. Also, keeping a free-surface (an air-water interface) on the descending, swirling flow minimizes pressures within the swirling flow and against the dropshaft's perimeter, until the swirling water eventually reaches the base of the dropshaft, where the water impacts the dropshaft's base or enters a reservoir of water contained at the base.

Usual physical characteristics of vortex-flow intakes are that they have no moving parts (e.g., hydro-machinery) and cause flow to assume a swirling trajectory as water enters the intake then descends the circular cross-section of the dropshaft extending below the intake. Vortex intakes often are used for drainage systems involving relatively large drops (5 to 100 m). To reduce construction costs typically incurred with underground construction, dropshafts may need to be kept comparatively compact or narrow, more-or-less the same as the width of flow approaching the intake.

1.3.3 | When swirl at intakes is undesirable

Intake designs avoid (or minimize to an acceptable level) flow swirl and consequent vortex formation in situations when flow energy is to be conserved, added energy minimized, and flow must pass practically uniformly into an intake. These intakes may comprise a simple outflow conduit, or they may have a crest, a gated crest, and possibly they may involve hydro-machinery located relatively close the intake entrance (e.g., a pump or a run-of-river turbine). The vortices begin upstream of these facets of the intake or occupy a small percentage of the intake's volume.

Further, when an intake transitions from a free-surface approach flow to a closed-conduit flow (e.g., in a pump column), air entrainment via intense swirl (vortex formation) into the intake should be avoided, because air entrainment bulks flow within the closed conduit and, thereby, reduces the conduit's capacity to convey water. Also, the concomitant problem of vibration must be avoided, as vibration reduces flow capacity, consumes energy, and may increase wear of intake entrances and especially the rotating bearings of hydro-machinery (notably, turbines and pumps) connected with

the intake. This paragraph uses the word “avoid” recurrently, as the flow-field features of swirl and vortices are incompatible with the required performance of an intake, in most situations; exceptions do arise, as explained in Chapter 5.

1.3.4 | Swirl decay

Swirl decay, or swirl decrease, is a consideration for flow in dropshafts extending below vortex-flow intakes. For a given dimensions of vortex-flow intake, flow’s initial swirl reduces as dropshaft length increases. Gravity acceleration acts to overcome centrifugal acceleration. The ratio of centrifugal acceleration to gravity acceleration could be expressed as $V^2/(Dg)$, where V = the average velocity of the flow entering the dropshaft; D = diameter of dropshaft, as noted above; and g = gravity acceleration (e.g., Knauss 1987). Additional parameters influencing swirl decay are angle of vertical incline of flow entering the dropshaft, relative roughness of the dropshaft wall, and dropshaft length relative to dropshaft diameter.

As explained in Chapter 2 of this monograph, there are three main types of swirl flow in pipe flows, in accordance with the tangential flow field each flow produces. Tangential flow field influences swirl decay. In addition to the wall-jet type produced by vortex-flow intakes, for pipe (closed conduit) flows there also are concentrated swirls and solid-body swirls. The concentrated swirl type concentrates flow so that the maximum tangential velocity is near the center of a pipe. The solid-body type has almost uniform rotation (like a forced rotation) such that the maximum tangential velocity is near the outer edge of the pipe.

For pipe flow (no air core), swirl decay is shown to depend on flow Reynolds number, relative roughness of the dropshaft wall, and initial swirl angle (e.g., Steenbergen and Voskamp, 1998). For example, experiments involving pipe flows with relatively small-diameter pipes (e.g., 25.5-mm-diameter pipe) indicate that, after an axial length of flow equivalent to about 50 pipe diameters of conduit, swirl produced by a wall-jet is about 10–20% of its original value (e.g., Kreith and Soniu, 1965; Steenbergen and Voskamp, 1998). Rates of swirl decay for dropshafts conveying wall jets with free-surface flow are documented for hydraulic models of vortex intakes and dropshafts, but those hydraulic structures usually are comparatively short relative to dropshaft diameter; common ratios of dropshaft length to dropshaft diameter are less than about ten.

1.3.5 | Other advantages of swirl

The generation of swirl by wall-jets in flows has other advantages, though energy dissipation remains an ever-present consideration. Those advantages stem from the flow-field features mentioned above

and relate primarily to the effects of lengthened flow path and centrifugal acceleration. This monograph briefly mentions them and cites a few selected references where interested readers may learn more about the mentioned other advantages of swirl.

The other advantages usually pertain to closed-conduit flows in pipes of circular cross-section, and concern heat-transfer from (or to) a flow, separation of material in a flow, and mixing of particles in a flow (especially of sediment or insoluble powder):

- Swirl increases heat transfer. The increased flow path enables more heat exchange. The literature on heat transfer in a swirling flow is extensive (e.g., Hay and West, 1975; Chang et al., 1995; Mariemianov and Okulov, 2003; Sielbold et al., 2022).
- Swirl in a hydrocyclone helps separate material in a flow (gas-liquid, liquid-liquid, and solid-liquid). Centrifugal acceleration causes the heavier material to move to the outer boundary of flow, whence it is separated from the flow. An extensive literature exists on hydrocyclones or swirl concentrators (e.g., Svartovsky and Thew, 1992; Cilliers, 2000).
- Swirl may enhance transport capacity of sediment which is used in certain flushing systems of desanders or in vortex-tube sediment extractors at headrace channels of hydropower plants to evacuate deposited solid material and bedload, respectively, through slotted tubes with a minimum of water (Atkinson, 1994a, b; Meier, 2003; Rachelly et al., 2022).
- Swirl enhances mixing in pipe flow. Heavier material in pipe flow becomes mixed over the cross-section of flow, rather than accumulate at locations along a pipe's lower boundary. The literature on swirl to aid sediment transport in pipes, and to address accumulation and abrasion problems in liquid-solid conveyance along pipes is quite well developed (e.g., Schmidt and Ghosh, 2019; Zhou et al., 2022).
- Swirl may enable suitable distribution of flow entering reaction hydropower turbines. Barrows (1943), for example, gives early dimensions of scroll-form intakes used to feed flow to turbines intended to harvest flow energy.

1.4 | Structure of monograph

Following this chapter introducing the monograph, Chapter 2 is a concise refresher about the fundamentals of vortices and their swirling flows. The refresher usefully reminds readers about the complexities and the three-dimensional nature of such flows.

Chapters 3 and 4 cover physical (laboratory) and numerical (office) hydraulic modeling of vortices and swirling flows, respectively. Chapter 3 extends a chapter in Knauss (1987) by adding recent

experiences regarding modeling of vortices and vortex-flow intakes. Chapter 4 is wholly new. That chapter explains how advances in computational techniques, software, and computers themselves increasingly enable modelers to use numerical methods for examining flows likely to form vortices. But challenges continue. As does physical modeling, numerical modeling wrestles with issues regarding how best to handle stratified, highly turbulent, unsteady, and highly aerated flows. These challenges are discussed in the context of vortices and swirling flows, and the chapter outlines recent successes in numerical modeling of flow in vortex intakes.

The next three chapters describe common instances where vortices are prominent traits of flows fields, and where the main features of vortices become desirable and undesirable. Chapter 5 deals with drainage intakes and dropshafts. These hydraulic structures have significantly gained in prominence over recent decades, and increasingly (though not always) involve vortex-flow intakes and the desirable attributes of swirl and vortex-flow fields. Chapters 6 and 7 concern undesirable aspects of swirl and vortices at intakes used for dam outlets and pump intakes, respectively. Also, Chapter 7 deals with swirling flows and vortices at spillway crests. Indeed, vortices are to be avoided for intakes conveying water flow to pumps or turbines, because swirl and vortices diminish pump or turbine performance. Design and operation guides are suggested regarding intakes for drainage structures, pumps, turbines, and spillways. Chapter 7, focused on intakes to turbines, is new, though many of the considerations for hydropower intakes are essentially the same as for pump intakes, notably in the importance of avoiding vortices, especially air-entraining vortices. One difference is that turbines for medium- and high-head hydropower facilities are positioned substantial distances downstream of the intakes directing water to them.

This monograph ends with Chapter 8, which links back to Chapter 8 of Knauss (1987). The chapter in Knauss, and written by George Hecker, frames itself in terms of five questions revolving around swirling flows, pump intakes and physical modeling. The questions are germane, partially answered, and now augmented by contemporary questions especially regarding vortex-flow intakes and numerical modeling.

Hecker's questions were as follow:

a) Should vortices be prevented?
b) What are the practical results of basic research?
c) Is the intake geometry important?
d) Do published guidelines work?
e) How may vortices be dissipated?

Hecker addressed the questions and ended with recommendations for future research, notably regarding pump intakes. He concluded that considerable knowledge existed on the basic aspects of vortices, and that physical models of pump intakes can be reliably designed and operated to aid the design of prototype intakes. This knowledge should help designers determine the need for a site-specific study, especially one that examines flow patterns at the specific site of an intake. The present monograph also addresses these questions but goes further by showing how the features of vortices deemed undesirable for the intakes of many hydraulic structures (e.g., hydropower intakes) are wanted for the intakes of other intakes (e.g., drainage dropshafts).

CHAPTER 2

Fundamentals of Vortices and Swirling Flows

SUSAN J. GASKIN
Civil Engineering, McGill University, Canada. E-mail: *susan.gaskin@mcgill.ca*

SEAN MULLIGAN
VorTech Water Solutions Ltd, Galway, Ireland. E-mail: *sean.mulligan@vortechws.com*

2.1 | Introduction

Free-surface vortices occur in flows at hydraulic structures with submerged intakes and occasionally at the approach to outflow structures like spillways. Circulation in the approach flow, or swirl and vorticity, imparted to the approach flow due to upstream flow boundaries or from flow separation from a sharp boundary (e.g., a pier) is concentrated by discharge to an intake, located below the free-surface, and may evolve into a free-surface vortex. The circulation in the vortex is concentrated and intensifies due to axial stretching as flow is drawn downward to the intake and accelerates, as Fig. 2.1 shows. The low pressure at the center of the vortex produced by centripetal acceleration produces a depression of the free surface, which, with increased vortex strength defined by its circulation, becomes an air-core vortex.

Free-surface vortex behavior is typically classified into two main types, as shown by Fig. 2.1:

- Weak vortices (that are generally not desirable in hydraulic structures design), in which the axial flow concentrates the circulation into a coherent vortex that may increase in strength to an air-entraining vortex. Fig. 2.1a illustrates the critical submergence, S_c, of an intake; and
- Strong vortices that are designed by inducing a strong circulation which forms a vortex flow with a large air-core. Fig. 2.1b shows a vortex with an air-core penetrating into the intake.

Weak-vortex flows can occur at reservoir intakes and pump intakes (discussed in Chapters 6 and 7). They develop when submergence (i.e., intake depth below the free surface) is low and are of concern as they can generate flow asymmetry or unsteadiness, or entrain air, floating debris, or ice, which may reduce plant performance and/or cause premature failure of mechanical components. Strong vortex

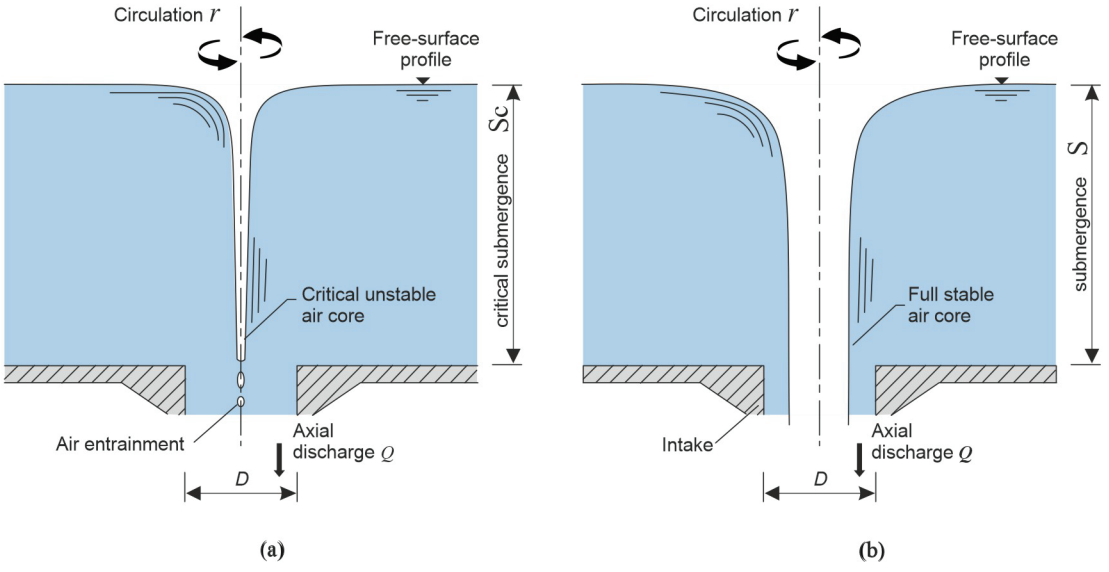

Figure 2.1 | Sketch of a typical, vertical intake structure with a swirling flow producing a vortex: (a) a weak vortex during the onset of air entrainment at the critical submergence S_c; and (b) a stable full air core vortex under strong circulation conditions (Mulligan 2015).

flows form owing to induced circulation or a steady supply of vorticity to the flow field producing a free-surface vortex with a stable full air core extending deep into the intake. Their most common design application is to safely convey flows vertically downward in swirling-flow intakes, such as used for stormwater dropshafts (discussed in Chapter 5).

2.2 | General description of vortices

A vortex is a local concentration of vorticity surrounded by irrotational fluid (Saffman, 1992) within which streamlines follow a circular path or a helix with a reducing radius (i.e., three-dimensional [3D] spiral path). The streamline pattern can be used to classify vortices into two- or three-dimensional structures (Lugt, 1983). An ideal planar vortex is two-dimensional (2D) with concentric or asymmetric streamlines. In real systems, planar vortices are quasi two-dimensional with a large diameter to axis length ratio (e.g., 100/1 for hurricanes). A 3D vortex has helical or 3D-spiral streamlines due to the component of velocity along the axis of rotation, while their diameter to axis length ratio is small (e.g., 1/100 for dust devils). In engineering applications, such as free-surface vortices at water intakes or in dropshafts, the diameter to axis length ratio is of the order of 1/2.

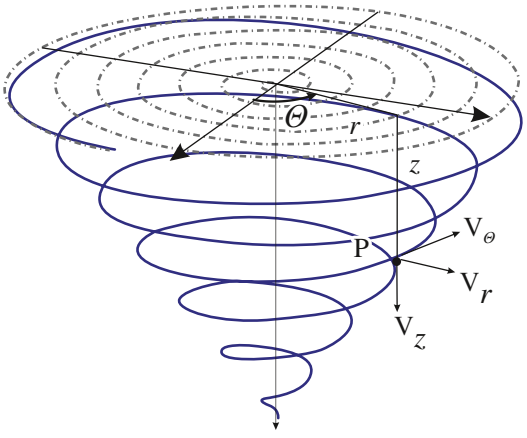

Figure 2.2 | The coordinate system (r, θ, z) for analysis of a spiral vortex.

2.2.1 | Fundamental mathematics of swirling flow

The velocity field in a vortex is described using a local cylindrical coordinate system (r, θ, z), with z orientated along the central axis of the vortex (axis of rotation), and with corresponding radial, azimuthal and axial velocities V_r, V_θ and V_z, as shown in Fig. 2.2. For a free-surface vortex, z is typically defined pointing vertically down from the free surface.

A vortex is a local concentration of vorticity within which streamlines follow a circular, helical, or 3D-spiral path. Vorticity in the flow is a result of the shear deformation of a fluid element entering into rotation. Vorticity, $\vec{\omega}$, defined as the curl of the velocity vector, describes the rotation of a local fluid particle about its center of mass (Helmholtz, 1867),

$$\vec{\omega} = \nabla + \vec{V} = \begin{pmatrix} \frac{\partial V_z}{\partial y} - \frac{\partial V_y}{\partial z} \\ \frac{\partial V_x}{\partial z} - \frac{\partial V_z}{\partial x} \\ \frac{\partial V_y}{\partial x} - \frac{\partial V_x}{\partial y} \end{pmatrix} \tag{2.1}$$

As vorticity is concentrated in the core of the vortex ($r < r_0$, where r_0 is the characteristic radius), circulation, Γ_∞, can be estimated by integrating the azimuthal (circumferential) velocity, V_θ, along the circumference of a circle of radius $r \gg r_0$ (Thomson, 1869). Equivalently, circulation is the surface integral of vorticity (Lugt, 1983),

$$\Gamma_\infty = \Gamma(r \gg r_0) = \int_0^{2\pi} V_\theta r d\theta = \int\int_A \vec{\omega} \cdot d\vec{A} \tag{2.2}$$

Helmholtz (1867) first described vorticity using the concept of vortex filaments or tubes, which have the following properties. Vortex tubes must either be closed loops or must end at a surface. The strength of a vortex filament is constant along its length and its circulation is the same for every contour enclosing it. As angular momentum in a vortex is conserved (if viscous losses are negligible), vorticity in the vortex increases in proportion to the axial gradient, a, of the axial velocity component, V_z, (Helmholtz, 1867). The axial velocity gradient results in axial stretching of the vortex, an increase in the azimuthal velocity and a pressure drop at the center of the vortex.

2.2.2 | Free-surface vortices

Free-surface vortices form in open channel flows due to vorticity generated from boundary shear in a boundary-layer flow or from boundary discontinuities (e.g., Quick, 1970). A free-surface vortex will be located at the boundary discontinuity or where swirl in the approach flow is concentrated by the flow accelerating axially towards an outflow (e.g., a hydropower intake). The interaction of a vortex with the free surface is defined by the deformation of the free surface, such that the tangential stress is equal to zero and the normal stress is a constant (Green, 1995).

The potential of a free-surface vortex to cause damage to a turbine or pump is a function of its strength. With increasing strength, the vortex will result in a non-uniform flow and may entrain air or debris, which will lower efficiency, causing increased wear or damage to the pump or turbine. A qualitative classification system has been developed to predict vortex strength, which is characterized by its circulation. The original system (Denny 1956) was refined by the Alden Research Laboratory (Hecker, 1987) and is commonly referred to as the Hecker scale for vortex type (VT). Vortex strength varies from VT0 with no vortex activity, VT1 with coherent surface swirl, up to VT6 with a full air-core extending into the intake, as demonstrated in Fig. 2.3.

Vortex types VT1 to VT5 contain a forced vortex in their cores (where vorticity is concentrated) and a potential (or free) vortex in their outer fields, where vorticity is much lower and is approximated as zero in some models. The air-core vortex, VT6, can be assumed to be entirely a free vortex. Vortex types VT1 and VT2 are considered to have general swirl, vortex type VT3 is identified by a dye core and is the lowest strength vortex considered to have concentrated vorticity. VT3 has a small free-surface depression or dimple. The free-surface depression increases in depth with increasing vortex strength, VT4 entrains debris, VT5 entrains air bubbles, and VT6 has a full air core extending all the way to the inlet.

The Hecker scale primarily relates to the “weaker” and unstable range of vortex flows, with further classification for the “stronger” more stable (than VT6) full air-core range not available due to the

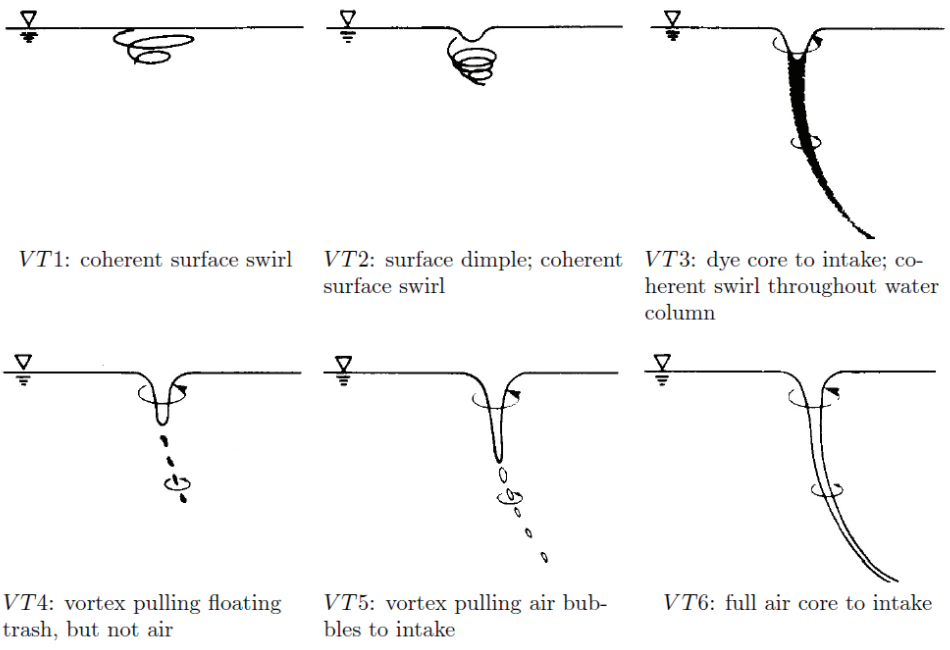

Figure 2.3 | The Hecker vortex classification scale (VT) for the strength of a free-surface vortex (Hecker, 1987); VT is vortex type.

qualitative nature of the classification system. Therefore, there is a need to further develop this classification system, perhaps through quantitative, non-dimensional variables, to provide a universal classification system for the full spectrum of vortex flows at intakes.

2.3 | Analytical and semi-analytical models

2.3.1 | Free and forced vortices

A forced vortex can be described as a solid body rotation of the fluid, such that

$$V_\theta = \vec{\omega} \times \vec{r} \tag{2.3}$$

A free vortex, which has no vorticity and is fully irrotational, can be described with an equation developed from the Navier-Stokes equations, the momentum equations in the radial, tangential, and axial directions (Hall, 1966). These equations simplify when assuming flow is steady, ideal (zero viscosity), axisymmetric and that derivatives in the axial direction can be neglected. Integration of the transverse momentum equation yields,

$$V_\theta = \frac{\Gamma}{2\pi r} \tag{2.4}$$

The simplification of the radial momentum equation describes the variation of the pressure, p, from its value at an infinite radius of p_∞ to a minimum at zero radius as

$$p_\infty - p = \frac{\rho\Gamma^2}{8\pi^2 r^2} \tag{2.5}$$

which, when divided by the specific gravity of the fluid, γ, gives the depth, h, or deformation of the free surface,

$$h_\infty = h_r - \frac{\Gamma^2}{8g\pi^2}\left(\frac{1}{r_\infty} - \frac{1}{r}\right) \tag{2.6}$$

2.3.2 | Vortex model

Rankine (1876) modelled a vortex as an inner forced vortex region of radius, r_c, of constant vorticity surrounded by a free vortex region of zero vorticity having the same circulation as the periphery of the forced vortex core, as Fig. 2.4 shows. This vortex requires work to be done in the viscous core to dissipate kinetic energy. The tangential velocity and pressure of the vortex are given as

$$V_\theta(r) = \begin{cases} \dfrac{\Gamma_\infty r}{2\pi r_c^2}, & 0 \le r \le r_c \\ \dfrac{\Gamma_\infty}{2\pi r}, & r_c \le r \le \infty \end{cases}, \quad V_r = 0, V_z = 0 \tag{2.7}$$

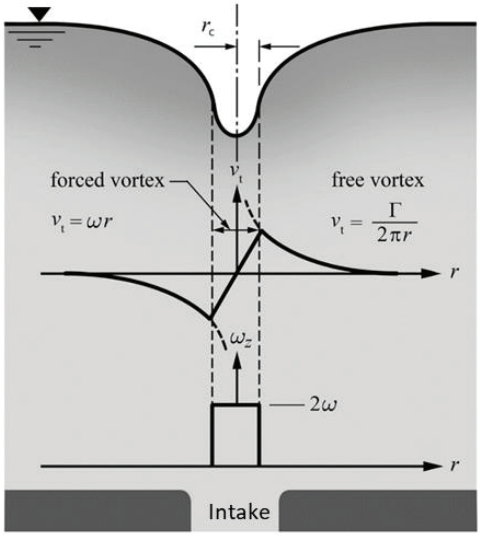

Figure 2.4 | Rankine vortex, with an inner forced vortex and an outer free vortex, at an intake (adapted from Möller, 2013).

$$p_\infty - p = \begin{cases} \dfrac{\rho\omega^2 r^2}{8}, & 0 \le r \le r_c \\ \dfrac{\rho\Gamma_\infty^2}{8\pi^2 r^2}, & r_c \le r \le \infty \end{cases}, \quad V_r = 0, V_z = 0 \tag{2.8}$$

where Γ_∞ is the bulk circulation, assumed to be a constant value far from the vortex center.

In Rankine's model, there is a discontinuity at r_c between the rotational and irrotational fields (Rouse, 1963), that will not exist in a real fluid as viscosity diffuses vorticity outwards producing a Gaussian-like profile (Rott, 1958; Rouse, 1963; Saffman, 1992). In a full-air-core vortex, the air core replaces the viscous core, whose periphery is the air-water interface beyond which is the free vortex (Quick, 1970). Burgers (1948) and Rott (1958) independently developed a vortex model incorporating the diffusion due to viscosity, thus removing the discontinuity found in Rankine's model, and incorporating the concentrating effect of axial stretching of the vortex.

A vortex is said to be axially stretched if the axial velocity, V_z, increases along its axis, which, due to conservation of angular momentum, causes its streamlines to converge towards the axis ($V_r < 0$). Burgers (1948) and Rott (1958) assume that the radial profiles of V_θ and V_r are constant along z and that the axial velocity V_z is independent of r and increases linearly with z,

$$V_z(z) = az, \qquad V_r(r) = -ar/2 \tag{2.9}$$

where the axial gradient a is a constant with units of s^{-1}. If the profile of V_r were set to satisfy continuity, the axisymmetric Navier-Stokes equations can be solved to obtain

$$V_\theta(r) = \frac{\Gamma_\infty}{2\pi r}\left[1 - \exp(-(r/r_0)^2)\right] \tag{2.10}$$

The characteristic radius, r_0, is determined from the ratio of viscosity, υ, to the axial gradient as

$$r_0 = 2(\upsilon/a)^{1/2}, \quad a = \partial V_z/\partial z \tag{2.11}$$

Petitjeans (2003) verified Eq. (2.11) for experiments of a stretched vortex in the wake of a step, demonstrating the importance of axial stretching in determining the characteristic radius r_o. The model was refined by Odgaard (1986) to predict the critical submergence for an air core vortex in a cylindrical tank with imposed flow rotation. He assumed a linear profile of the axial velocity varying from 0 at the free surface to U_i at the bottom outlet as $a = U_i/h$ where h is the water depth and U_i the mean outflow velocity. The diffusion of vorticity at r_c from the forced vortex to the free vortex, occurs due to viscous diffusion, which is proportional to $Re^{-1/2}$ and is a slow process at large Reynolds number (Cotel and Breidenthal, 1999).

A model with a Burgers vortex in the vortex region surrounded by an external zone with no axial velocity was proposed by Einstein and Li (1951). Bøhling et al. (2010) adjusted the model to obtain smooth azimuthal and radial velocity profiles and a continuous axial velocity profile. Burger's model is the base of many numerical and analytical variants proposed, for example by Lewellen (1962), Toyokura and Akaike (1970), Lundgren (1985), Hite and Mih (1994), Miles (1998), Vatistas and Li (1988), Rossi et al. (2004), Anh and Hosoda (2005), Stepanyants and Yeoh (2008), Ito et al. (2010), and Wang et al. (2011). Andersen et al. (2006) extend Lundgren's (1985) model to include surface tension. The free-surface depression for a mild depression in a Burgers vortex is computed by Miles (1998), while Anh and Hosoda (2005) computed the free-surface profile for a full air core vortex.

The models described above are for time-independent vortices continuously provided with kinetic energy from outside the vortex system (Rouse, 1963) by the radial or axial velocity component (Daggett and Keulegan, 1974; Lugt, 1983). Kinetic energy is dissipated through shearing and growth of the viscous core.

The Rankine model can also be treated as time-dependent because the vortex evolves over time. This can be due to growth of intensity, as more kinetic energy is supplied, or decay, if energy is lost over time. Oseen (1912) and Lamb (1932) developed a time-dependent model (t is time), which is an exact solution to the one-dimensional laminar Navier-Stokes equations:

$$V_\theta(r,t) = \frac{\Gamma_\infty}{2\pi r}\left[1 - \exp\left(-\frac{r^2}{4\upsilon t}\right)\right] \tag{2.12}$$

The radius of the viscous core, r_0, which is the location of the maximum tangential velocity, can be found from the maximum of Eq. 2.12 as

$$r_0(t) = \sqrt{4\varphi\upsilon t} \tag{2.13}$$

where φ is the Oseen parameter, O(1), which provides a fit to experimental data.

The free-surface profile can be calculated from the azimuthal velocity profile, $V_\vartheta(r)$, of Burgers model (Eq. 2.10), including the surface tension effects, as

$$h_\sigma(r) = \int_\infty^r \left(\frac{V_\theta(\acute{r})^2}{g\acute{r}} - l_\sigma^2 K(\acute{r})\right) d\acute{r} \tag{2.14}$$

(Andersen et al., 2006; Suerich-Gulick, 2013), where σ is the surface tension coefficient, $l_\sigma = \sqrt{\rho g}$ is the characteristic length scale for the air-water interface (i.e. the scale at which surface tension effects become significant) and $K(r)$ is the mean local curvature profile. The pressure drop associated with the kinetic energy of the radial and axial velocity is negligible compared to that of the azimuthal

velocity and is not included (Odgaard, 1986). This approximation neglects the effect of the depression on the velocity field resulting in a negligible error for dimples but gives an error of up to 26% for a deep funnel-type depression (Stepanyants and Yeoh, 2008).

The mean local curvature $K(r)$ can be calculated from the azimuthal velocity profile, $V_\vartheta(r)$, of Burgers model, including the surface tension effects, as

$$K(r) = -\frac{1}{2}\left\{\frac{h_r}{r[1+(h_r)^2]^{1/2}} + \frac{h_{rr}}{[1+(h_r)^2]^{3/2}}\right\} \qquad 2.15$$

where h_r and h_{rr} are the first and second derivatives of h with respect to r, respectively (Andersen et al., 2006). The first and second terms in the parentheses are the curvature about the horizontal axis and the curvature about the axis of rotation (vertical). A vertical section through the free surface shows the concave curvature (positive) at the tip, changing to convex (negative) beyond the inflection point a distance past r_0. Surface tension therefore pulls the interface upward in the core and pulls it down very slightly outside the core.

In the case of strong, full-air-core vortices (VT6), the solid body region of Rankine's model does not exist due to the position of the air core. Therefore, the ideal, irrotational model (Eq. 2.4) is applied to predict the tangential velocity field up the radial position of the air water interface. This theoretical tangential velocity profile was found to diverge from the experimental data in the near-field close to the core by as much as 50% (Quick, 1961; Anwar, 1965; Mulligan et al., 2019), as the tangential velocity field in this region strongly depends on axial flow conditions (Mulligan et al., 2019). See Fig. 2.5.

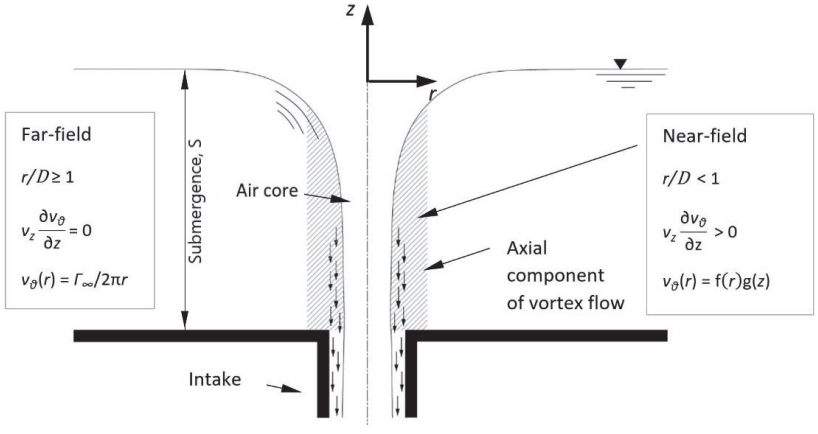

Figure 2.5 | Schematic representation of the axial flow component in a strong full air-core, free-surface vortex extending to an intake. (Here, the z-axis is upward.)

Anwar (1965), presented an alternative model for the tangential velocity of the full air core vortex, defined as

$$\left(\frac{v_\theta}{v_{\theta_o}}\right)^2 = 1 - 2\frac{1-\sqrt{1-(2n)^2}}{1+\sqrt{1-(2n)^2}}\log_e\frac{\tan\emptyset}{\tan\emptyset_0} \tag{2.16}$$

where ϕ is the so called "*angle of conical coordinates*" that defines the angle of the tangent to the free-surface on the $r-z$ plane:

$$\phi = \tan^{-1}\frac{r}{z} \tag{2.17}$$

and subscript 0 refers to that of the characteristic radius; and n is the ratio of the tangential velocity to the axial velocity.

To account for the effects of axial flow near the full air core, Mulligan et al. (2019) developed an alternative tangential velocity model that depends on the circulation number and geometry of the intake as:

$$v_\theta(r) = \frac{\Gamma_\infty}{2\pi r}\left(1-\left(\frac{4}{\pi N_\Gamma}\right)^{\frac{mr}{d}}\right) \tag{2.18}$$

where m is an empirical constant. When $m \to 0, v_\theta(r) \to 0$. Additionally, when $m \to \infty, v_\theta(r) \to \Gamma_\infty/(2\pi r)$, the model is bounded and exhibits no singular behaviour. Values for the exponent m then provide a family of curves for the tangential velocity distribution, which must be validated using data sets from physical experiments. A value of $m = 2$ provided acceptable results when applied to a scroll type vortex intake application (Mulligan et al., 2019) (see Chapter 5).

2.3.3 | Measurements of velocity profiles and free-surface depression

In recent years, laboratory measurements of velocity profiles and free-surface depressions have been compared to models, facilitated by the development of non-intrusive velocity measuring techniques such as particle image velocimetry (PIV) and particle tracking velocimetry (PTV).

The azimuthal velocity profiles are modeled using the Burgers (1948), Rott (1958) or Lamb–Oseen model (Eqs. 2.10 and 2.12). These models then were modified (e.g. Rosenhead, 1930; Anwar, 1965; Odgaard, 1996; Vatistas et al., 1991; Hite and Mih, 1994; Mulligan, 2018) to improve the fit of the azimuthal velocity profiles to experimental data, as Fig. 2.6a shows for the free-vortex region of a strong vortex in a cylindrical tank and Figure 2.6b for an air-core vortex in a cylindrical tank.

Fig. 2.6 shows comparisons of vertical profiles of the azimuthal velocity within and outside the vortex predicted by the modified model and compared to measured data. For the case of a horizontal intake,

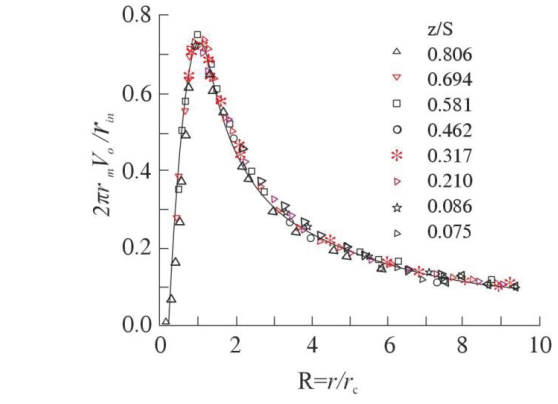

(a)

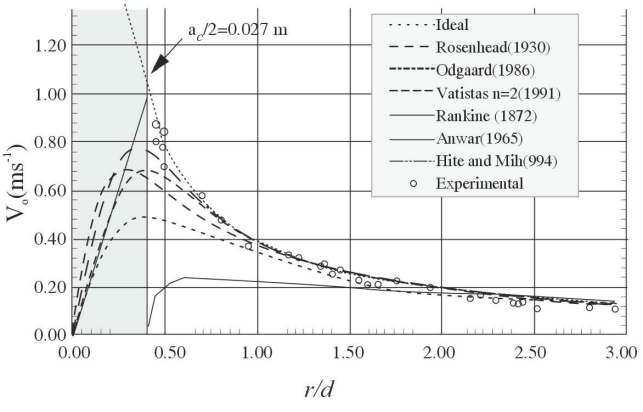

(b)

Figure 2.6 | Comparison of computed values with measurements: (a) experimental azimuthal velocity profile, $V_\vartheta(r)$, in a free-surface vortex, where S is submergence (Figure 9 of Song and Li 2015); and (b) comparison of azimuthal velocity profile models and data from a strong free-surface, air-core vortex, where a_c is the critical air-core diameter. (Figure 11 of Mulligan, 2019.)

the flow outside the vortex can be well approximated as a slice of a two-dimensional potential flow into a horizontal line sink located at the upper edge of the intake opening (Yildrim et al., 2000; Bøhling et al., 2010; Suerich-Gulick et al., 2014b) as

$$\frac{|U|(\eta)}{U_i} = \frac{c_1}{4k}\left(\frac{d}{\eta} - c_2\right) \qquad 2.19$$

where $|U|$ is the magnitude of the velocity outside the vortex, U_i is the mean velocity across the intake opening, η is the distance from the top of the inlet opening, k is the distance between the piers

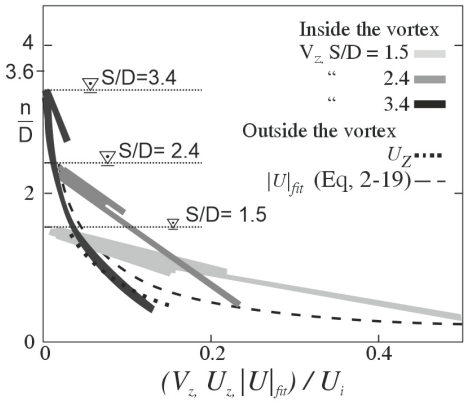

Figure 2.7 | Vertical velocity profiles in a free-surface vortex into a horizontal intake at the end of a channel flow (adapted from Suerich-Gulick et al., 2014b). Note, as mentioned in text, (V_z, U_z, $|U|_{fit}$ are the velocity profile inside and outside the vortex and best fit outside the vortex; U_i is outlet velocity, S is submergence, D is the intake diameter).

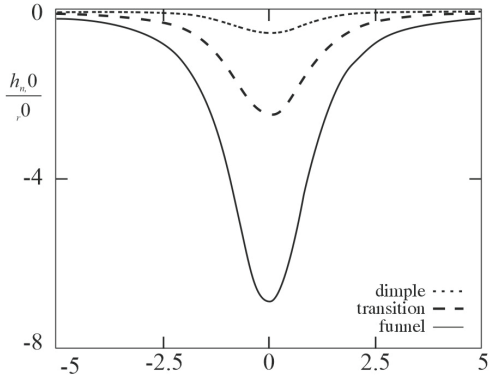

Figure 2.8 | Shape of the free-surface depression provided by Burger's model, including surface-tension effects. (Figure 7 of Suerich-Gulick et al., 2014c), where $h_{n,0}$ is the nominal maximum depth of the surface depression.)

flanking the inlet, c_1 and c_2 are coefficients that account for the specific geometry, as graphed in Fig. 2.7. The vertical velocity V_Z, within the vortex is given by Eq. 2.9 and is shown in Fig. 2.7.

The free-surface depression increases with increasing strength of the vortex, starting as a dimple and developing into a funnel shape. Fig. 2.8 shows the depression predicted using Burgers model, including surface-tension effects (Eq. 2.14), and images of funnels of increasing depth for a free-surface vortex in a cylindrical tank.

2.3.4 | Critical submergence

A major concern for water intakes is the occurrence of a strong, free-surface vortex that reduces the discharge into the intake, can entrain floating debris or air, and results in non-uniform or unsteady flow that may reduce plant efficiency and longevity. A key parameter to predict the occurrence of a problematic vortex is its critical submergence $(S/D)_c$ for a given discharge Q, as Fig. 2.1 illustrates.

The critical state has been defined as a change from a dimple to a funnel-shaped surface depression (Anwar et al., 1978; Anwar and Amphlett, 1980; Anwar, 1983), when bubble entrainment begins (Denny, 1956; Markland and Pope, 2003; Eguchi et al., 1994, Kimura et al., 2008), or when the air-core reaches the intake; (Daggett and Keulegan, 1974; Jain et al., 1978; Anwar, 1983; Odgaard, 1986; Gulliver, 1988; Hite and Mih, 1994; and Yildrim et al., 2012).

Critical-submergence, $(S/D)_c$, is a function of the intake Froude number, defined as $\mathrm{Fr}_s = U_i/\sqrt{gD}$ or $\mathrm{Fr}_s = U_i/\sqrt{gS}$; again, here U_i is mean velocity in the intake pipe, g is acceleration due to gravity and S is submergence (Quick, 1962b; Toyokura and Akaike, 1970; Jain et al., 1978; Blaisdell, 1982; Anwar, 1983; Chang and Posser, 1987; Schäfer and Hellman, 2005). The variation of critical submergence with Froude number (the slope and shape of the curve) depends on the intake configuration and geometry (Knauss, 1987; Kacabaş and Yildrim, 2002) and imposed circulation (Jain et al., 1978; Kacabaş and Yildrim, 2002).

Many expressions take the form

$$\left(\frac{S}{D}\right)_c \sim BFr_s^A \tag{2.20}$$

The coefficient B may incorporate factors, including the influence of viscosity or turbulence (Jain et al., 1978) or circulation (Jain et al., 1978; Rao et al., 1997). The power, A, can vary from $1/2$ (Jain et al., 1978; Gulliver et al., 1986), to 2/3 (Gulliver, 1988; Rao et al., 1997), or 1 (Reddy and Pickford, 1972). Alternatively, over a greater range of Froude numbers, the critical-submergence parameter has been observed to scale with Fr_s^A at small Froude number, but tends to flatten out at larger Froude number (Jiming et al., 2000; Hebaus, 1979; Amphlett, 1979), Alternatively, critical submergence, $(S/D)_c$ has a linear increase with intake velocity, U_i, at low values of velocity, but the rate of increase decreases at higher intake velocities (Markland and Pope, 2003). As empirical correlations for critical submergence are very sensitive to the geometry of the intake structure and to the associated velocity distribution, the values are used for preliminary design. Physical models are used to optimize layout, but models introduce uncertainty, as water's physical properties (surface tension and viscosity) affect the forces that control vortex characteristics (known as scale effects).

2.4 | Other considerations

Several other considerations arise that may affect vortex formation at intakes. The next chapter discusses several of the factors, especially factors influencing the veracity of physical hydraulic modeling of intakes where vortices form.

2.4.1 | Turbulence and vortex instability

Free-surface vortices interact with turbulent approach flows. Such interactions can modify vortex characteristics and scaling behavior (see Chapter 4 for scaling between models and prototypes). Turbulent mixing in the vortex could increase radial diffusion of momentum and vorticity (Rouse 1963), resulting in more diffuse vortices with greater characteristic radius and smaller free-surface depression for a given bulk circulation. High levels of turbulent intensity in the surrounding flow can either prevent vortices from forming or intensify them (Padmanabhan and Hecker, 1984; Tastan and Yildrim, 2010), disrupting the smooth trend of increasing vortex intensity at increasing flow rates. Vortex breakdown may also be provoked by instability of the vortex or by certain boundary conditions. As these processes are transient and evolve at higher temporal and spatial resolution, they are difficult to study experimentally.

The radial turbulent velocity fluctuations in a vortex are suppressed, although the radial velocity gradient is large. This effect is seen by the formation of a continuous and coherent dye core along a free-surface vortex axis when dye is injected into its core (Anwar, 1983; Echavez and McCann, 2002; Carriveau et al., 2009, Rajendran and Patel, 2000; Schafer and Hellman, 2005; Walder and Rutschmann, 2007). Dye injected outside the core is quickly mixed and diluted by the turbulent flow (Anwar 1983). The suppression of radial turbulent fluctuations in a vortex core has been studied extensively (White, 1964; Bradshaw, 1973; Beninati and Marshall, 2005a), particularly for the case of a wingtip vortex in turbulent flow (e.g., Adams and Gilmore, 1972; Spalart, 1998; Jacquin and Pantano, 2002). As a result, radial diffusion in a vortex core has been observed experimentally to be governed by viscous diffusion rather than turbulent diffusion (Zeman, 1995; Cotel and Breidenthal, 1999). This phenomenon is used as a defining characteristic in the classification of vortex types, as well as to detect their presence and assess the persistence and trajectory of vortices in physical scale models (e.g., Schäffer and Hellman, 2005; Walder and Rutschmann, 2007). For example, in the classification system proposed by Alden Research Laboratory (ARL), the strength of the vortex is assessed in terms of the behavior of dye in the vortex core until the air-core is formed (Padmanabhan and Hecker, 1984).

The issue of how to account for turbulent effects in analytical models of intake vortices remains challenging. Early research (Einstein and Li, 1951) suggested using eddy viscosity, υ_T, to account

for increased mixing of momentum due to turbulent fluctuations, although experimental evidence indicated that the eddy viscosity was not constant across the vortex radius (Anwar, 1969). Similarly, Odgaard (1986) replaced the molecular viscosity with a constant viscosity equal to the sum of the molecular viscosity and an eddy viscosity proportional to the circulation, Γ_∞, in the equation used to predict the characteristic radius in Burgers' model (1948). The resulting model predicts that, as intake size increases, and the circulation increases proportionally, eddy viscosity eventually dominates, so that at high Reynolds number, viscosity scale effects become negligible. This approach reproduces trends observed experimentally wherein the influence of Reynolds number decreases at high Reynolds values. However, this approach fails to account for the suppression of viscous diffusion by rotation in the core and, therefore, was found to significantly overestimate the core radius (Suerich-Gulick et al., 2014b).

Other research on vortex-turbulence interaction is driven by the interest in the life-span and persistence of trailing wing-tip vortices that are hazardous to airplanes (Saffman, 1992; Beninati and Marshall, 2005a, b). These vortices have a Gaussian vorticity distribution and an axial flow jet in the core but are not subject to axial stretching. They form as a pair of counter-rotating vortices, as can form from piers at intakes, that can interact (Crow, 1970; Jacquin et al., 2005). Hurricanes and tornados experience axial stretching (Levi, 1972; Klimenko, 2007), but thermal effects are also significant and, the boundary conditions, driving forces and scales are different from vortices formed at intakes.

Linear stability theory can be used to assess the stability of a vortex, which can depend on the vortex velocity field, and the associated boundary conditions (Benjamin, 1962), including the presence or absence of physical boundaries (Ash and Khorrami, 1995). These analyses indicate that instabilities in most rotating flows are inviscid, and viscosity is assumed to be stabilizing (i.e., damping of flow energy). The conditions under which external turbulence may destabilize or break down vortices remain unclear (Cotel and Breidenthal, 1999; Beninati and Marshall, 2005b; Jacquin et al., 2005).

2.4.2 | Submerged vortices

In contrast to free-surface vortices that extend from the free surface to the intake opening, submerged vortices extend from a solid surface such as the floor or a wall, to the inlet, or between adjacent intakes. For the case of an outlet located a certain distance above the bed, a free-surface vortex will always be accompanied by a mirroring submerged vortex that extends and attaches to the bed (Suerich-Gulick et al., 2014a). Several submerged vortices commonly form in pump intakes where the intake pipe extends into the reservoir (see Chapter 7); they form also where the opening is not

mounted flush to the wall, as common in hydropower intakes. Unless the inlet extends upward from the bed of the reservoir, a submerged vortex tends to occur, connecting the intake to the bed unless a vortex breaking device is installed on the bed (Padmanabhan and Hecker, 1984).

2.4.3 | Effect of geometric configuration

The configuration of the approach flow results in different mechanisms of generating circulation or vorticity into the flow. A hydraulic structure can provide the source of vorticity due to an asymmetric approach flow, velocity gradients due to boundary friction, and flow separation behind an obstruction (Durgin and Hecker, 1978). Vortex generators in dropshaft applications provide a generally constant bulk circulation to maintain a stable vortex air core (Hager, 1985; Mulligan et al., 2016) where there is a strong correlation between the depth and discharge (see Chapter 5).

2.4.4 | Coriolis effect

The sense of rotation of large-scale rotations at the earth's surface is determined by the Coriolis acceleration (counterclockwise in the northern hemisphere and clockwise for the southern hemisphere for ocean and atmospheric circulation). Coriolis acceleration can be neglected for a Rossby number, $R_o = V/2\omega L$, much greater than 1, where V is velocity, ω is Earth's rotational velocity, and L is the scale of the motion. A typical intake has a Rossby number of 700 and, therefore, Coriolis acceleration can be neglected (Möller, 2013). The influence of the Coriolis effect on axially stretched vortices was examined by Shapiro (1962), Binnie (1964) and Trefethen et al. (1965) at different latitudes in the Northern (Shapiro, 1962; Binnie, 1964) and Southern hemispheres (Trefethen et al., 1965).

2.4.5 | Taylor-Couette analogy

As mentioned above, a complete description of the turbulent, three-dimensional flow field and its stability properties remains elusive. Recent physical and numerical observations made of the turbulent free-surface vortex revealed distinguishable, time-dependent "Taylor-like" vortices in the secondary flow field (Mulligan et al., 2018). These vortices were concluded to be like the secondary vortices of the well-known Taylor-Couette flow system. Consequently, a free-surface vortex can be treated analogously to the Taylor-Couette flow, thereby permitting a potential advancement of understanding of the general flow structure and the various states of free-surface vortex flow stability. For example, using Rayleigh's stability criterion, analysis showed that a wall-bounded, free-surface vortex can become unstable due to a centrifugal driving force in a similar manner to the Taylor-Couette flow. A schematic comparison of both systems in this analogue is outlined in Fig. 2.9.

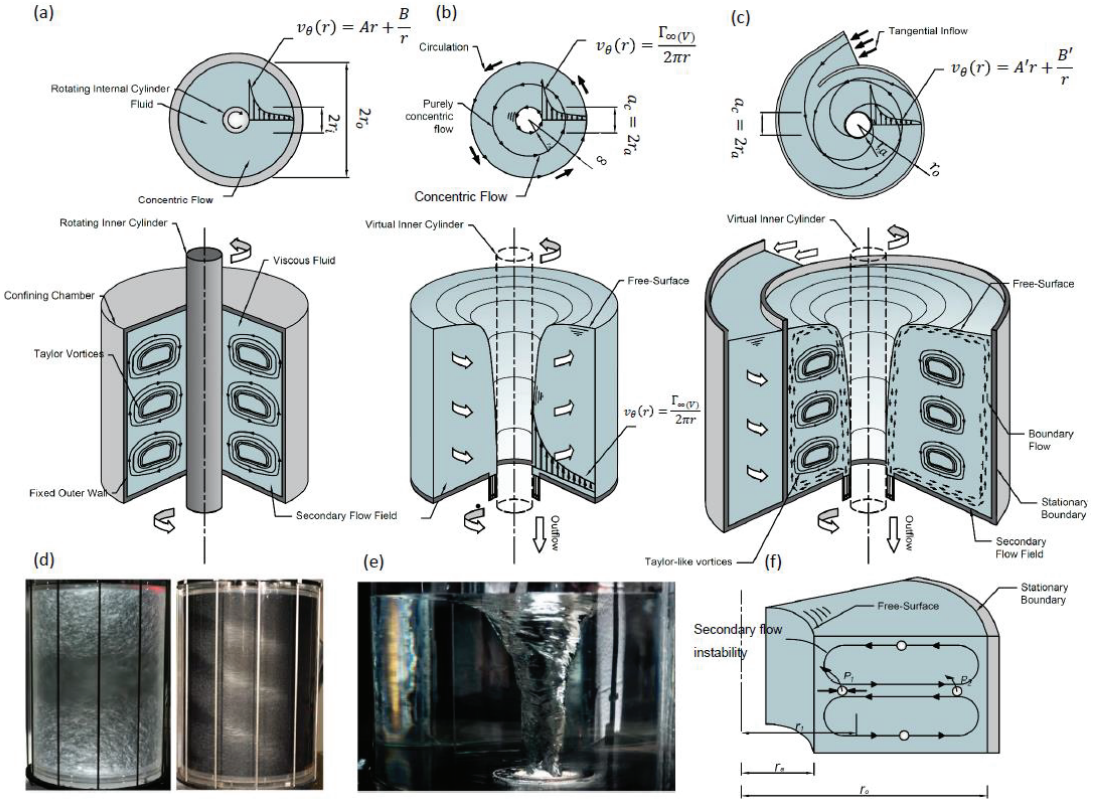

Figure 2.9 | The analogue between secondary flow: (a) Taylor-Couette flow (TCF) system; (b) a laminar free-surface vortex (FSV); (c) a turbulent vortex flow in a vortex chamber; (d) an enclosed Couette; (e) a free-surface Couette; and (f) flow in a vortex intake (Mulligan et al., 2018).

CHAPTER 3

Physical Hydraulic Modeling

ROBERT ETTEMA
Civil & Environmental Engineering, Colorado State University, Colorado, USA.
E-mail: *Robert.Ettema@colostate,.edu*

TROY C. LYONS
IIHR-Hydroscience and Engineering, The University of Iowa, Iowa City, Iowa, USA.
E-mail: *troy.lyons@uiowa.edu*

ROBERT M. BOES
Laboratory of Hydraulics, Hydrology and Glaciology (VAW), ETH Zurich, Switzerland,
E-mail: *boes@vaw.baug.ethz.ch*

3.1 | Introduction

Physical hydraulic models are commonly used for investigating flow fields of concern involving vortices and swirling flows in hydraulics. Water intakes, by involving these flow-field concerns, frequently require physical modeling, which entails replicating intakes at reduced scale.

The primary objective of physical modelling of an intake is to assess the design and modify the geometry as needed so that an intake flow field satisfies requirements ensuring that the intake performs as necessary. The requirements for acceptable flow conditions may be determined from laboratory-space or discharge constraints (notably, for dropshafts, pump intakes, and hydropower intakes), or size constraints specified by the manufacturers of pumps and turbines.

Reduced-scale modeling of flow may incur scale-effects (facets of flow inadequately simulated), as water typically is used to simulate water, and air to simulate air. Similitude criteria and engineering judgment may be required to set size limits for models, and to assess the impact of a scale effect and for a design or operation to the impact into account. This chapter presents the main similitude criteria associated with physical modeling of water intakes, indicates similitude limits, discusses several potential scale effects, and briefly mentions aspects of physical modeling in need of further research.

As of this writing, air entrainment poses a major challenge in physical modeling. The limits suggested for physical models involving vortices and swirling flows partly stem from this challenge. Another

scale-effect arises when simulating vorticity (rotation of a fluid moving in a vortex) because vorticity involves velocity and length, two variables that differ in scale, and contribute to shortcomings in Froude similitude. Consequently, models, by simulating flow velocity at a larger scale (length ratio of prototype/model) than the length scale, usually amplify vorticity relative to prototype conditions. The shortcoming is compounded by the limits associated with using water and air to model the behavior of prototype flows of water and air.

The ensuing coverage of modeling considerations uses Figs. 1.1 and 2.1 in the preceding chapters. Of prime importance are flow rate, conduit diameter and submergence, and air entrainment that may occur when water flows at high velocities or assumes vortical and spiraling motions.

Engineers at several hydraulics laboratories have published design recommendations based on their experiences in modeling intakes of various types (e.g., for pump intakes, Prosser, 1977; Tullis, 1979; Sweeney et al., 1982; Padmanabhan and Hecker, 1985; Gulliver et al., 1986; Ettema et al., 1998; and Möller et al., 2010). However, aspects of swirling flows and vortices, not to mention site peculiarities, often require a physical model to assist designers of intakes.

3.2 | General similitude considerations

The use of a physical hydraulic model to simulate a prototype flow requires that certain dimensionless parameters describing the geometric, kinematic, and dynamic properties of the model assume similar (or acceptable) values in the model and prototype. The basic similitude conditions for modeling flow processes involve a free surface; flow with an air-water interface, such as an open-channel flow. When flows also involve air entrainment, they become mixed — or multi-phase — flows of water and air. For mixed flows, four forces usually are considered:

- Inertial force (a contact force) associated with rate of change of flow momentum.
- Gravitational force (a body force) associated with the Earth's gravitational field.
- Fluid-viscosity force associated with shear forces (fluid resistance against shear) and internal fluid friction forces.
- Surface tension (a force per unit length across a water surface), associated with the molecular structure of water.

The relative magnitudes of these forces are expressed in the dimensionless Froude, Reynolds, and Weber numbers. The ensuing description, beginning with geometric similitude, defines these numbers and shows how kinematic and dynamic similitude stem from them. A key notion is that scales

are based on Froude similitude, but the values of Reynolds and Weber numbers are suitably large that their effects do not adversely affect the overall capacity of the model to simulate flow processes with acceptable fidelity.

3.2.1 | Geometric similitude

The model should be geometrically like the prototype. If L represents some characteristic length, then the length scale is

$$L_r = \frac{L_p}{L_m} \tag{3.1}$$

Here, suffix r denotes the scale for the quantity (length); and p and m refer respectively to prototype and model. Additionally, as vortex or swirling flows are markedly three-dimensional, models of intake flows should be undistorted geometrically (i.e., vortices should feature identical length scales in horizontal and vertical directions). For example, the application at the end of this chapter refers to a $L_r = 16$-scale model.

3.2.2 | Water flow similitude

The basic requirement for dynamic similarity of free-surface flow is satisfied if the prototype and the model have the same value of Froude number, Fr, which expresses a balance of inertial forces relative to gravitational forces:

$$\mathrm{Fr}_m = \mathrm{Fr}_p \tag{3.2}$$

Here,

$$\mathrm{Fr} = \frac{V}{\sqrt{gY}} \tag{3.3}$$

with $V =$ flow velocity, $Y =$ representative length scale (typically flow depth or hydraulic radius); and $g =$ acceleration due to gravity.

Eqs. (3.2) and (3.3) lead to respective, Froude-number scaling criteria for velocity and discharge:

$$V_r = L_r^{1/2} \tag{3.4}$$

and

$$Q_r = V_r L_r^2 = L_r^{5/2} \tag{3.5}$$

Here, $V_r =$ velocity scale, $Q_r =$ discharge scale, and $L_r^2 =$ area scale.

To be kept in mind is that vorticity has units of time^{-1} (i.e., velocity/distance), and so vorticity in a model must be interpreted accordingly. For Froude-number similitude,

$$T_r = L_r^{-1/2} \tag{3.6}$$

The Reynolds number, Re, of a flow expresses a balance of inertial forces relative to fluid-viscosity forces:

$$\mathrm{Re} = \left(\frac{VY}{\nu}\right) \tag{3.7}$$

where, ν = kinematic viscosity of water, a water property that is mildly sensitive to water temperature (e.g., a 27% decrease in ν when water temperature changes from 4°C to 16°C). Eq. (3.7) typically has flow depth or hydraulic diameter as representative length, Y.

A scale-reduced model usually does not maintain the prototype value of Re associated with a prototype flow. However, strict equality is not necessary if the value of Re in the model were above the critical value needed to ensure fully turbulent flow. From Eqs. (3.1) and (3.4), and assuming the use of water to model water at the same temperature,

$$\mathrm{Re}_m = \frac{\mathrm{Re}_p}{L_r^{3/2}} \tag{3.8}$$

If values of Re_m in the model were fully turbulent, exact replication of Re_p is unnecessary. Similarity of a flow's energy gradient in boundary roughness is affected by the resistance of the channel boundary. For fully turbulent flow, flow resistance is affected primarily by flow geometry and boundary roughness.

3.2.3 | Air-entrainment similitude

Air entrainment occurs naturally in high speed, free-surface flows (e.g., dropshafts, around objects piercing the free surface, spillways, and jets) and at submerged inlets (e.g., pump intakes, hydropower intakes, and partially open spillway gates). Consequently, air entrainment has several primary design implications for vortex intakes to dropshafts: entrained air may bulk water flows, so that they become air-water, two-phase flows; entrained air may blow-back, sometimes in a geyser-like manner; and entrained air may occupy substantial space in a conduit or an underground storage reservoir. For pump and hydropower intakes, entrained air may cause force imbalances on the pump or turbine impeller, substantially decreasing the efficiency of hydraulic machinery and potentially causing premature failure.

Surface tension of water is an important aspect of air entrainment, and its significance is expressed using the Weber number, We, a ratio of inertia forces to surface tension force:

$$\mathrm{We} = \left(\frac{\rho V^2 L}{\sigma} \right) \tag{3.9}$$

Here, σ = surface tension of water, a water property that is mildly sensitive to water temperature (e.g., a 2% decrease when water temperature increases from 4°C to 16°C); ρ = water density, a water property that is only slightly sensitive to water temperature (e.g., a 0.10% decrease when water temperature changes from 4°C to 16°C); and L = representative length (usually flow depth, intake diameter, or air-bubble diameter).

Because of practical limitations of simultaneous Reynolds, Froude, and Weber numbers similarity between prototype and model, air entrainment is impossible to model accurately (unless replacing the fluid). Therefore, the Reynolds and Weber numbers usually are relaxed in the design of physical models involving air entrainment. To address the effect of incomplete similitude, modelers choose the model scale with discernment (ensuring that air entrainment is acceptably simulated), then interpret and scale up the results with due caution. An important point to mention is that air bubbles formed from free-surface breakup depend on fluid properties not on model scale. Consequently, forces associated with fluid properties may be of comparable size in model and prototype, and not reduced with scaling ratio.

Insights regarding air entrainment observed at various physical models of other hydraulic structures (especially spillways) are useful for vortex entrainment of air. Modeling experience generally indicates that scale effects attributable to inadequate air entrainment are small when the value of Re exceeds about 1.5×10^5, and We exceeds about 2×10^4 (e.g., Pfister and Chanson, 2014); here, Re uses flow depth as representative length in Eq. (3.7). Pfister and Hager (2010a, b) identified a gross underestimate (by up to one magnitude in terms of local bottom air concentration downstream of a chute aerator) when $\mathrm{We} < 1.9 \times 10^4$. They proposed $\mathrm{Re} = 2.2 \times 10^5$ as a limiting value for void fraction modelling; representative length based on flow depth (i.e., Re exceeds about 3.5×10^6, with representative length being ramp distance or air-slot length. Hohermuth et al. (2021), for a spillway outlet of a dam, compared air concentration and velocity data obtained from a large-scale laboratory model with data from a prototype tunnel spillway. In the model, Re was between 6.6×10^5 and 3.2×10^6 (with L = hydraulic diameter and V = cross-sectional average clear-water velocity), and We was between 6×10^3 and 8.4×10^4 (with V being mean clear-water velocity from flow continuity, and L = half of equivalent hydraulic radius of clear-water flow according to Dai et al. (1998) for the scaling of droplet size); in the prototype the ranges were $7.8 \times 10^6 \leq \mathrm{Re} \leq 2.4 \times 10^7$, and $3.7 \times 10^5 \leq \mathrm{We} \leq 1.8 \times 10^6$.

The geometric scale of the model, based on gate width, was 1:5. The data agreed acceptably well for the purpose of the physical model. The quantities of immediate engineering interest (bottom and depth-averaged air concentration, flow depth of mixed air-water flows, velocities, and flow resistance) were comparable and, therefore, showed no scale effects. However, laboratory model data did indicate scale effects regarding air-water-flow properties, such as droplet sizes, despite the large-scale model.

To be kept in mind, however, are regions of flow separation and inadvertent formation of vortices, and that swirling flow may form air-entraining vortices. The turbulence generated by vortex structures, and local contractions of flow, induce air entrainment at greater rates than suggested by the references mentioned in the preceding paragraph. The studies of aerators on a spillway (Pinto et al., 1982a; Pinto et al., 1982b), for example, suggest model values of length scale should be less than 12 or 15, to accurately reproduce the values measured in the prototype. Based on protype chute aerator measurements, Gardarsson et al. (2015) observed an air demand ratio of 16.5 on average (for two discharges tested) for a model scale of 45. A potential scale effect is that the prototype flow likely will experience more air entrainment than observed for the model. Besides spillway flow, this process is also true in vortex intakes for dropshafts. A study by Lyons (2021), and analysis of his data and those of Jain and Kennedy (1983), suggest air entrainment rates for vortex dropshafts to be about four times higher at prototype scale than in a 10-scale model; and up to seven times higher when measured in a 20-scale model (length scale = prototype/model). Hohermuth et al. (2020) suggest an aeration demand 2.2 times higher in prototype low level outlets compared to length scales of 5.5 to 9 based on gate-width ratios. This scale effect can be addressed by keeping the dimensions of the intake (and downstream appurtenances, including air vents and sidewalls) sufficiently large to accommodate more bulking of flow (air entrainment) than observed at model scale. More research though is needed regarding the complex flow fields at intakes.

Further discussion of model-scale effects on air-water flows can be found in Kobus (1984), ASCE (2000), and Heller (2011). Typically, the length scale of a model should not exceed about 10, though we hesitate to state a scale limit, given intake size and the requirement that judgment of the modeler is always needed.

3.3 | Additional similitude criteria for dropshafts

Additional criteria for vortex intakes to dropshafts (mainly used for drainage of water) relate primarily to the approach flow conditions necessary for acceptable performance of vortex-intake dropshafts used for draining water. Generally, these criteria were developed to ensure flow uniformity

and stability upstream and inside of the vortex intake and dropshaft. Some intake types are suited for subcritical flow while others perform acceptably with subcritical and supercritical flows. Approach channel length, width, and other geometric features necessary to create acceptable flows in several types of vortex inlets have been developed experimentally (Drioli, 1969; Hager, 1985, 1990 and 2010; Jain and Kennedy, 1983; Yu and Lee, 2009). Chapter 5 presents and discusses design criteria for vortex intakes to dropshafts.

3.4 | Additional similitude criteria for hydropower intakes

Additional criteria for hydropower intakes relate to flow conditions deemed acceptable for the performance of low-head and run-of-river hydropower plants. For such plants, the turbine is typically a bulb or pit, impulse turbine located close to the entrance of the flow intake. Therefore, flow distribution at the intake entrance essentially is the flow distribution encountered by the turbine's propellor. The criteria (e.g., Fischer and Frankee, 1988; Gulliver and Arndt, 1991; Godde, 1994; Voith, 1996) include the following guidelines for flow distribution at the trashrack or stoplog cross-sections of flow entry into an intake:

- The flow should not have air-entraining vortices (VT5 and VT6 in accordance with the vortex classification by Hecker, 1984).
- The velocity distribution should fall within limits prescribed by the turbine manufacturer.
- All crossflow components of velocity should be less than 5% of the average axial component of velocity at the trashrack cross-section of an intake.
- Deviations of average axial velocity for the four quadrants of an intake cross-section should not vary more than 10% from the average axial velocity.

Frequent factors causing vortex formation, both for run-of-river hydropower intakes and storage hydropower reservoir intakes, are inadequate submergence, S, of an intake and intake Froude number $\mathrm{Fr}_D = V/\sqrt{(gD)}$; here, $D =$ diameter of intake entrance. Submergence usually is related to intake diameter, as S/D (see Chapter 6). As a rule of thumb for horizontal intakes (Gulliver et al., 1986), when $S/D < 0.7$ and $\mathrm{Fr}_D = V/\sqrt{(gD)} > 0.5$, vortex problems are likely and, therefore, a physical model is needed.

Use of a physical model enables evaluation of whether an intake design meets the criteria mentioned above, or the design should be modified. Deviation from these criteria mean reduced efficiency and

possible vibration of a turbine. Further similitude criteria exist for turbines as hydropower machines (e.g., Gulliver and Arndt, 1991). More details on critical submergence at hydropower intakes are given in Chapter 6.

3.5 | Additional similitude criteria for pump intakes

Pump intakes are common subjects of hydraulic models, as pump-intake geometry readily causes pump intakes to form vortices and swirling flows. Also, low submergence of a pump intake may produce vortices. The additional criteria concern vortex formation and flow conditions to facilitate pump performance.

For correct reproduction of free-surface vortices, Daggett and Keulegan (1974), and Anwar et al. (1978) recommend the following Reynolds-number criterion for physical hydraulic models:

$$\mathrm{Re} = \frac{Q}{\upsilon D} \geq 1.5 \times 10^4 \tag{3.10}$$

in which Q = design pump discharge, and D = pump-bell diameter. The limits of Re and Fr_D for accurate model similitude are explored numerically later in this chapter.

Several additional similitude parameters (based on the theory presented in Chapter 2) have been identified for various types of intake flow. For example, the following set of additional dimensionless parameters are usually considered for pump intakes designed for vertical pumps:

- Submergence Froude number, essentially is a form of Froude number written in terms of pump-bell submergence S, which is a fraction of approach-flow depth, Y, and V_D = flow velocity at a pump's bell entrance,

$$\mathrm{Fr}_S = \frac{V_D}{\sqrt{gS}}$$

  with velocity at the base of the pump's suction bell assessed as

$$V_D = \frac{4Q}{(\pi D^2)}$$

- Radial Reynolds number, with Q = pump discharge and R = pump-bell radius,

$$\mathrm{Re}_R = \frac{Q}{\upsilon D}$$

- Weber number, with V = local flow velocity,

$$\mathrm{We} = \frac{\rho V^2 D}{\sigma}$$

- Relative submergence, S/D

An important dependent parameter for pump intakes is circulation number, $N_r = \Gamma D/Q$, in which Γ = flow circulation (m^2/s). Experiments by various investigators, including Anwar et al. (1978), show that surface-tension effects are negligible when $\mathrm{We} \geq 10^4$. The requirements for Re_R are those for Re_D, differing by a factor of 2. For the typical diameter range of prototype vertical pumps, the critical values of Re_D and We are comfortably exceeded, so the dependency of vortices on these parameters is relevant mainly in hydraulic models.

The length scale (prototype/model) for a pump-intake model is often recommended not to exceed about 10, with greater scale reduction being acceptable for very large pumps. In most cases, to provide additional proof of satisfactory flow conditions, it is necessary near the completion of modeling to run a special test condition whereby the model is operated at 1.5 times the Froude-scaled discharge, as obtained from Eq. (3.5). This test condition increases Re_D and pushes the model to reveal the formation of vortices not illuminated by flow at the lesser value of Re_D (Ettema et al., 1994).

In terms of flow distribution, the following considerations typically are included in guidelines for flow to and within pump intakes:

- No detectable vortices extending into the pump column.
- No surface attached vortices stronger than type 2 (Hecker, 1984).
- No measured velocities that vary more than 10% from the average of all the velocities measured on the same circle in the pump-column throat (just downstream from the pump bell).
- Vortimeter-tip-velocity angles (swirl angles) no greater than 5°. This angle equals arctangent of vortimeter-tip velocity/average axial velocity of flow in the pump column.

3.6 | Instrumentation

Extensive advances since Knauss (1987) have been made regarding instrumentation used to measure variables in physical models. Muste et al. (2020) describe many of the advances and indicate usual precisions associated with diverse instruments. Kramer et al. (2020) provide a summary of studies reporting accuracies for phase detection probes. Hohermuth et al. (2021) may be an interesting reference for velocity accuracy. This chapter offers only a short summary and indicates the precisions typically attainable.

3.6.1 | Elevations

The elevations of all key elevations of a model can be determined and periodically checked using the following instruments:

- A LiDAR, whose measurement resolution varies with range, but is typically about 3 mm at about 150 m.
- A Survey Total Station, whose measurement resolution varies with range, but is typically about 2 mm for distances at about 500 m.

Both instruments commonly are used to check a model's elevations when a model is being assembled and at several times after a model had been operated. To be sure, point-gauges, and scales also are frequently used to check elevations.

3.6.2 | Flow discharges

Discharges through a model commonly are measured using an electromagnetic flow meter installed in the pipeline supplying water to the head tank of a model. These flowmeters are factory-calibrated and give a data record of discharge to a model. Maximum measurement error for discharge is about $\pm$0.5% of the reading (measured quantity). The repeatability of the flowmeter is about $\pm$0.1% of the set reading. The influence on discharge of the ambient temperature of water is $\pm$0.005%/°C.

3.6.3 | Flow velocities

Of principle concern is that the flow approaching an intake (or outlet such as a spillway crest) is suitably distributed such that the flow is discharged uniformly over the crest's segments separated by the two piers, thereby making optimal use of the crest. To help ensure this distribution is attained, and augmenting visualization methods, flow velocity may be measured using the following techniques:

Point velocities of approach flow can be measured at verticals along transects within the approach flow, using the following instruments.

- Usually, an Acoustic-Doppler can be used for this purpose and yields a record of velocity at about 10 Hz. ADV's can be used to obtain high-frequency (for water flow) data for velocities up to 4.5 m/s with resolution of $\pm$1% of measured velocity. However, to be kept in mind is that the ADV concept does not work reliably well in aerated flows.
- For enclosed flow, such as within a pump column or hydropower penstock, flow velocities can be obtained using a Pitot-static tube, whose precision depends on reading differences in water level

between the total-head and the static port (Munson et al., 2013). For water levels less than about 10 mm of water, additional instrumentation is needed for estimating pressure difference. These probes do not yield high-frequency data of velocities.

- Sometimes (close examination of flow behavior), flow velocities are measured using laser-based instruments, such as Particle Image Velocimetry (PIV), Particle Tracking Velocimetry (PTV), or Laser-Doppler Anemometry (LDA).

The distribution of water-surface velocities of flow to the intake may be measured using Large-Scale Particle Image Velocimetry (LSPIV). This technique enables definition of the streamlines around in the water-surface flow field. LSPIV precision depends closely on video-camera quality, image rectification and software. Precision estimates of about $\pm 3.5\%$ of actual velocity magnitude is obtained for many hydraulic models.

3.6.4 | Water-surface levels

Water-surface levels can be measured using a point-gauge, an ultrasonic sensor, or a pressure gauge. Typically, a point-gauge is used when the water surface does not vary considerably in elevation at the measurement location (e.g., flow over the crest of the spillway). The measurement precision of a standard point-gauge is about ± 0.1 mm, but the placement of the point gauge tip on the surface may retain a subjective aspect and, therefore, be less precise (if the surface is not 100% still).

Ultrasonic or acoustic sensors are used when the water-surface is flat, so that the sensor's conical beam (8° cone angle is common) emitted by the instrument intersects a water surface that is flat (on average); turbulence at locations caused some temporal fluctuations of water surface at certain locations. Such sensors have a measurement precision of $\pm 0.1\%$ of the set reading. A common frequency of sensor sampling frequency is 10 Hz. Acoustic sensors can be used to measure water levels in the piezometers fitted along a model. The effect of temperature and humidity might need to be considered as they affect acoustic wave speed.

3.6.5 | Flow pressures

Ambient, or low-amplitude, pressures at selected locations can be measured using a variety of pressure sensors. The selected pressure-range of probe and sampling frequency depends on expected pressures and pressure-fluctuation rates.

Dynamic pressures at selected locations can be measured using pressure sensors, set to measure pressures in estimated ranges (model scale) with an accuracy of $\pm 1.0\%$ of the pressure reading.

Common sampling rates can be up to about 5 kHz and are aided by appropriate data-acquisition systems. For vortex-flow intakes, of possible interest may be pressures at the base of a dropshaft where the downward spiraling flow hits the more-or-less horizontal base of a de-aeration chamber. If the flows are aerated, air-water phase-detection probes must be used to measure the equivalent clear water flow depth.

3.6.6 | Air concentration

Two types of air-concentration (phase-detection) probe are used for measuring air concentration in flows:

- Fiber optic probes.
- Conductivity probes.

Fiber-optic probes use the different refractivity of a laser in air and water, whereas the conductivity probes use the different electrical resistivity of air and water. A study of the efficacy of each type of probe showed that the two types were of comparable accuracy, though each type had some advantages (Felder and Pfister, 2017; Felder et al., 2019). The study involves sampling rates of 500 kHz. For example, the conductivity probe could be slightly more reliable for flows whose velocity exceeds about 10 m/s, though the fiber-optic probe may perform slightly better for flow velocities below that rate. Other criteria for probe selection are bubble diameter, chord lengths, and particle count rate that are targeted to be sampled. In regions close to the invert, where bubbles are rare and small, Felder et al. (2019) observed a slight underestimation in void fraction for the conductivity probe (compared to fiber optic probes); a key finding was that the probe tips should be placed side-by-side instead of inline. Fiber-optic probes tend to have smaller probe tips, thus allowing for smaller droplets to be detected. However, these probes are quite fragile, so that they are not suitable for large-scale or prototype investigations.

A useful variable from both probes was measurement of the velocity of aerated flows. The velocity probes mentioned in Section 3.6.3 may not function reliably for such flows. Hohermuth et al. (2021) explains the accuracy of velocity measurements in air-water flows, including downwards directed flows that may be found in vortex intakes.

3.7 | Application

Physical modeling increasingly is done in concert with numerical modeling (next chapter), as each approach has its strengths and limitations. The combination of approaches, also termed composite

or hybrid modelling, potentially enables overcoming some of the limitations yet using the strengths of both approaches.

A 16 length-scale (prototype/model), Froude-similitude physical model played a significant role in developing the design of a vortex intake and dropshaft for the Lower Middle River Des Peres, Combined Sewer Overflow, Storage Tunnel Project (Lyons, 2019). The intake and dropshaft are in metropolitan St. Louis, Missouri.

The physical model included a complex, approach channel featuring an abrupt change in channel elevation and alignment, horizontal trash racks, flow control gates, channel narrowing, and an overflow bypass pipe. The geometry of the vortex intake was designed in accordance with guidelines in Jain and Kennedy (1983). The dropshaft is a terminal shaft (i.e., located at the upstream end of the tunnel) and incorporates an in-line deaeration chamber and vent shaft to manage entrained air. The vortex-flow intake and 6.1-meter-diameter dropshaft were tested for water flow rates up to 213 m^3/s, and the intake discharged into a 10.4-meter-diameter by 117.0-meter-long deaeration chamber, making this shaft potentially the largest vortex shaft presently in existence. Fig. 3.1 shows the 16-scale, physical model in operation.

Figure 3.1 | View of the 16-length-scale physical model of the vortex intake and dropshaft and deaeration chamber used to aid design of the vortex intake and dropshaft for the Lower Middle River Des Peres, Combined Sewer Overflow, Storage Tunnel Project. This view shows the model in operation. (Scale = prototype/model).

Three-dimensional-flow, numerical modeling (CFD) was initially used to develop the overall design features, and physical modeling was used to refine the design and evaluate air-entrainment and deaeration-venting requirements. The physical model revealed undesirable flow features in the approach channel for certain operational conditions that had not been detected using a numerical model. Also, the physical model demonstrated that the deaeration-chamber diameter should be enlarged from 9.15 m to 10.37 m to achieve acceptable deaeration performance. Additionally, the physical model showed the deaeration-chamber vent was more effective when moved further downstream than initial design suggested. Ultimately, the physical model led designers to consider venting air at an existing access shaft further downstream. An orifice configuration was developed for the revised venting location to optimize deaeration and enable the chamber to pass the design flow rate of water. This change of shaft use eliminated the need for a dedicated vent shaft, thereby reducing construction cost.

Chapter 4 elaborates the use of numerical models to simulate flows into vortex intakes. The development and use of numerical models of flow in vortex intakes and dropshafts is an active topic of research at this moment. The topic of air entrainment requires more research, as does the general topic of the complex flow field associated with vortex formation at intakes.

CHAPTER 4

Numerical Modeling of Vortices and Swirling Flows

SEAN MULLIGAN
VorTech Water Solutions Ltd. Galway, Ireland. E-mail: *sean.mulligan@vortechws.com*

SUSAN J. GASKIN
Civil Engineering, McGill University, Canada. E-mail: *susan.gaskin@mcgill.ca*

4.1 | Introduction

Vortices and swirling flows at intakes are among the most complex flow structures in hydraulic structures engineering. Intakes tend to have irregular three-dimensional geometries that have a strong influence on the flow, which in turn often include strong free-surface deformations, adverse velocity gradients, unsteadiness, and anisotropic turbulence. In some cases, these flows can also include both stratified or annular (vortex dropshafts) and bubbly flows (downstream of an air entraining vortex at a pump intake). Given this three-dimensional complexity, one-dimensional, and two-dimensional modelling approaches had been unsuccessful in accurately reproducing swirling flow characteristics in practical applications in the past.

Three-dimensional numerical flow models, or computational fluid dynamics (CFD), present a promising alternative that has evolved significantly over the past twenty years. The affordability and accessibility of CFD for simulating turbulent, multiphase flow features have been enhanced by the dramatic growth in computational power and the development of several commercial and open-source CFD codes such as Flow3D, Fluent, CFX, Star CCM+, OpenFoam etc. These codes are now well equipped to tackle both single and multiphase turbulent three-dimensional flows and there has been widespread use of CFD in vortex intake research since the early 2000s. This chapter summarizes advances in the numerical modeling of flow in vortex intakes through a selection of key studies of free-surface swirling flows and approaches to meshing, unsteadiness, and turbulence. This chapter also highlights areas that require further development and that inevitably will occur as numerical models and computing capabilities evolve.

4.2 | Modelling studies

4.2.1 | Early approaches

The earliest work recorded on numerical approaches to solving free-surface vortex flow fields was presented by Binnie and Davidson (1949) who applied a finite-difference approximation to the free-surface problem. Later, finite element method (FEM) modelling of vortex circulation was employed by Brocard et al. (1983) using the two-dimensional depth integrated conservation of mass and momentum equations. Brocard et al. (1983) formulated the conservation equations for turbulent flow by replacing the Reynolds stresses using the turbulent eddy viscosity approach. However, Brocard et al. (1983) applied the results to an idealised case of vortex flow, which did not agree well with experimental data. Building on this work, Trivellato and Ferrari (1997) later adopted a finite-difference method formulated from the hydrostatic shallow water equations which were solved using the Euler-Lagrange approach. The results captured the tangential motion and the radial flows which form near the floor of the structure near the intake. However, the shallow water approximation used failed to capture the fully three-dimensional nature of the flow at actual intakes and the finite-difference model cannot be applied to complicated fluid domains. Trivellato et al. (1999) addressed these limitations in later work using the finite-volume method (FVM) to analyse a free-surface vortex over a vertical intake. The model captured the radial jet or radial band near the vessel floor well, as it did the larger flow circulation, when compared to the time-averaged experimental results of Daggett and Keulegen (1974) (see, for example, Fig. 4.1).

The past twenty years have seen an increase in advanced simulation benchmark studies as commercial CFD codes capable of solving more complex three-dimensional turbulent flow conditions became more readily available in the 2000s (Tokyay and Constantinescu, 2005; Okamura et al., 2007; Suerich-Gulick et al., 2006). These studies enabled researchers to identify key challenges of simulating free-surface vortex flows, including mesh configuration and time step dependencies, multiphase modelling, velocity, unsteadiness, and turbulence modelling. The following sections describe several key studies and begins with a geometrically simple configuration of the intake being on the floor of a reservoir containing water.

4.2.2 | Free-surface modelling

One of the characteristic features of vortex flows is the transient, hyperbolic deformation of the free surface near the location of the intake, when the intake is directly beneath the water surface. Researchers in the past have approached this problem using (a) single phase, or (b) multiphase approaches with a computational mesh, or (c) smoothed particle hydrodynamics, a Lagrangian

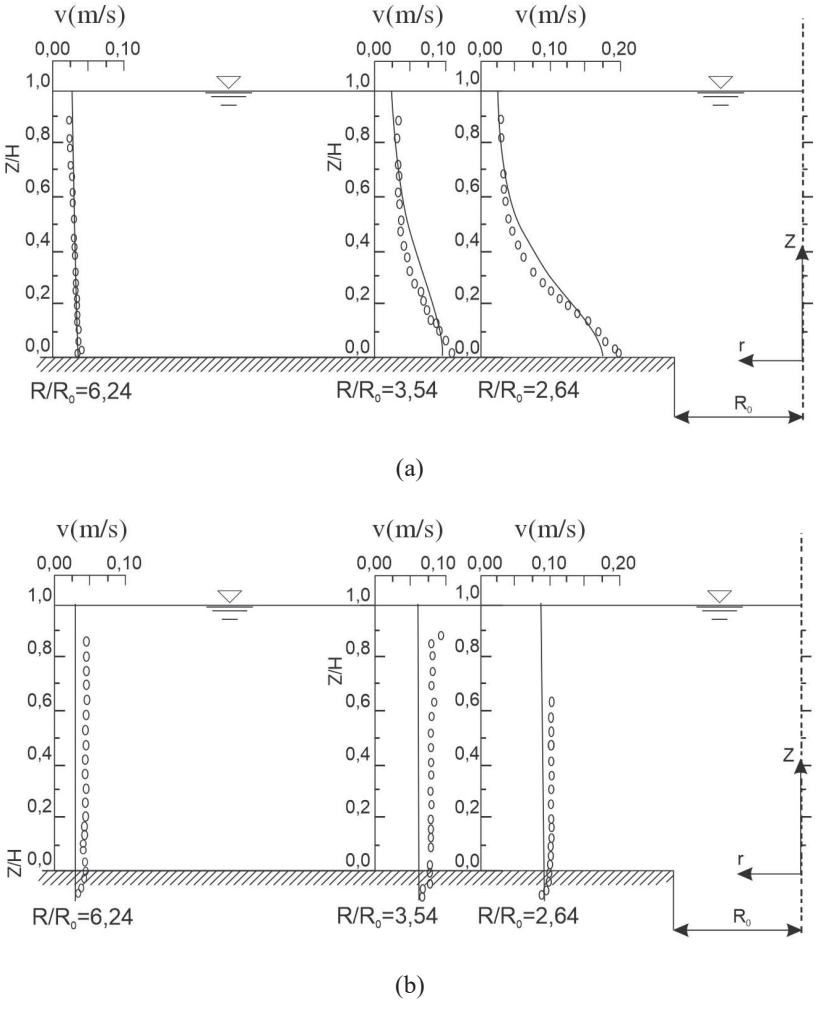

Figure 4.1 | An example showing a comparison between the numerical (line) and experimental (dots) data (Trivellato et al., 1999): (a) vertical distribution of radial velocity near a vortex intake; and (b) vertical distribution of tangential velocity profile near a vertical vortex intake.

approach. Several single-phase investigations (Rajendran et al., 1999; Ansar et al., 2002; Li et al. 2004) have been performed by modelling the free surface as a fixed, free-slip (frictionless) surface to approximate the air-water interface. This single-phase approach is often referred to as a "fixed lid boundary condition", which was employed by Constantinescu and Patel (1997), Rajendran et al. (1999), Li et al. (2004), Tokyay and Constantinescu (2005), Okamura (2007), Li et al. (2004), Li et al. (2008) and Škerlavaj et al. (2014). Modelers generally conclude that bypassing the need to model the interface

through the fixed lid condition allows reasonable qualitative flow information to be obtained at a low computational expense. However, the validity of the quantitative results is limited, particularly in strong vortex flows where there is a steep depression and high curvature of the free-surface in the vortex core region.

In multiphase approaches, Eulerian-Eulerian or volume-of-fluid (VOF) (Hirt, 1992) methods are extensively used to capture interface processes deforming free-surface flows (Suerich-Gulick, 2013; Cristofano et al., 2014; Mulligan, 2015; Chan et al., 2018; Chan et al., 2022). In their study using VOF, Suerich-Gulick (2013) found that CFD solutions could approximately predict the range of vortex characteristics, although the core radius was over-estimated, and the free surface depression was underestimated. Fig. 4.2 illustrates two cases simulated by Suerich-Gulick (2013).

Cristofano et al. (2014) studied a central vertical vortex intake using the VOF method with the commercial CFD software Fluent and found good agreement with the shape and position of the vortex over time, as Fig. 4.3 indicates.

Additionally, Mulligan (2015) and Mulligan et al. (2018) studied a vortex flow having a strong circulation. They used the coupled Eulerian-Eulerian approach to capture time-averaged water levels and the transient evolution of the vortex structure. Fig. 4.4 shows the comparison. Again, good predictions in the free-surface shape and position were obtained when compared to available experimental data, but the approach flow depth was significantly underestimated. Chan et al. (2022) also investigated a scroll vortex chamber using the VOF approach and found good agreement between the experimental and numerical free-surface profiles. Plant and Crawford (2016), Carty et al. (2019), and

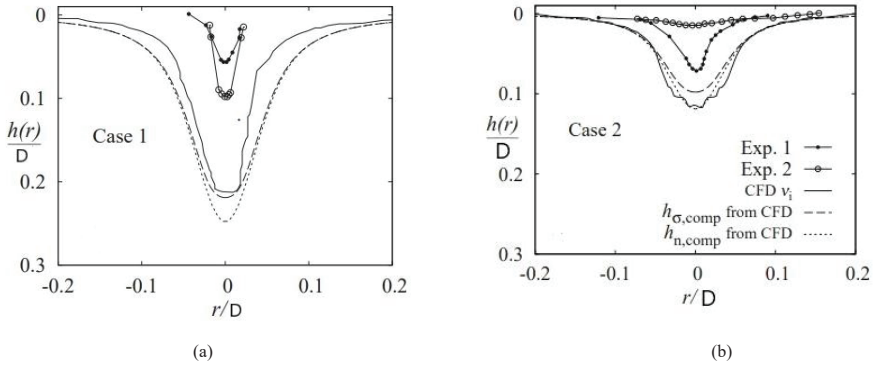

Figure 4.2 | Experimental and numerical free-surface profiles for vortex formation at a hydropower intake (Suerich-Gulick 2013): (a) case 1 is for marked deformation of the water surface; and (b) case 2 is for mild deformation of the water surface.

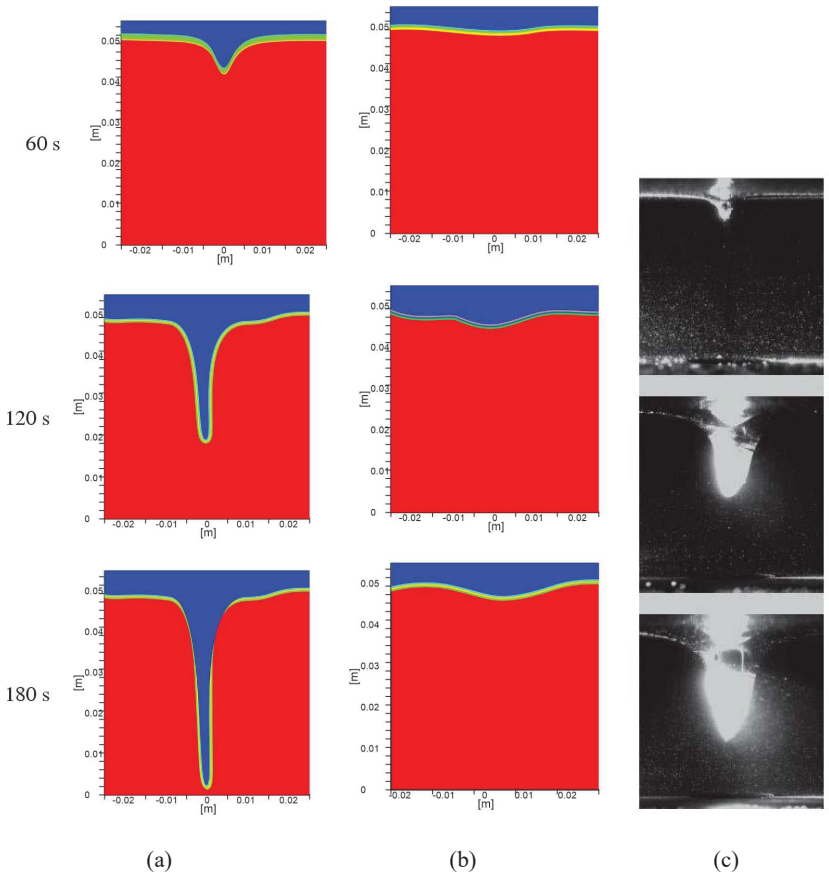

Figure 4.3 | Numerical and physical free-surface profiles for transient evolution of a vortex over a vertical intake for different turbulence models (Cristofano et al., 2014): (a) laminar flow; (b) Scale Adaptive Simulation based on Shear Stress Transport turbulent model (SAS-SST); and (c) physical experiment.

Chan et al. (2018) reported on the use of ANSYS CFX to analyse tangential vortex intakes with the Eulerian-Eulerian approach and found good agreement with experimental data. Chapter 5 describes the three predominant types of vortex intake i.e., (scroll, tangential, spiral).

The only applications of smoothed particle hydrodynamics (SPH) to vortex intake studies were performed by Bart et al. (2020) and Azarpira et al. (2021). The free-surface shape and position from the SPH free-surface simulations of Bart et al. (2020) compared well with the experimental and simulation data by Mulligan (2015) as shown in Fig. 4.5. Azarpira et al. (2021) found good agreement of the free surface and velocity profiles obtained in their physical model and numerical simulations of a draining rotating reservoir with an axisymmetric vortex flow, as Fig. 4.6 indicates.

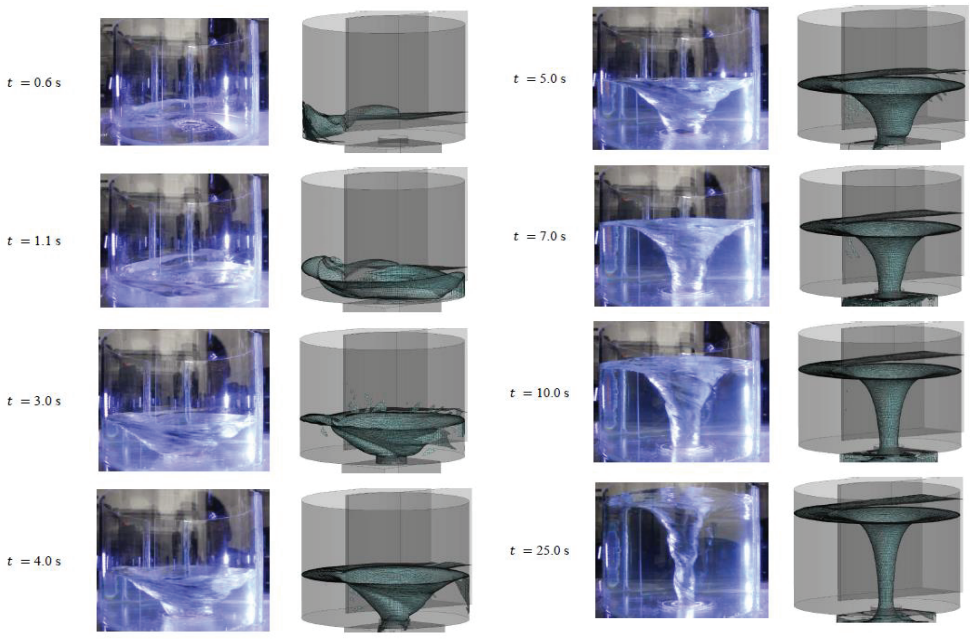

Figure 4.4 | A sequence of numerical and physical free-surface profiles for transient evolution of a vortex in a scroll vortex intake (Mulligan, 2015). The times are indicated (t = 0.6 s to 25.0 s). The physical images are evident with purple dye, and the numerical profiles are visible in blue-green shading.

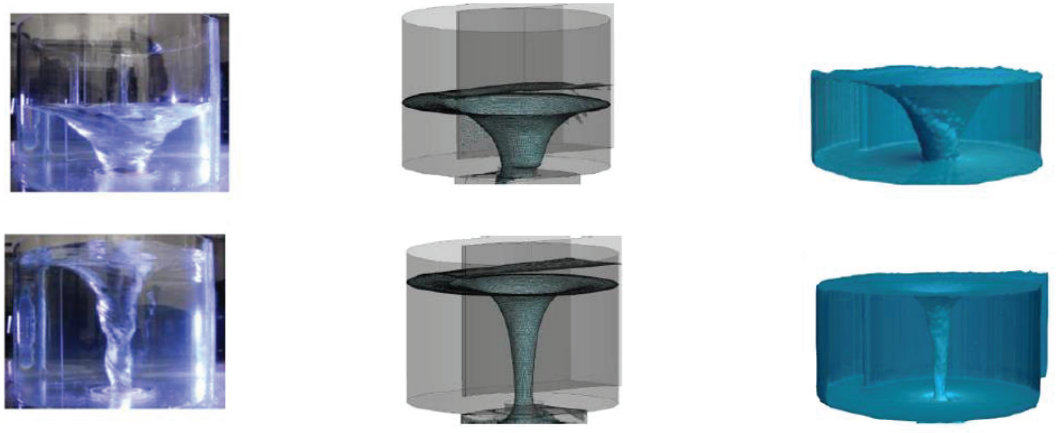

Figure 4.5 | Free-surface comparisons for a subcritical scroll vortex intake using Eulerian-Eulerian and smoothed particle hydrodynamics modelling (Bart et al., 2020): (a) physical model; (b) numerical, VOF, approach; and (c) numerical, SPM, approach.

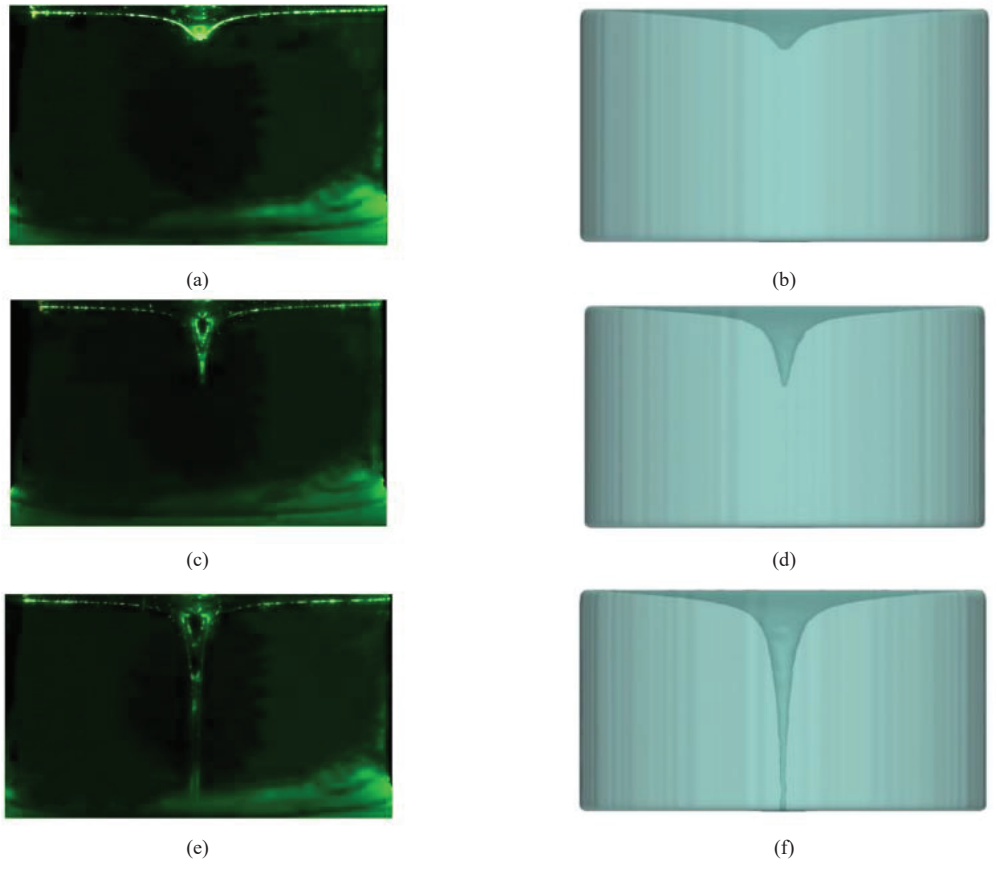

Figure 4.6 | Free-surface vortex formation over a vertical intake; comparison between a physical model (a, c, e) and a numerical model that used smoothed particle hydrodynamics (SPH) simulation output (b, d, f) (Azarpira et al., 2021): (a) $t/t_o = 2.2$; (b) $t/t_o = 2.28$; (c) $t/t_o = 2.38$; (d) $t/t_o = 2.45$; (e) $t/t_o = 2.62$; and (f) $t/t_o = 2.78$.

4.3 | Mesh configuration

Various mesh configurations and strategies have been employed for numerical models requiring a computational mesh. Suerich-Gulick et al. (2006) used the structured hexahedral mesh shown in Fig. 4.7. Simulations were initiated with a coarse mesh and then the solution was interpolated onto a finer mesh as the simulation progressed. Cristofano et al. (2014) used a semi-structured hexahedral grid for their simulation of axisymmetric flow around a centrally located intake, as shown in Fig. 4.8. In both cases, the authors concluded that grid sensitivity had been addressed, to the extent that the effect of errors due to turbulence modelling (see Section 4.5) likely exceeded any benefits that might be achieved from further mesh refinement.

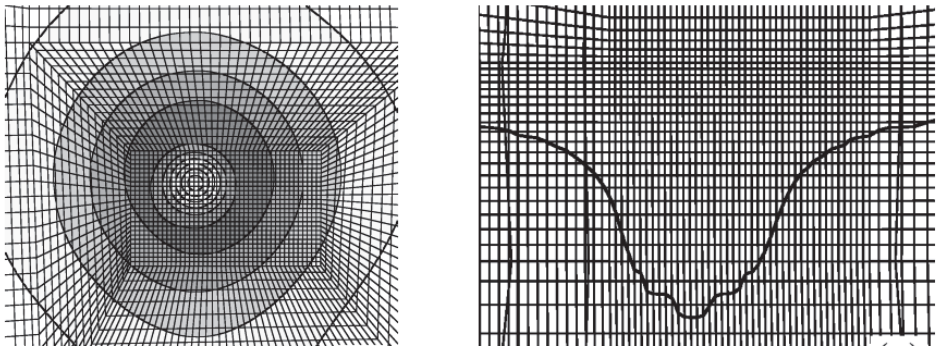

Figure 4.7 | Mesh structure through the vortex in the study by Suerich-Gulick et al. (2006): (a) plan view; and (b) side view.

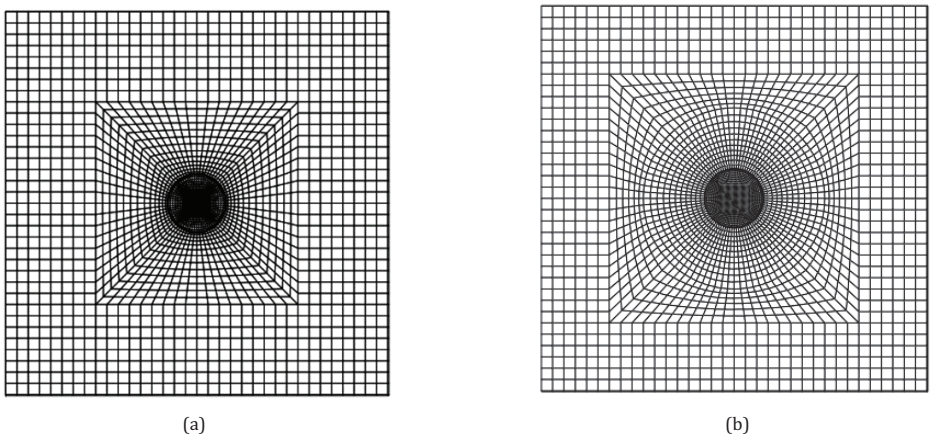

Figure 4.8 | Plan views of mesh structure through the vortex in the study by Cristofano et al. (2014): (a) and (b) involve differently structured mesh grids.

Other studies have used a mixture of structured and unstructured meshing approaches, as the latter approaches are easier to generate. Mulligan (2015) compared results from structured and unstructured meshes (for a fixed turbulence model in a scroll vortex generator) and found that a significant amount of numerical diffusion was produced with the unstructured mesh, exceeding the magnitude of physical diffusion that would normally occur in the flow. He concluded that this excess numerical diffusion limited the generation of a radial gradient in the tangential velocity in the chamber, thus limiting the magnitude of the steady state circulation that was produced. Therefore, he recommended avoiding unstructured meshes when modelling vortex intake flows. Furthermore, a structured mesh

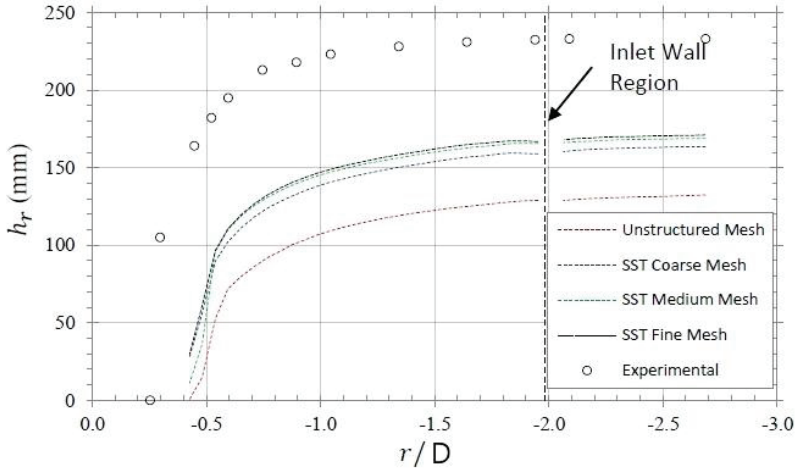

Figure 4.9 | Comparison between physical and numerical data. The comparison illustrates the sensitivity of the solution to the mesh type and density. (Mulligan, 2015)

strategy should be developed on a case-by-case basis, depending on the specific flow features that are to be expected (i.e., vortex location, position of the free surface, etc.). His findings are illustrated in Fig. 4.9 (Mulligan, 2015).

4.4 | Unsteadiness and turbulence modelling

As discussed briefly in previous sections of this chapter, several studies (Tokyay and Constantinescu, 2005; Stephens and Mohanarangam, 2010; Chen et al., 2012; Suerich-Gulick, 2013; Mulligan, 2015) have found that accurate modelling of vortex flows depends highly on the approach to turbulence modelling. Strong streamline curvature (Shur et al., 2000) in vortex dominated flow results in highly anisotropic turbulent conditions (Scorer, 1967; Dyakowski and Williams, 1993). Neglecting these conditions can have a detrimental effect on the accuracy of the results.

Early CFD research on vortices at pump-intake structures (Constantinescu and Patel, 1997; Rajendran et al., 1999) using standard eddy viscosity models (e.g., k-ε or k-ω) yielded significant discrepancies between numerical and physical data. The authors of those studies concluded that anisotropic turbulence and unsteadiness must be accounted for to improve accuracy. Studies with slightly more sophisticated eddy viscosity models (e.g., Menter's (1994) shear stress transport (SST) model) was inadequate compared to results from the far more complex and computationally expensive Large Eddy Simulation (LES) approach (Tokyay and Constantinescu 2005). An overall conclusion is that eddy viscosity models significantly overestimate the turbulence and diffusivity in the vortex core by

failing to account accurately for the fact that strong rotation suppresses turbulence (Shur et al., 2000; Tokyay and Constantinescu, 2005; Chen et al., 2012; Suerich-Gulick, 2013). Variations of the eddy-viscosity models attempt to account for the effect of system rotation and streamline curvature through the addition of a curvature correction (CC) to the Reynolds averaged Navier-Stokes (RANS) equations (Spalart and Shur, 1997). Curvature correction reduces the production of turbulent kinetic energy and increases its rate of dissipation in regions of streamline curvature. So far, only a few vortex-intake studies have tested turbulence models with CC (Stephens and Mohanarangam, 2010; Škerlavaj et al., 2011; Škerlavaj et al., 2014; Mulligan, 2015). These studies present quite variable findings.

Other turbulence models, such as the SST scale adaptive simulation (SAS) model and the Reynolds stress model (RSM), were investigated with and without CC by Skerlavaj et al. (2011), Skerlavaj et al. (2014) and Cristofano (2014) and Mulligan (2015). The SST-CC and SAS-CC models provided a better fit to experimental data at lower than at higher approach flows (Škerlavaj et al. 2014). Full Reynolds stress models (RSM) have a fundamental advantage over simpler eddy viscosity models because they model the three-dimensional components of turbulence and rotation, and curvature terms appear explicitly in the turbulence equations (Spalart and Shur, 1997; Wilcox, 1998). Previous investigations formulations of the RSM (e.g., Škerlavaj et al., 2011) have proven to be very accurate but at much higher computational cost (approximately 5–9 times the CPU time required to run the SST model) (Škerlavaj et al. 2011).

Mulligan (2015) compared several turbulence models for the Eulerian-Eulerian simulations of a flow in a vortex intake, including: laminar, RNG k-ε, SST, SST-CC, SAS and RSM models. Curvature correction improved simulation accuracy compared to eddy viscosity approaches (confirming Škerlavaj et al. 2014). RSM further improved accuracy by 2–3%, but was more prone to failure due to numerical instability and was 7.5 times more computationally expensive. The studies by Plant and Crawford (2016) and Carty et al., (2019) on tangential vortex intakes using SST and SST-CC approaches demonstrated greater accuracies ($\leq$ 5% differences between physical and numerical free-surface profiles) than that of Mulligan (2015). These studies were for scroll vortex intakes, and the differences arise possibly due the complex three-dimensional nature of the flow and free surface in this type of application. Consequently, the accuracy of numerical results may vary widely between applications.

An alternative approach to address the over-estimation of the turbulent viscosity in the vortices was employed by Muntean et al. (2005), Sakai et al. (2008), Ito et al. (2010) and Suerich-Gulick (2013). A static eddy viscosity distribution is explicitly defined over the computational domain using an analytical expression, with higher eddy viscosity in the upstream and air-water interface portion of the flow, and lower eddy viscosity in the region where the vortices form. The resulting simulated vortices

remain too diffuse (though far less so than with the k-ε model) and the circulation tends to be overestimated, but the magnitude and effect of axial stretching appears to be more accurately captured.

Another related factor is that most vortices that occur in industrial applications, such as hydropower and pump intakes are extremely transient, shifting position and re-forming intermittently. The transient nature of the vortices further complicates the evaluation and comparison of simulated vortices obtained from RANS and even URANS simulations, because such models average the fluctuating velocities over relatively large time and length scales. This tendency was noted by Rajendran et al. (1999), who performed RANS simulations of highly unstable pump intake vortices revealing significant discrepancies relative to experimental data. Even with vortices that are stable (such as in vortex dropshafts), transient modelling and choice of time step proved critical to resolve the turbulent flow field. Mulligan (2015) demonstrated this concern for the stable flow in a scroll vortex chamber, for which it was concluded that natural unsteadiness of the free-surface and internal flow features was limiting the solutions accuracy. Mulligan (2015) demonstrated that accuracy was increased by switching from a steady-state model to a transient model.

In summary, the transient and anisotropic turbulent qualities of the flow in vortex intake studies significantly increase the modelling challenge. Care must be taken in choosing an unsteady turbulence model, and transient modelling configuration (duration and time step) to ensure that the full transient and turbulent nature of the specific flow problem is being correctly captured.

4.5 | Application

4.5.1 | Vortex-intake dropshafts

Vortex-intake dropshafts are a common application modelled by vortex-intake CFD studies. (Chapter 5 gives details). With recent advances in the field of CFD modeling, vortex-intake dropshafts have been increasingly modelled to enhance understanding for practical design, optimization and research purposes as outlined below.

To accurately model the free-surface flows in the vortex drop shaft, the two-phase (air-water) flows are commonly modelled using the homogeneous Eulerian-Eulerian multiphase or Volume of Fluid (VOF) methods described previously. Several studies have been undertaken on supercritical vortex generators. ANSYS CFX was used by Plant and Crawford (2016) to analyze tangential intakes using an inhomogeneous multiphase approach to model interphase momentum transfer between air and water with homogeneous turbulence using shear stress transport (SST). The fine mesh (9 million elements) results compared well to the physical model. A similar study by Carty et al. (2019) used

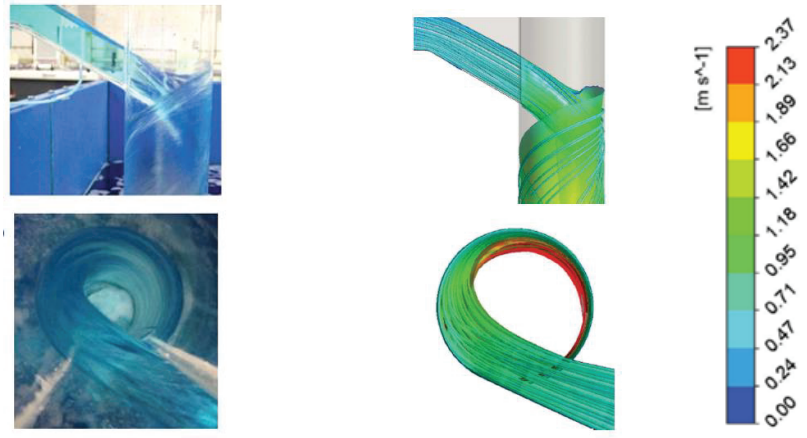

Figure 4.10 | Comparisons between numerical and physical-model data on free-surface profiles in a tangential vortex drop-shaft: (a) physical model; and (b) numerical model (with velocity scale). (Carty et al., 2019)

the transient model (0.01-s timesteps) in ANSYS CFX with a homogeneous multiphase approach and different turbulence models finding similar levels of accuracy ($\leq$ 5% differences) in modeling the free surface, see Fig. 4.10.

Chan et al. (2018) simulated a tangential vortex generator using "interFoam" solver in OpenFOAM 4.0 for two incompressible, immiscible fluids based on the interface capturing approach (Fig. 4.11). They validated their model predictions with detailed point velocity measurements using LDA for a wide range of inflow conditions. The good agreement between the numerical and experimental velocity profiles for the inlet channel and vortex generator confirmed that the multiphase CFD simulation is capable of accurately capturing the velocity field in the tangential intake structure.

Mulligan (2015) undertook several multiphase simulations on the subcritical vortex generator using a homogeneous Eulerian-Eulerian model with different turbulence models. Despite the differences in modelling approaches, the simulations found that the standard eddy viscosity models significantly overestimate turbulence production in the vortex core due to the strong curvature and rotation in this region. The simulations concluded that the results can be significantly improved through implementation of curvature correction in standard eddy viscosity models (e.g., SST). Mulligan (2015) also concluded that, to model the free-surface and depth discharge relationship in a subcritical vortex chamber accurately, it was necessary to resolve the mesh in a radial fashion to avoid false diffusion. Refinement of the mesh density near the core was also essential to ensure the hydraulic control is

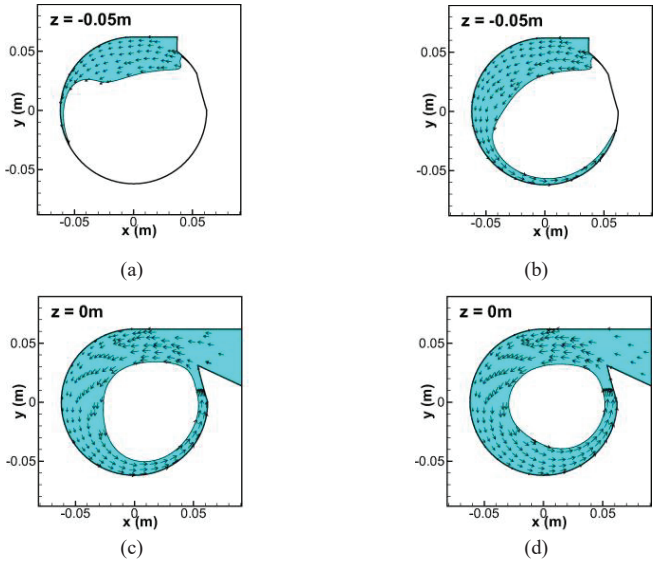

Figure 4.11 | Numerically predicted shapes of the minimum air core with velocity vectors at different flowrates and elevations in a tangential drop structure: (a) 2 l/s($z = -0.05$ m), (b) 4 l/s ($z = -0.05$ m), (c) 8l/s ($z = 0$ m), (d) 10 l/s ($z = 0$ m) where the free surface is defined as 50% air concentration. (Chan et al., 2018).

properly captured to derive the correct depth-discharge relationship. Finally, a first modelling of the subcritical vortex drop shaft with smoothed particle hydrodynamics (SPH) was presented by Bart et al. (2020). Although a comparison between the simulation and physical-model data in this study was only qualitative, the good agreement of the free-surface position bodes well for further investigation of this approach.

4.5.2 | Reservoir intakes and hydropower intakes

The viability of numerical models is increasing for predicting the formation of free-surface vortices at reservoir intakes and hydropower intakes with the increasing accessibility of high-performance computing. The two main challenges are modelling the interaction of the vortices with turbulence and with the air-water interface. Both challenges require a very high resolution in the intake region to capture the formation of the free-surface vortex, while also modelling the very large upstream domain containing the approach flow, which is particularly important for run-of-the-river plants.

A limitation, within the constraints of RANS models used in industry, is modelling turbulence, commonly with two equation models such as the k-ε or the shear stress transport (SST) model. In these models, turbulence intensity is linked to velocity gradients in the flow field. The two equation

turbulence models, therefore, generate artificially high turbulence in the vortex core, which contain high velocity gradients but low vorticity, resulting in unphysical diffusive flow behavior. As an improvement, model add-ons, such as the curvature correction, can be used to partially reduce turbulence production owing to streamline curvature or rotation. The performance of RANS approaches (using the k-ε and SST turbulence models) to model physical hydraulic models of intakes has been assessed by comparison with laboratory measurements of velocity fields, vortex locations and free-surface depressions. Single-phase simulations do not model the deformation of the free surface, which is modelled as a free slip boundary (Li et al. 2008, Škerlavaj et al., 2014). The location of the free-surface vortex is assessed using a post-processing code, which identifies the location of the vortex as where the strength of the rotation is greater than the local strain rate (e.g., the Q criterion used by Škerlavaj et al., 2010). Turbulence models with curvature correction improve the fit with observed data (Škerlavaj et al., 2014). Two-phase simulations use the volume of fluid (VOF) method to resolve the free-surface level, which requires a very fine mesh and becomes computationally expensive (Ito et al., 2009; Shi et al., 2012; Zi et al., 2020). A two-phase approach (GENTOP) was implemented improving predictions of bubble entrainment at free surface vortices (Putra and Lucas, 2020). Commercial codes (Start CD, CFS-Ansys, Flow 3D) and open-source codes (OPENFOAM) have been used, and provide good qualitative agreement. However, the resulting vortices tend to be overly diffusive due to the limitations of the turbulence models, with the error decreasing when curvature correction methods are used (Li et al., 2008; Galuška, 2017; Sungur, 2018; Domfeh et al., 2020; Yildrim, 2020).

In an industry setting, initial assessments of an intake for risk of vortex formation could be made using a fixed lid approximation with RANS simulations using the k-ε turbulence model to estimate bulk circulation and the velocity field around the vortex, which can then be used with the analytical Rankine model to obtain the geometry, and hence strength, of the vortex (Suerich-Gulick et al., 2014a).

Large eddy simulations have been used to model physical scale models of hydropower intakes using the standard Smagorinsky model with near-wall damping and correction for irrotational strain to evaluate the sub-grid scale stresses (Nakayama and Hisasue, 2010; Rabe et al., 2017). The results replicate the main flow behavior, doing so with improved fit to measurements compared to the results obtained using RANS approaches with two equation turbulence models. Lagrangian methods, or Smooth Particle Hydrodynamics approaches (DualSPhysics), used to model a laboratory scale cylindrical rotating tank with bottom drain showed good agreement with experimental data (Azarpira et al., 2022). A comparison of Lagrangian (SPH) and Eulerian LES methods modelling a laboratory cylindrical tank with bottom drain both showed qualitative agreement with the SPH. However, such models are computationally more expensive and less accurate (Azarpira et al., 2021).

Lastly, several neural network methods have been explored and are guardedly promising. These methods (using critical spherical sink surface — CSSS, general linear model — GLM and radial basis functions based on neural network approaches — RBNN) have been trained on 44 sets of data to predict critical submergence levels in hydropower intakes (Kocabaş and Ünal, 2010).

Much progress has been made in the development of numerical methods for hydropower intakes with models validated against physical scale models. The assumption is that results validated against physical models also will be valid at prototype scales (e.g., Guyot et al., 2015). However, the larger domain of the prototype incurs greater computational expense. If the laboratory scale numerical model is used, the model will suffer from the same scale effects when interpreting the results to the prototype scale as does a physical scale model (see Chapter 3 for elaboration).

4.5.3 | Pump intakes

Pumps withdraw water from a river or reservoir via an intake structure. The intake structure typically has an approach channel with a free surface from which a pump column (horizontal, inclined upwards or downwards) or a vertical upward or downward (Bauer and Nakato, 1997) directs the water to a pump. Highly intermittent vortices occur, which are of two types, a free-surface vortex extending from the free surface and submerged vortices that originate at a boundary of the intake bay. Both forms of vortex are undesired and lead into the pump reducing the flowrate, causing flow disturbance or cavitation, and possibly entraining air, sediment, or debris. Designs aim to avoid both formation of problematic vortices and entrainment of air (see Chapter 6).

Pump designs are traditionally refined using scale-model studies (see Chapter 3), while over the last two decades numerical models have complemented or replaced them. RANS approaches with a standard one or two equation turbulence models, typically k-ε and SST turbulence models, are used. As in free surface vortices at hydropower intakes, these models lead to artificially high turbulence intensities in the vortex, as they link turbulence intensity to velocity gradient, leading to vortices that are unphysically diffuse (i.e., underestimating the vortex strength). Earlier simulations used single-phase models with the free surface represented with a no-slip fixed lid and thus were not able to resolve the deformation of the free surface by the vortex (Lu et al., 1997; Constantinescu and Patel, 1998; Rajendran et al., 1999; Constantinescu and Patel, 2000; Li et al., 2004; Okamura et al., 2007; Tang et al., 2011).

Later two-phase approaches, using the VOF method, could define the free surface of water and have demonstrated more accurate predictions when free-surface depressions are relatively small (e.g., Qian et al, 2016; Ahn et al., 2017; Guo et al., 2017). As vortices are generally unsteady phenomena

(and undesired for pump intakes), unsteady RANS models (URANS) are inherently an improvement over RANS (Guo et al., 2017), although the velocity distribution and shape of the funnel are not well predicted (Wu et al. 2020). Further improvement in simulating time dependent processes and of quantifying air entrainment in two-phase models is obtained using hybrid RANS-LES or detached eddy simulations (DES) (Wu et al. 2020) or LES (Tokyay and Constantinescu, 2006; Nakayama and Hisasue, 2010; Chuang et al., 2014: Pan et al., 2019: Yamade et al., 2020). LES approaches typically use the standard Smagorinsky model as the subgrid scale model (Tokyay and Constantinescu, 2006).

4.6 | Concluding remarks

Vortices and swirling flows at intakes are among the most complex of flow processes in hydraulic engineering and, therefore, require additional considerations during three-dimensional numerical modelling campaigns. This Chapter summarizes key numerical aspects that should be considered based on existing research. It should be noted that the quantitative accuracy (uncertainty) of numerical models has been found to vary widely between vortex intake applications. Therefore, further work is required. In some cases, the uncertainty may still be too significant for the numerical model to be suitable for detailed design purposes, unless considerable, application-based safety factors or coefficients are integrated with the simulation outputs. However, the qualitative results could provide guidance. The following recommendations maximize the quantitative accuracy of numerical results.

Mesh Structure and Resolution: Due to the swirling nature of vortex flows, past research indicates that structured meshes should be developed to ensure that the grid is aligned with the general flow structure to avoid false diffusion. The mesh should be refined closer to the air core region where the transient interface and high velocity gradients are expected. In applications of pump or hydropower intakes, the mesh should maintain the required resolution close to the intake, whilst a less dense mesh can be implemented far from the vortex intake to maintain efficiency of the numerical simulations.

Multiphase Flow Considerations: Single-phase "fixed lid" methods can be useful when the objective is to obtain efficient, qualitatively accurate results, such as location(s) of vortex appearance and design modifications to avoid undesirable vortices. However, past research indicates that two-phase flow models (i.e., VOF or Eulerian-Eulerian) should be adopted when quantitative accuracy is required.

Turbulence Model Considerations: Care should be taken when choosing the turbulence model for the application. Standard models tend to be too diffusive and they underpredict the vortex strength. Curvature correction approaches should be adopted when feasible, otherwise, RSM,

LES or DNS approaches should be considered for maximum quantitative accuracy. Also, the Very-Large Eddy Simulation (VLES) method can be suitable to avoid turbulence diffusion when a single-phase approach flow is used (e.g., Tiwari et al. 2020).

Transient Considerations: The correct strategy should carefully consider the choice of the unsteady turbulence model and the correct transient modelling configuration (duration and time step) to ensure the full transient and turbulent nature of the specific flow problem is being correctly captured.

Dependence on Application: Quantitative accuracy of results will vary between applications. For example, higher accuracies have been demonstrated in tangential vortex intakes using basic turbulence models as compared to the scroll intake. This result likely is due to the position and three-dimensional structure of the controlling hydraulic section. In pump intakes, the transient position of the vortex may pose additional challenges not resolvable by a fixed mesh. Therefore, the physical characteristics of each problem should be considered carefully to ensure that any unique flow features are being properly resolved before a simulation campaign is conducted.

Vortices and swirling flows at intakes are among the most complex flow processes in hydraulic engineering and therefore require additional considerations during three-dimensional numerical modelling campaigns. Based on the above review of past studies, it is noted that in many cases, the results from CFD studies at vortex intakes still have significant uncertainty, that may limit viability for practical application. Therefore, to further strengthen our understanding and the validity of CFD studies, the following aspects have been identified for future research studies:

Physical-Numerical Transient Analysis: Further detailed CFD validation studies are required using data available from advanced high resolution transient measurements of, for example, vortex location, air core free-surface unsteadiness, sub-surface three-dimensional velocity distributions and secondary flow mechanisms. The CFD studies should advance existing developments and guidelines by integrating the following aspects to determine sensitivity to uncertainty and to improve simulation accuracy.

Mesh Adaptation: Mesh adaptation (or Adaptive Mesh Refinement) is an emerging tool available for three-dimensional CFD studies. The tool enables automatic mesh refinement in regions of interest. Due to the time dependent nature of the free surface in vortex flow studies, the tool could be used to automatically refine the mesh in the vortex core region (mesh adaptation by adverse velocity or volume fraction gradients). This process may be particularly useful when the vortex tends to migrate around the intake structure. Such refinement studies should reference

findings using the Courant number and other numerical residuals in the air core region to establish relevant guidelines for future practical application.

Prototype Studies: Many of the previous numerical validation studies leverage data available from physical models only. There is a growing need to gather data at prototype scale for full-scale validation of CFD models to fully close the model verification circle and to further de-risk the use of these models for design purposes.

Momentum Advection: The minimum momentum advection is essential when using a VOF method. A minimum second-order closure is needed, though further investigation is required here.

Bubbly Flow Considerations: Previous studies used the Homogeneous Eulerian-Eulerian or VOF approaches, which are viable for cases where the flows are stratified. Under some conditions of vortex intake flow, the flow can become a mixture of stratified and bubbly flow, where the air phase is dispersed in the water phase. Examples of these conditions are near pump or hydropower intakes where vortex characteristics will be dependent on the bubble formation. In such conditions, it may be important to ensure that the bubbly flow is accurately modelled to ensure the accuracy of the overall solution. In this case, mixture models or decoupled, inhomogeneous two-phase models with or without population balance methods may need to be considered and thus, a study focusing on these multiphase modeling approaches would be useful. Further research is needed in this regard.

Advanced Turbulence Models: Further validation studies using advanced turbulence formulations such as the SST-CC, RSM, LES or even direct numerical simulation are required to fully understand the sensitivity of numerical results on turbulence modelling.

Meshless Approaches: Only two studies currently available in the literature adopt meshless smoothed particle hydrodynamics (SPH) methods for investigating vortex intakes. The studies have demonstrated that SPH is a viable method for generating qualitative results, which agree well with measured data from laboratory models, at a lower cost and complexity compared to the mesh-based approaches. The research community should continue to explore and develop SPH based studies to advance the use of this technique and understand its limitations (if any) for practical application.

CHAPTER 5

Vortex-Intake Drop Structures

SHU NING CHAN
The Hong Kong University of Science and Technology, Hong Kong SAR, China.
E-mail: *treechansn@gmail.com*

TROY C. LYONS
University of Iowa, IIHR, USA. E-mail: *troy-lyons@uiowa.edu*

DAVID Z. ZHU
University of Alberta, Canada. E-mail: *dzhu@ualberta.ca*

JOSEPH H. W. LEE
Macau University of Science and Technology, Macau SAR, China. E-mail: *jhwlee@must.edu.mo*

5.1 | Introduction

Vortex-intake drop structures (herein also termed dropshafts) are commonly used in water supply, drainage, sewer, and combined-sewer-overflow systems. The primary function of drop structures is to convey flow efficiently and safely from an upper level to a lower level, typically a subterranean tunnel system. Plunge-type drop structures convey water directly from an upstream channel to a vertical dropshaft or from a pool via a radial inlet (i.e., morning-glory-type) intake, commonly used for reservoir spillways (e.g., Vischer and Hager, 1998; Hager et al., 2020).

A vortex-intake drop structure (e.g., Hager, 2010) is a specific type of drop structure that mainly consists of the vortex intake, the dropshaft, and the outlet structure typically connected to a tunnel. Often, the outlet structure contains a deaeration chamber and deaeration shaft, to aid in removal of air entrained into the dropshaft. Vortex flow is intentionally created in the dropshaft and induces a continuous air core in the dropshaft. The air core acts as a conduit for air to move freely and avoiding flow instability. Fig. 5.1 illustrates a typical vortex-intake drop structure.

Additionally, vortex-intake drop structures have been increasingly used for urban flood protection in densely populated cities, particularly because urbanization and global climate change lead to more frequent occurrences of extreme rainfall events and consequent urban flooding. Such structures are

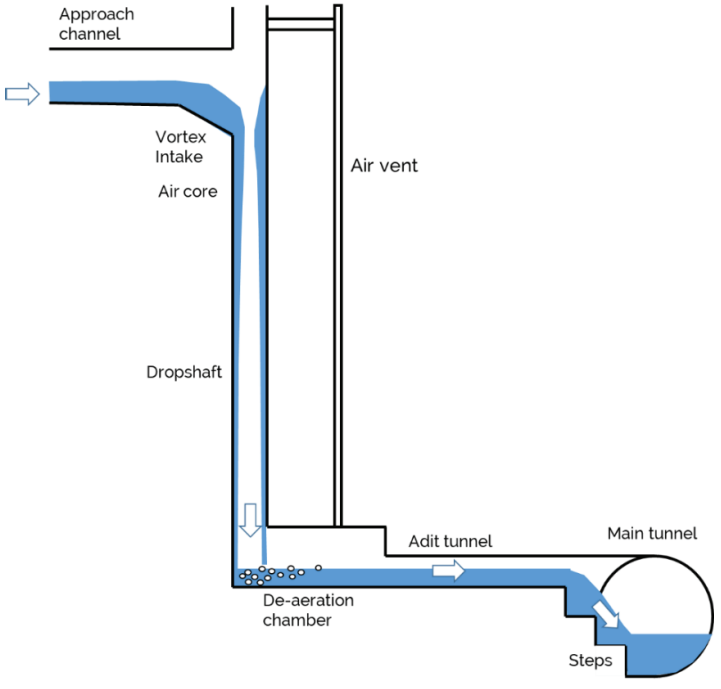

Figure 5.1 | Schematic of the structure of a vortex drop and connection to a main tunnel that collects the drainage flow.

an effective, economic flood protection measure that act by intercepting the upstream stormwater and discharging it to a safe downstream location (e.g., Drioli, 1947; Mortara, 1948; Stevens and Kolf, 1957; Yu and Lee, 2009). Vortex drops have also been adopted for intercepting runoff from hilly terrain for storage in coastal reservoirs (e.g., the Plover Cove Water Scheme in Hong Kong, HRS 1965), and for conveying treated sewage effluent to submarine outfalls (e.g., Brooks and Blackmer 1962) and deep sewage tunnels (e.g., scroll vortex intakes to convey screened sewage in preliminary treatment plants to the deep tunnels of the Hong Kong Harbour Area Treatment Scheme). For combined sewer overflow systems, vortex dropshafts also benefit ventilation, minimize pressurized conditions in sewer headspace and the potential release of sewer odour (e.g., Holstad, 2020).

Theoretical, computational, and physical hydraulic models are of great importance to aid the engineering design of vortex intakes. Though computational fluid dynamics (CFD) modelling tools are developing, as Chapter 4 explains, robust theories are still useful to provide preliminary guidance and fast screening of overall design features to determine the type and geometry of the vortex intake and associated structures. CFD models are a useful tool for evaluating the flow details of vortex intakes

and aid the detailed design. Physical models are commonly used to confirm the hydraulic features of the selected design, improve the design, evaluate air entrainment and deaeration characteristics over a wide range of flow conditions, and study the fate and transport of debris and sediment.

The original chapter in Knauss (1987, i.e., the chapter by Jain and Ettema, 1987) mostly focused on theoretical considerations based on simplified one-dimensional assumptions and limited physical model tests. In the past three decades, the understanding and design of vortex-intake drop structures have greatly benefited from the advancement of sophisticated measurement techniques and full three-dimensional computational modeling, resulting in more robust design theories and a blooming number of applications worldwide. This chapter aims at providing a comprehensive introduction to the different types of vortex intakes, their design dimensions, and their applications, updating readers about the latest development on the topic.

5.2 | Configurations and general design considerations of vortex intakes

Water can be conveyed efficiently as a spiraling flow down a vertical or nearly vertical dropshaft. This process requires that the approach flow enters a vortex-flow intake at the top of the dropshaft and then spirals down the dropshaft. The vortex intake imparts an angular motion to the flow which then enters the dropshaft as a spiraling annular jet with an air core at the center of the dropshaft (Fig. 5.1). The air-core area initially decreases, forming a throat, and then increases down the dropshaft. As the flow drops, its vertical velocity component increases, swirl in the spiral attenuates due to energy dissipation, and the flow direction gradually approaches vertical. The flow, however, continues to adhere to the dropshaft wall. The spiraling flow along a dropshaft wall can result in considerable energy dissipation. Further, significantly less air is entrained by a coherent, wall-attached, spiraling flow than by a plunge flow (Camino et al., 2015; Lyons, 2021), and the entrained air migrates toward the air core due to the outward (towards the air core) pressure gradient produced by flow rotation.

A typical design of the vortex-intake drop structure consists of a vortex intake, a dropshaft, a deaeration chamber and an adit tunnel (or pipe) connecting the dropshaft to the tunnel. An air shaft is installed in the crown of the deaeration chamber for releasing any air entrained by the intake flow, the downward spiraling flow, and the plunging flow impacting the shaft base. The design of the vortex intake is an important aspect to maintain a sufficient air-core size to allow movement of air past the dropshaft throat, thereby satisfying the upstream constraint in water level and avoiding flow instability. The air core must be sufficiently large to enable free passage of air and ensure the stable operation of the vortex drop structure. A typical criterion is that the ratio of the air core area to the dropshaft cross-sectional area, λ, is greater than 0.25 (Jain and Ettema, 1987).

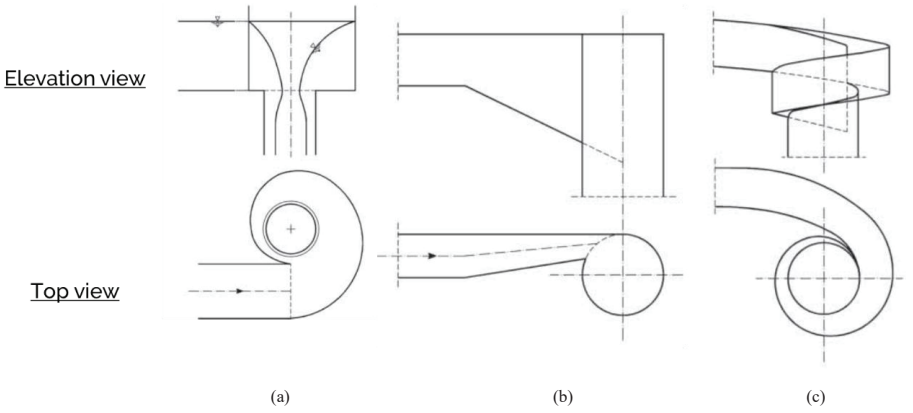

Figure 5.2 | Types of vortex flow intakes: (a) scroll, (b) tangential; and (c) spiral.

Different types of vortex intakes have been proposed. Among earlier configurations, circular intakes feature a horizontal floor and a circular vortex chamber concentric within the dropshaft, with a tangential approach flow channel. They require larger intake depths to discharge the required discharge compared with other types of intakes (Weiss et al. 2010). More efficient types of vortex intakes are the scroll, tangential and spiral intakes (Fig. 5.2). Whereas tangential (Zhao et al., 2006; Yu and Lee, 2009; Chan et al., 2018a) and spiral (Pfister et al., 2018; Crispino et al., 2019) vortex intakes are suitable for both subcritical and supercritical approach flows, scroll vortex intakes are often used only for subcritical approach flows (Drioli, 1969; Del Giudice et al., 2010).

5.2.1 | Scroll vortex intakes

First introduced by Drioli (1947), a scroll vortex intake consists of a vortex chamber with a horizontal floor whose walls curve continuously inwards to the dropshaft. A standard design of the scroll intake geometry was proposed by Drioli (1969) and Jain and Ettema (1987). Various experimental and numerical modelling studies have been conducted for studying its hydraulic characteristics. Importantly, a sufficient air core facilitates free passage of air, ensuring stable operation of the vortex drop structure.

The geometry and key dimensions of the scroll vortex chamber are designed based on the standard geometry. Fig. 5.3 depicts a scroll vortex intake and gives the important length variables. The chamber wall consists of four arcs with decreasing radii in the flow direction. The centre of each arc is offset from the dropshaft centre by a certain distance determined by an eccentricity, e, such that

$$e = \frac{B + s}{7} \tag{5.1}$$

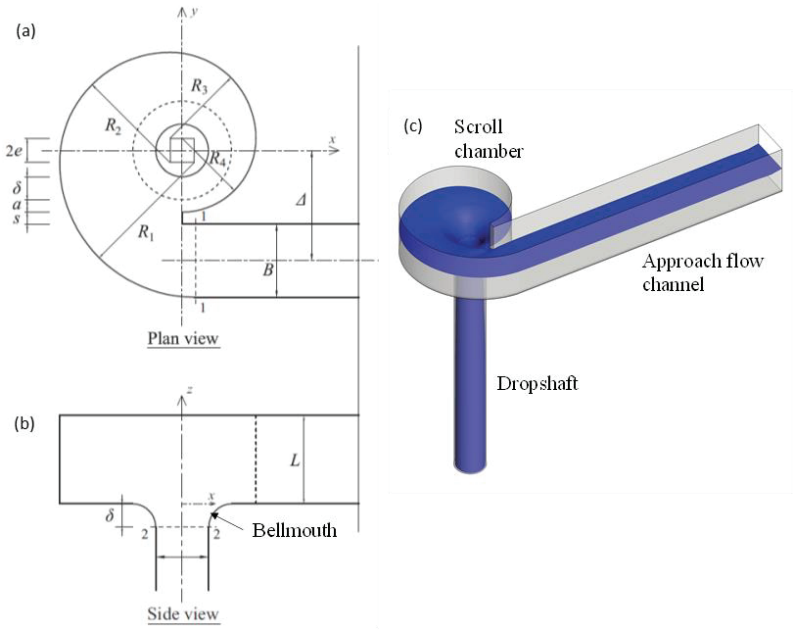

Figure 5.3 | The scroll form of vortex intake: (a) plan geometry; (b) elevation geometry; and (c) a 3D depiction of the intake and free surface flow profile.

where B = approach channel width, and s = offset distance between the approach channel wall and the chamber wall. The radius of each arc, R_i, is then determined by following relations:

$$R_4 = \frac{D}{2} + \delta + a + e, \quad R_3 = R_4 + e, \quad R_2 = R_3 + 2e, \quad R_1 = R_2 + 2e, \quad \Delta = R_1 + e - \frac{B}{2} \qquad 5.2$$

where D = dropshaft diameter, δ = radius of curvature of the dropshaft entrance, a = distance between the top of bellmouth and the chamber wall (Fig. 5.3a), and Δ = the eccentricity between the approach channel and the dropshaft. B and D are first determined based on the design discharge; Δ, s, and a are chosen based on structural considerations. Then e and the radii of the four arcs can be determined based on Eqs. 5.1 and 5.2 (Drioli, 1969; Jain and Ettema, 1987; Chan et al., 2022).

Water flows into the intake via the eccentric approach channel. Thus, the intake imparts swirl to the flow so that a tornado-shaped free-surface vortex with a stable air core is formed along the dropshaft (Fig. 5.3c). The air core allows the air brought by the approach flow to escape freely, and the extended flow path enhances energy dissipation. The swirling flow gradually drains down the dropshaft through the bellmouth at the top of the dropshaft (Fig. 5.3c). The air core area decreases with increasing discharge. The minimum area of air core occurs around the level of the bellmouth.

Experimental and numerical evidence (Mulligan et al., 2019a; Chan et al., 2022) shows that the tangential velocity in the vortex chamber decreases with radial distance from the center of dropshaft to the side walls, like a strong free-surface air core vortex (see Chapter 2). Vortex flow adheres to the free vortex rule, whereby the vortex circulation is approximately constant over the radius of the chamber and equals the circulation imparted at the inlet; except near the chamber bottom where friction dissipation dominates. The average circulation decreases gradually along the chamber, as flow spirals down the dropshaft. The vortex circulation at the bellmouth and dropshaft is less than that at the vortex chamber and gradually decreases due to viscous dissipation and friction (Chan et al. 2022). The vertical velocity at the dropshaft increases with increase in the air core area and can be estimated based on the below equation (Kellenberger, 1988; Hager, 2010):

$$\left(\frac{V}{V^*}\right)^2 = \tanh\left(\frac{z}{z^*}\right) \tag{5.3}$$

where $z^* = (1/n)^{6/5}(Q/\pi D)^{4/5}/2g$; $V^* = (1/n)^{3/5}(Q/\pi D)^{2/5}$; n = Manning's resistance coefficient; and V^* = the uniform shaft velocity established, provided shaft length, z, exceeds $3z^*$.

Several design theories for scroll vortex intake have been proposed (e.g., Viparelli, 1950; Ackers and Crump, 1960; Pica, 1970; Hager, 1985; Jain and Ettema, 1987; Chan, 2022). The theories aim at estimating the approach flow depth, h_a, and the air core size ratio at the dropshaft, λ, for a given scroll intake geometry and the discharge, Q. A control volume is selected for the analysis between Section 1.1, just upstream of the inlet of the vortex chamber, and Section 2.2, the entrance to the dropshaft (Fig. 3a). The following six assumptions apply: uniform approach flow velocity at Section 1.1; atmospheric pressure inside the air core; the throat (control) section is located at Section 2.2; axisymmetric vortex flow; negligible radial velocity component at the throat; and total-energy conservation occurs between Sections 1.1 and 2.2.

Design theories assume different distributions of tangential, vertical velocities and pressure at the bellmouth, resulting in differences for the predicted head-discharge relationship and air core relationship:

- Ackers and Crump (1960) assumed that the tangential velocity and pressure at the bellmouth are those of a free vortex:

$$Q = \sqrt{\frac{2g h_a^2 (h_a + \delta) B^2}{\left(\frac{\Delta}{R}\right)^2 \left(\frac{1+\lambda}{2\lambda^2}\right) - 1}}, \qquad h_a = \frac{\pi R \Delta}{\sqrt{2}B} \frac{(1-\lambda)^{3/2}}{\lambda} \tag{5.4}$$

- Pica (1970) assumed that the pressure at the core is zero over the entire vortex cross-section and the tangential velocity is constant:

$$Q = \sqrt{\frac{2g\left(h_a+\delta\right)}{\left(\frac{1}{C_{x0}\pi^2R^4}-\frac{1}{B^2h_a^2}\right)}}, \qquad h_a = \frac{\pi R\Delta}{B}C'_{x0} \tag{5.5}$$

$$C_{x0} = 0.95-\sqrt{\lambda}, \qquad C'_{x0} = \frac{3}{2}\left(\frac{1-\lambda}{1-\lambda^{3/2}}\right)\frac{C_{x0}}{\sqrt{1-C_{x0}^2/\left(1-\lambda\right)^2}}$$

- Jain and Ettema (1987) assumed that the pressure distribution at the air core is zero over the entire vortex cross-section and the tangential velocity at the bellmouth follows that of a free vortex:

$$Q = \sqrt{\frac{2gh_a^2\left(h_a+\delta\right)B^2}{\left(\frac{\Delta}{R}\right)^2\left(\frac{1}{\lambda}\right)-1}}, \qquad h_a = \frac{\pi R\Delta}{B}\frac{C_{x0}}{\sqrt{\lambda}}, \tag{5.6}$$

$$C_{x0} = \sqrt{1-\lambda}-\lambda\ln\left(\frac{1+\sqrt{1-\lambda}}{\sqrt{\lambda}}\right)$$

- Chan (2022), using experiment-measurement and CFD predictions, proposed that the tangential velocity and pressure distribution at the bellmouth follow that of a forced vortex:

$$Q = \sqrt{\frac{2gh_a^2\left(h_a+\delta\right)B^2}{\left(\frac{\Delta}{R}\right)^2\left(\frac{5-3\lambda}{2}\right)-1}}, \qquad h_a = C\frac{\pi R\Delta}{\sqrt{2}B}\left(1-\lambda\right)^{3/2}, \qquad C = 1.52 \tag{5.7}$$

Fig. 5.4 shows that Pica's (1970) equations (Eq. 5.5) best predicts the head-discharge relationship, whereas Chan's (2022) equations (Eq. 5.7) better estimate the air-core ratio.

5.2.2 | Tangential vortex intakes

A tangential vortex intake consists of a linear approach flow channel and a tapering sloped section leading to a dropshaft, as Fig. 5.5 shows. Inflow enters tangentially into the dropshaft via the tapering channel, and the flow spirals down the dropshaft. Centrifugal acceleration in the swirling flow results in a stable air core, which enables entrained air to escape upwards. It is well accepted that a tangential intake is a compact design that possesses the hydraulic advantage of a stable flow with high energy dissipation and manageable air entrainment. Tangential intakes are particularly suitable for intercepting supercritical flows, and intake geometry is simple and relatively easy to construct.

Physical hydraulic modeling studies have provided valuable experience for designing tangential intakes (Jain and Kennedy, 1983; Lee et al., 2006). One-dimensional (1D) theories have been proposed (e.g., Jain, 1984; Yu and Lee, 2009) for estimating the head-discharge relationship and the air core

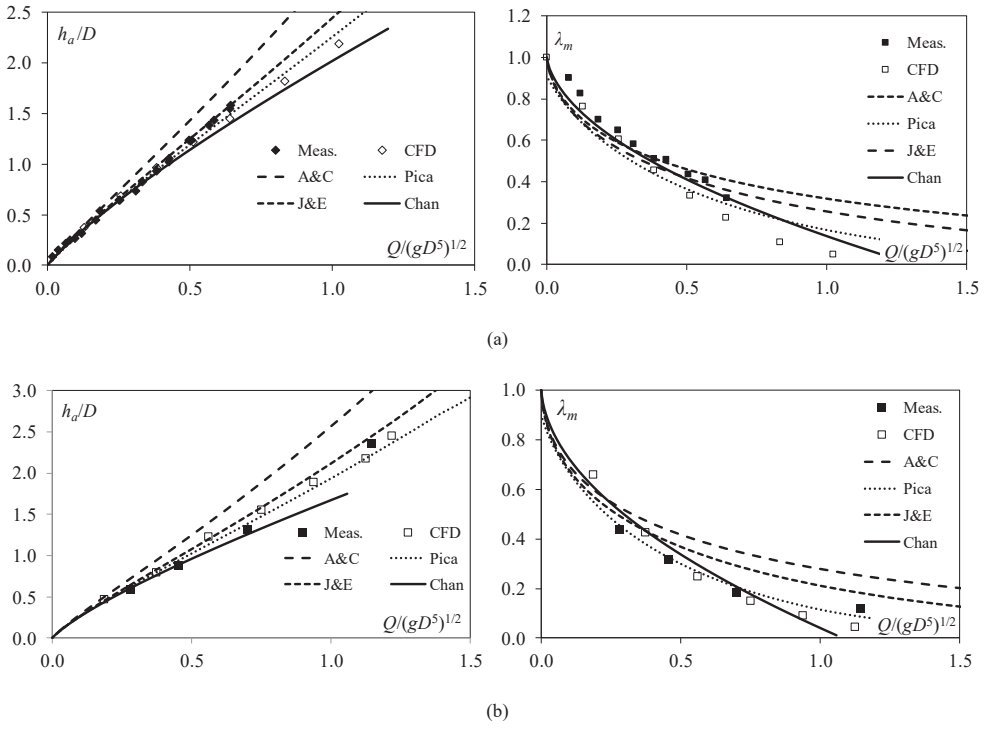

Figure 5.4 | Head-discharge relationship and air-core size for a scroll vortex intake: (a) experiments by Guo (2012); and (b) experiments by Viparelli (1950). {A&C = Ackers and Crump (1960) (Eq. 5.4), Pica = Pica (1970) (Eq. 5.5), J&E = Jain and Ettema (1987) (Eq. 5.6), Chan = Chan (2022) (Eq. 5.7)}.

size, assuming that the spiraling flow at the dropshaft is axisymmetric. However, model studies have revealed that, under certain conditions, a significant hydraulic jump can occur in the inlet channel, leading to undesirable overflow situations and violations of energy conservation implicit in the 1D model (Yu and Lee, 2009).

5.2.2.1 | *Hydraulic control of the intake*

For a given geometry of a tangential intake and a given discharge, Q, the flow depth in the approach flow channel, y_{ca}, can be determined. For small discharges, the flow control is at the transition from the approach channel (critical flow) to the steep tapering inlet channel (supercritical). y_{ca} can be determined using the equation for critical depth in an open channel:

$$y_{ca} = \left[\left(\frac{Q}{B}\right)^2 \frac{1}{g}\right]^{1/3} \tag{5.8}$$

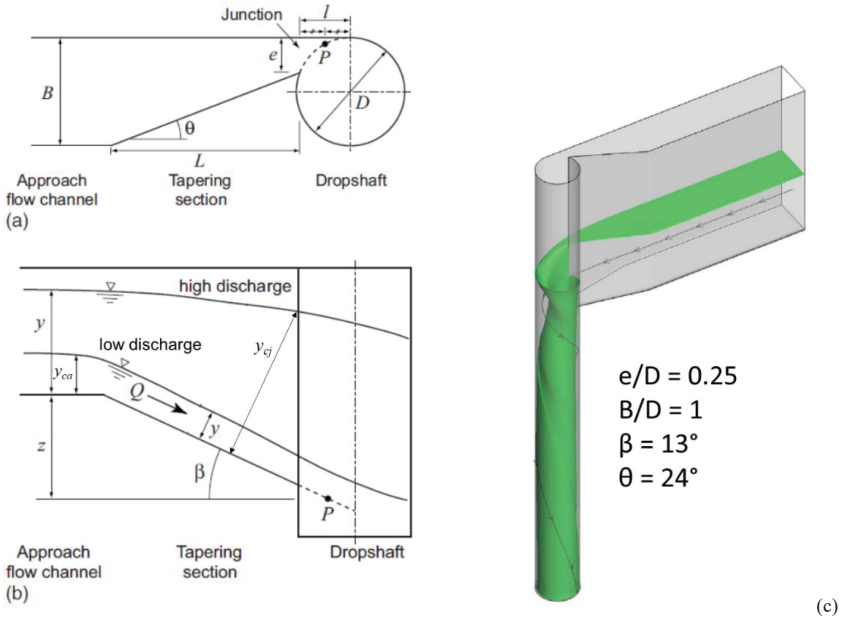

Figure 5.5 | Geometry of a tangential form of vortex-flow intake: (a) plan view; (b) elevation view; and (c) flow profile at intake (CFD prediction).

where B is the width of the approach flow channel. For high discharges, however, the control is at the junction between the tapering section and the dropshaft. The control at the junction drowns the control at the upstream end of the tapering inlet; flow in the approach and inlet channels remains subcritical. For the tapering inlet channel, the specific energy of the flow is $E = V^2/2g + y\cos\beta$, where V and y = velocity parallel to and depth normal to the bed, respectively, and β = bottom slope angle. The critical depth y_{cj} at the junction is $y_{cj} = [(Q/e)^2/(g\cos\beta)]^{1/3}$. Assuming negligible hydraulic losses, the specific energy in the approach flow channel can be related non-dimensionally to specific energy at the junction

$$y_* + \frac{1}{2y_*} = E_* \qquad 5.9$$

where $y_* = y/y_{ca}$; $E_* = 1.5\,(B\cos\beta/e)^{2/3} - z_*$ and $z_* = z/y_{ca}$. For $E_* \leq 1.5$, the flow control is at the approach flow channel. For $E_* > 1.5$, the flow control shifts to the inlet junction (Jain, 1984). The above equations can be used to determine the depth-discharge relationship at the approach flow channel end, assuming a smooth transition from the upstream to the downstream control as

Q increases. The shift of the flow control occurs at $Q = Q_c$, i.e., when the flow is critical both at the upstream channel and at the junction:

$$Q_c = \frac{\sqrt{g}e\,(2z/3)^{3/2}}{\left[\cos^{2/3}\beta - (e/B)^{2/3}\right]^{3/2}} \tag{5.10}$$

Q_c increases with e and most importantly $z = (B-e)\tan\beta/\tan\theta$ (the drop in elevation between the approach flow channel and the junction) for given β and B. The above 1D theory is valid only when this shift of flow control occurs smoothly without flow instability and energy loss.

5.2.2.2 | *Free drainage condition and stable intake design*

Under some conditions, the supercritical inlet flow does not flow smoothly into the vertical dropshaft even when the discharge is smaller than the control shift discharge. The vortex flow, after turning 360° in the dropshaft, may reenter the inlet or disturb the parallel inflow jet, leading to a local swell that creates a backflow or even a hydraulic jump in the tapering section (Fig. 5.6). Hence, a tangential vortex intake must be designed to avoid this condition.

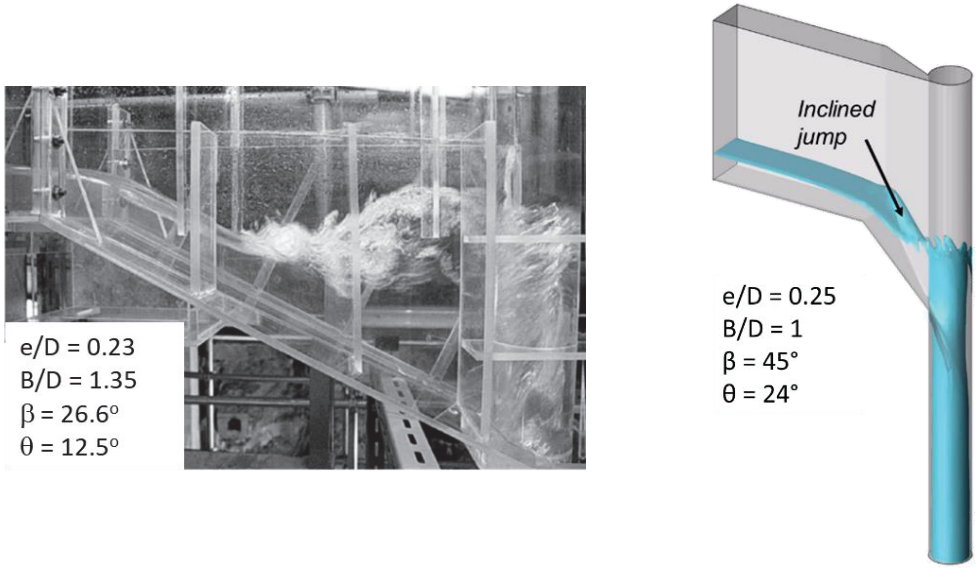

Figure 5.6 | Hydraulic jump on an inclined surface, with air entrainment occurring as water flow interacts with the junction of a tangential form of vortex intake: (a) experiment (Yu and Lee, 2009); and (b) a CFD simulation. The symbols are as shown in Fig. 5.5.

As a first-order approximation, Yu and Lee (2009) derived the limiting condition of "free drainage". Flow from the tangential inlet swirls down the dropshaft as an annular jet. Swirling flow inside the dropshaft can be approximated as a free irrotational vortex (e.g., Jain and Ettema, 1987), characterized by a constant circulation. Assuming a constant horizontal velocity at the inflow junction, and constant vertical velocity in the annular jet outflow in the dropshaft. For the free drainage condition, Q_f can be estimated in terms of the intake geometry

$$Q_f = \left(\tan\beta \frac{\pi D}{1 - e/D}\right)^{3/2} e\sqrt{g}\cos^2\beta \tag{5.11}$$

If $Q_f < Q_c$, a hydraulic jump likely occurs in the tapering section due to the flow-contracting effect of the junction. This condition leads to undesirable fluctuating of flow. Therefore, to maintain smooth and stable flow along the tapering section, experimental observations indicate that $Q_f > Q_c$ (Yu and Lee, 2009). The value of Q_c and occurrence of flow stability are governed by the geometry of the intake.

5.2.2.3 | *Air core size*

This section assumes that a critical section develops at the throat of the drop structure and that the air core is axisymmetric (Binnie and Hookings, 1948). By estimating the pressure change and the corresponding change in velocity head, the vertical velocity can be estimated, and the discharge can be related to the air core size ratio λ. By assuming constant tangential velocity across the annulus at the throat, Jain (1984) derived the following relationship between air core size and discharge:

$$\sqrt{\frac{1-\lambda^3}{2\lambda}} = 4\left[\frac{Q^2 e}{g\pi^3 D^6 \cos^4\beta}\right]^{1/3} \tag{5.12}$$

Yu and Lee (2009) assumed a free vortex at the throat and derived the following relationship:

$$\sqrt{\frac{1-\lambda^3}{2\lambda}} = 4\left[\frac{Q^2 e}{g\pi^3 D^6 \cos^4\beta}\right]^{1/3}\left(\frac{1}{1-e/D}\right) \tag{5.13}$$

The free-vortex assumption is supported by detailed measurement of flow and CFD modelling (Chan et al., 2018a). The predicted depth-discharge relationship and air core size compare well with measurements (Fig. 5.7). The air core is significantly asymmetrical, with the flow thickness being largest near the junction entry to the dropshaft. The air-core size increases gradually as it spirals around the circumference of the dropshaft. The tangential velocity of the vortex flow down the dropshaft increases linearly from near the air core in the center to a maximum, then declines in radius. The vortex resembling a Rankine type vortex (Chan et al., 2018a).

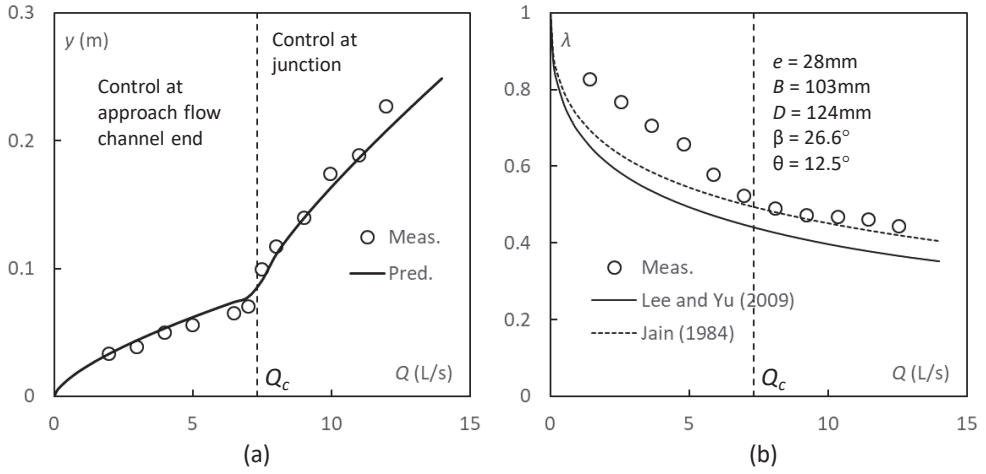

Figure 5.7 | (a) Depth-discharge relationship estimated from Eq. 5-9; and (b) air core size estimated from Eqs. 5.12 and 5.13 for a tangential intake ($e/D = 0.226$, $B/D = 0.831$, $D = 0.124$ m, $\beta = 26.6°$, $\vartheta = 12.5°$, measurements from Yu and Lee, 2009).

5.2.2.4 | *Worked example of designing a tangential intake*

The hydraulic design of a tangential intake is based on the basic guidelines mentioned above. The design discharge is typically based on the hydrologic assessment. The minimum dropshaft diameter can be sized from

$$D = \eta \left(Q^2/g\right)^{1/5} \tag{5.14}$$

where $\eta = 1.2-1.25$, is a safety factor for avoiding pressurized flow in the dropshaft (Hager, 1990; Yu and Lee 2009). A suitable value of e/D is required to produce an effective swirling flow and air core of adequate size, yet satisfying other constrains. Optimal design from model studies recommends $e/D = 0.2-0.25$ (Jain, 1984; Lee et al., 2006). The free drainage discharge condition should be satisfied to avoid unstable flow and hydraulic jump which may result in overflow, i.e., $Q_c < Q_f$. In addition, it is advisable to limit the maximum discharge not to exceed Q_f (Yu and Lee 2009). The air core area ratio at maximum discharge should be greater than 0.25 to enable free passage of air for stable operation.

This section shows an example for designing a stable tangential intake for a maximum discharge of 15 m^3/s and $B = 2.5$ m. Site constrains dictate that L (horizontal length of tapering section) should not exceed 10 m. The following steps ensue:

a) Taking $\eta = 1.25$, D can be sized as 2.34 m (Eq. 5.14). e can be estimated as $0.25D$, i.e., $e = 0.59$ m.
b) Try an initial design of $\beta = 27^\circ$ and $L = 10$ m. $z = L \tan\beta = 5.1$ m. From Eqs. 5.10 and 5.11, Q_c and Q_f can be determined as 28.4 and 16.2 m^3/s respectively. As $Q_f < Q_c$, the design will generate an undesirable hydraulic jump in the intake. Re-designing is required.
c) Keeping D, B and e unchanged, L is reduced to 5 m and β is increased to 32° ($z = 3.1$ m). In this design Q_c and Q_f are 14.8 and 20.0 m^3/s respectively (Eqs. 5.10 and 5.11). As $Q_f > Q_c$, a smooth transition of flow is expected to occur in the intake. Q_f is also sufficiently greater than the design maximum discharge.
d) From Eq. 5.8, y_{ca} can be estimated as 1.54 m, $z_* = 2.03$ and $E_* = 1.51 > 1.5$. The flow control is at the inlet junction. The water depth at the head of the tapering channel y is estimated as 1.59 m (Eq. 5.9).
e) The air-core area ratio, λ, can be estimated as 0.38 (Eq. 5.13) at the maximum discharge, greater than the minimum air core criteria of 0.25. This design satisfies all basic criteria and is expected to give satisfactory performance.

5.2.3 | Spiral intakes

The spiral form of vortex intakes is suitable for subcritical and supercritical approach flows, making the form preferable in congested hilly cities. The ability of spiral intakes to handle supercritical flows is an advantage over scroll vortex intakes, which require subcritical approach flow and a larger chamber footprint, thereby limiting their application within urban areas. Spiral vortex intakes were developed to transform the supercritical flow directly into a vortex flow with smooth transition into the drop-shaft. A spiral intake is relatively complex; the curvature effects result in a change of cross-sectional area from the rectangular inlet to almost triangular shape in the spiral inlet structure.

The recommended intake geometry (Fig. 5.8) is based on model tests that involved optimizing the height of standing wave, the reduction of cross-waves, and prevention of choking flow. Hager (1990) introduced a particular spiral intake design with four arcs of reducing radius:

$$R_1 = \frac{1}{2}(a + R + t + c), \quad R_2 = \frac{1}{2}(2R + t + c), \quad R_3 = \frac{1}{2}(a + R + t - B), \quad R_4 = R + t \qquad 5.15$$

where R = shaft radius; a = distance of shaft axis to outer approaching wall; B = the approach channel width; t = wall thickness; and c = channel width opposite the intake section. The centers of the circular arcs are

$$e_1 = a - R_1, \quad e_2 = R + t + c - R_2, \quad e_3 = a - B - R_3 \qquad 5.16$$

The thickness t_1 of the inner wall at the intake section is

$$t_1 = a - B - R \tag{5.17}$$

The following conditions should be satisfied:

$$R + t + c \leq a \leq 3R + t \quad \text{and} \quad 0.8R < B < 2R \quad \text{and} \quad 0.8R < c < 2R$$

Small values of both B/R and c/R are preferable. The bottom slope S_o of the approach flow channel is limited to 30% maximum. The longitudinal slope of the inlet structure S_{oi} should be larger than S_o. The radial slope in the intake can be designed as flat (zero slope) or warped (sloped down towards the dropshaft). For given design discharge Q, both B and R, depend on hydraulic radius.

To design a supercritical-flow, spiral vortex intake, the approach channel width B, and the dropshaft diameter D, are first determined based on Q and S_0. As the approach flow is supercritical and the intake does not act as a flow control, B can be designed in accordance with the inflow condition. Then D is related to Q, independent of the approach-flow condition; as $Q = \sqrt{g(D/\eta)^5}$. Hager (1990) suggests a safety coefficient of $\eta = 1.25$ to avoid pressurized flow in the shaft and to prevent the formation of excessive flow depth along the outer guiding wall and cross-waves along the inlet structure. The parameters c, t and t_1 are estimated from structural considerations. The inner and outer radii (Fig. 5.8) can be determined from the geometrical relationships. The longitudinal slope inside the intake can be assumed along the outer wall. For a flat invert, the outer invert level is first determined from the geometry and the inner invert level at the same angle are the same.

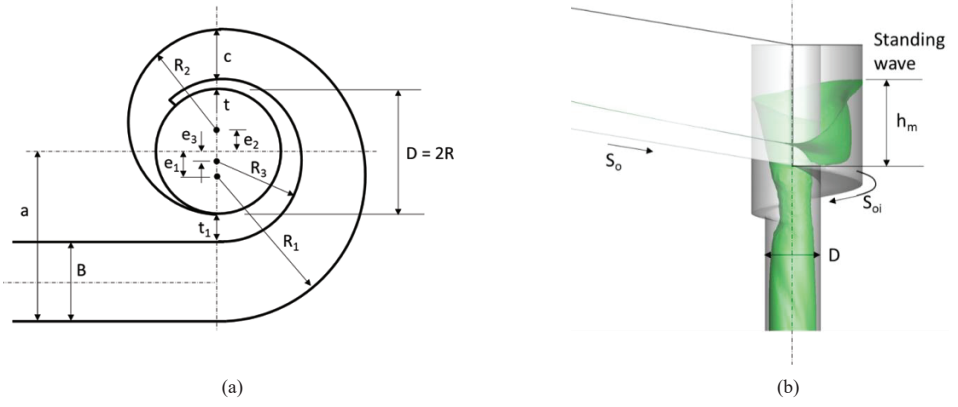

Figure 5.8 | Spiral form of a vortex intake: (a) plan view; and (b) elevation view (3D) showing flow within the dropshaft top.

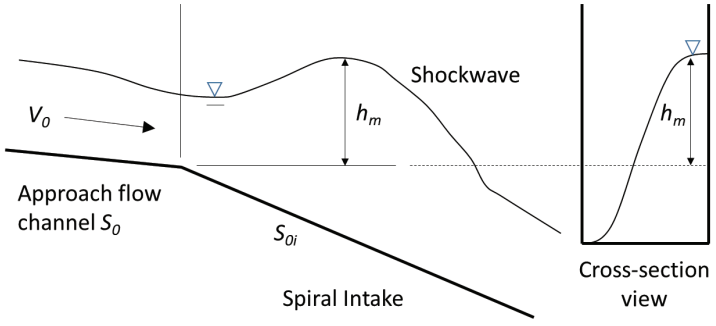

Figure 5.9 | Shockwave generated in the spiral form of vortex intake.

The hydraulics of spiral intakes have been studied using scaled hydraulic models (e.g., Kellenberger, 1988; Hager, 1990; Lee et al. 2005a). A standing wave was observed to form along the outer guide wall, the height of which is critical to avoid spilling and overtopping of the intake. Kellenberger (1988) and Hager (1990) deduced the maximum height of the shockwave with respect to the invert level of the inlet section (Fig. 5.9):

$$\frac{h_m}{R_1} = (1.1 + 0.15F_1)\left[F_1\sqrt{2Bh_1^2R_1^{-3}} - \frac{1}{2}S_{oi}\right] \tag{5.18}$$

where F_1 is the Froude number at the inlet. The location of the maximum wave height can be described using the angle $\alpha_m = s_m/R_1$ as

$$\frac{\alpha_m}{F_1} = 75\left(\frac{h_1}{R_1}\right)^{1/2} \tag{5.19}$$

The shockwave height is highly dependent on the approach flow condition. As the supercritical approach flow follows an S2 curve, F_1 increases along the channel length. Thus, long approach channels result in stronger and higher (and unstable) shockwaves. Predicted values of the maximum wave height were validated by several physical modeling studies (e.g., Lee et al., 2005a; Fernandes and Jonatas, 2019). The wall height can be determined from the above equations. Due to the complex flow nature of the spiral intake, prediction of air core size relies on laboratory experiments or CFD modeling. As found in Lee et al. (2005a), the warped invert design could result in a slightly smaller shockwave and larger air core.

5.3 | Energy dissipation

An important function of vortex-intake drop structures is to dissipate the energy of the incoming flow whilst transferring the flow to a substantially lower elevation. The spiral motion of flow results in an

extended flow path down a dropshaft. Consequently, the lengthened path enhances energy dissipation by wall friction. Increased turbulence production in the annular jet flow in the chamber and the dropshaft also causes dissipation of flow energy. Experiments show that wall friction associated with spiraling flow clinging to the dropshaft can contribute to about 30% of energy dissipation in the dropshaft of a tangential intake (Zhao et al., 2006). This amount of energy dissipation can be readily estimated using typical friction coefficients for pipe flow.

Energy dissipation can also result from the supercritical to subcritical transition, like the hydraulic jump in the tapering channel in a tangential intake. However, the most significant energy dissipation results from the plunge and the mixing in the air-water cushion in the stilling basin or deaeration chamber at the base of the dropshaft (Lee et al., 2005a; Lee et al., 2006), or due to the annular hydraulic jump in a surcharged dropshaft. Energy dissipation usually decreases with increasing discharge because less flow is in contact with the dropshaft's wall.

5.4 | Air entrainment by vortex dropshafts

Air entrainment is a critical issue in the design of intake structures. As water flows down a dropshaft, air mixes with water and causes a variety of potential problems. Trapped air can create pressure surges and oscillations in the water flow, and sometimes air can be released uncontrollably as "blowbacks" or explosive geysers (e.g., Wright et al., 2011; Cong et al., 2017). Entrained air can also cause insufflation (increased air flow), reducing the water-conveyance capacity of a drop structure. In combined sewer systems. The uncontrolled release of the entrained air can lead sewer-odor complaints. The primary objective of using a vortex intake is to create a stable flow, maximize the energy dissipation, and minimize the amount of air entrained by the flow. One advantage of vortex-intake dropshafts over simpler-to-construct plunge-flow dropshafts is that vortex intakes entrain significantly less air than do plunge-flow intakes. Experimental studies have shown that plunge-flow dropshafts entrain roughly 10–15 times more air than do vortex dropshafts of equivalent heights and flows (Lyons 2021). Lower air entrainment results in less air to manage at depth and lowers the risk of adverse conditions in the storage tunnel.

Air can be entrained into vortex-intake drop structures in a number of ways: (a) self-aeration by high speed inflow from a steep, upland catchment; (b) hydraulic jump or shock waves generated by flow in the vortex intake, notably tangential or spiral forms of vortex intake (Fig. 5.8a); (c) air dragged by water spiraling into a dropshaft; (d) entrainment by a hydraulic jump formed within a dropshaft or a subterranean tunnel (Fig. 5.10a); (e) entrainment by annular jet of water spiraling into the base of a dropshaft (Fig. 5.10b); and (f) entrainment by turbulent outflow from the drop structure. For submerged shafts

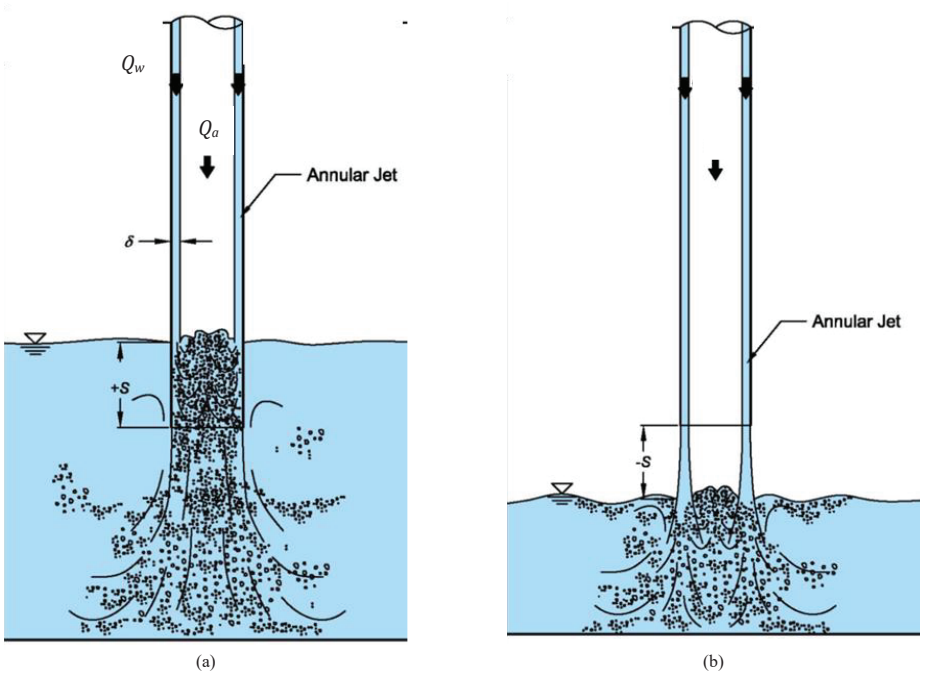

Figure 5.10 | Air entrainment in vortex-intake dropshafts: (a) dropshaft submerged ($+S$); and (b) dropshaft unsubmerged ($-S$). Note that here, δ is thickness of annular water jet.

(Fig. 5.10a), entrained air bubbles converge toward the center of the dropshaft, coalesce to form large bubbles or air slugs, then rise and release at the water surface (Jain, 1988), leading to less air transport to the tunnel. Unsubmerged shafts (Fig. 5.10b), more common in practice, always have net air transport through their dropshaft due to the annular jump occurring in the plunge pool below the dropshaft, and require air management measures to avoid potential problems (e.g., a venting pipe may be needed to exhaust entrained air).

5.4.1 | Air demand estimation

Empirical relationships for quantifying air flow (Q_a) or air demand ($\beta = Q_a/Q_w$, ratio of air flow entrained to water flow) in dropshafts have been developed based on experimental studies. Air demand depends on the type of dropshaft, water discharge, dropshaft diameter, falling distance of water, submergence of dropshaft end, and vortex circulation of the flow (e.g., Viparelli, 1961; Jain, 1988; Vischer and Hager, 1995; Zhao et al., 2006). Also, experimental studies have demonstrated that air flow is a function of dropshaft height (Kalinske, 1941; Laushey and Mavis, 1953; Viparelli, 1961; Ogihara and Kudou, 1996; Lyons, 2021).

Lyons (2021) developed an empirical relationship from experimental data collected on several drop-shafts of varying heights that can be used generally to predict β, in vortex-intake dropshafts before accounting for possible model-scale effects. A dimensional analysis of relevant parameters yielded three dimensionless relationships shown to influence air demand:

$$\left[\frac{L_s - S}{D_s}\right] = \text{drop length to shaft diameter ratio} \tag{5.20}$$

$$\left[\frac{Q_w^2}{D_s^5 g}\right] = \text{Froude number squared}$$

$$\left[\frac{Q_w}{D_s^2 V_p}\right] = \text{velocity number or area ratio (recognizing } Q = VA)$$

where L_S is the drop shaft length, S is submergence, Q_w is water flow rate, D_S is shaft diameter, V_p is velocity at the plunge point, and g is the gravitational constant (Fig. 5.10). A multiple linear regression of the experimental data yielded a mathematical model that describes the air demand:

$$\begin{aligned}\beta = {} & -5.4738 + 0.2142\left(\frac{L_s}{D_s}\right) - 4.8966\left(\frac{S}{D_s}\right) + 24.87\left(\frac{Q_w}{V_p D_s^2}\right) + 0.05\left(\frac{L_s}{D_s}\right)\left(\frac{S}{D_s}\right) \\ & - 0.9007\left(\frac{L_s}{D_s}\right)\left(\frac{Q_w}{V_p D_s^2}\right) \\ & + 14.1809\left(\frac{S}{D_s}\right)\left(\frac{Q_w}{V_p D_s^2}\right) - 1.1165\left(\frac{S}{D_s}\right)^2 + 0.0043\left(\frac{Q_w}{V_p D_s^2}\right)^2\end{aligned} \tag{5.21}$$

This relationship is like that proposed by Mahmoudi-Rad and Najafzadeh (2021) but is more generally applicable because it explicitly accounts for submergence and is developed from a larger data set. Lyons (2021) also developed a correction factor for adjusting air demand based on drop shaft height that is useful when modeling a shaft at one site but applying the same design to other sites with similar arrangements but different height requirements. The increase in air demand with increase in shaft height has also been demonstrated in laboratory studies and in field measurements involving plunge-flow drop structures (Camino et al., 2015; Ma et al., 2016, Zhang et al., 2016).

It should be noted that Eq. 5.21 is derived from scaled model experiment data and, therefore, under-predicts total air demand in the prototype. If the plunge velocity is high (say $>$ 5 m/s) in the prototype, the annular water flow clinging to the shaft could break up to form water drops which may create further air entrainment (e.g., Ma et al., 2016). Eq. 5.21 is intended to be used for guiding further detailed hydraulic model investigation, and the experimentally measured air demand can be adjusted for model scale effects (see Section 5.4.3).

5.4.2 | Effect of ancillary facilities

Significant amounts of entrained air can be transported downstream to the adit tunnel and main tunnel. A deaeration chamber with a vent pipe is often used to exhaust entrained air at the bottom of the dropshaft before connecting to the tunnel. The chamber dissipates flow energy, reduces flow speed and turbulence levels, and lets the air bubbles release from water, and thus exit from or recirculate in the structure via a vent pipe. Energy dissipating structures (e.g., plunge pools, steps, baffles) are installed at the base of the dropshaft. Conventional deaeration systems have been developed (e.g., Jain and Kennedy, 1983), including recirculation systems between the dissipation chamber and the drop shaft inlet (Kellenberger, 1988) and have been proven through extensive model testing and verified in several deep-tunnel systems.

Laboratory experiments show that submergence of the dropshaft outlet discharging into a plunge pool or deaeration chamber has a significant effect on air entrainment rates and should be considered during design. Lyons (2021) demonstrated that air flow rates could be reduced significantly by submerging the dropshaft outlet by as little as 0.5 diameter of dropshaft, and up to 90% reduction in air flow was achieved by submerging the dropshaft outlet by two diameters for dropshaft's design flow rate. The effectiveness of submergence was also shown to be a function of dropshaft height, with taller dropshafts requiring greater submergence to achieve the same air flow reductions as occur for shorter shafts. Increased air flow in tall dropshafts is likely due to higher energy at the plunge point and increased air drag downward in the shaft due to friction between the annular jet and air core inside the shaft. Additionally, for tall dropshafts, spiraling water can produce significant amounts of water drops or splash that can drag air down dropshafts (Ma et al., 2016).

5.4.3 | Scale effects

There still is a need for more research on the air transport of vortex dropshaft systems, particularly to address the problem of scale effects. Air entrainment or air flow is often underestimated in scaled model conditions, and care must be taken when extrapolating the results to prototype. Experimental evidence (e.g., Wood 1991) suggests that flow Reynolds number should be greater than 10^5 to prevent scale effects, whereas most hydraulic model experiments have been conducted at Reynolds numbers one to three orders of magnitude lower. An additional scaling factor k_a is suggested (Jain and Kennedy, 1983) for scaling the air flow rate from model measurement to prototype. The factor has the form

$$k_a = L_r^{\alpha} \tag{5.22}$$

where L_r is the prototype-to-model length ratio, and α is an exponent experimentally determined. Jain and Kennedy (1983) suggested $\alpha = 0.34$. More recently, Lyons (2021) conducted experimental

studies on vortex dropshafts that validated the scaling of air flows according to Froude's law but suggested α should be equal to 0.65. For example, air flow rate measured on a 1:10-model should be scaled up based on Froude similitude relationships, then adjusted by a factor of $k_a = 10^{0.65}$ or 4.5. Lyons demonstrated the factor suggested by Jain and Kennedy (1983) was underestimated due to differences in relative dropshaft height of their physical models. Once adjusted for shaft height, Jain and Kennedy's exponent increased to 0.67, which is very similar to the value proposed by Lyons (2021).

CFD modelling could complement physical modelling for the design of vortex-intake drop structures. CFD predictions demonstrate good agreement with measurements of free-surface profile, air-core size, and flow field, if air entrainment is not significant (e.g., Plant et al. 2016; Mulligan et al. 2018; Chan et al. 2018a; Chan et al. 2022). Nevertheless, numerical-model prediction of air concentration is still quite approximate and often lacks validation by measurements, as Chapter 3 elaborates. CFD models usually underpredict air concentration and air transport by vortex-intake drop structures (e.g., Plant et al., 2016). The processes attendant to bubble dynamics (coalescence and interaction with the highly turbulent flow) are often poorly understood and formulated. Semi-empirical air entrainment model (e.g., Hirt, 2003) have been proposed, yet their applicability remains unproven.

Though the relationships developed by physical and numerical modeling are useful, they were specific to given designs and arrangements, and care should be taken for applying them to other situations. Due to the site-specific nature of installed dropshafts, and the many factors that affect dropshaft performance, physical and numerical modeling always should be implemented to aid drop-structure design and evaluate their performance prior to construction.

5.5 | Application

Some of the earliest applications of vortex intakes for drop structures date back to the 1950-60's in Italy, where drop structures were installed for water collection from mountainous areas (Drioli, 1969). The present section briefly mentions several prominent example applications of projects employing vortex intakes and expands on facilities presently in operation in Hong Kong and London.

To be mentioned, by way of a brief example, is the Milwaukee Metropolitan Sewerage District's Inline Storage System, a 31-km-long tunnel system with a diameter of 5–9 m. The System, in Milwaukee USA, is an early example of tangential vortex-intake drop structures used together with deaeration and air-venting appurtenances. The design flowrates to each or the drop structures range from 6 to 70 m^3/s,

and dropshafts vary in diameter 1.8–3.6 m. Additionally, the System regulates combined and sanitary sewage interception with operation of a real-time control system to optimize storage and diversion to sewage treatment plants (Jain and Kennedy, 1983).

Also, to be briefly mentioned is the present development of Singapore's Deep Tunnel Sewerage System (DTSS), which includes over 80 km (50 km in Phase 1 and 30 km in Phase 2) of deep tunnels constructed at depths of 20–40 m below ground. DTSS connects stormwater and wastewater to two centralized sewage treatment plants. Eighteen tangential vortex-intakes will convey wastewater flow to the deep tunnels, with the provision of design flows up to about 20 m^3/s (Brocard et al., 2019).

5.5.1 | Hong Kong West Drainage Tunnel

Hong Kong is among the earliest places to adopt a system of vortex-intake drop structures and tunnels for collecting runoff from the hilly terrain to a coastal reservoir (the Plover Cove Water Scheme), solving the water-shortage problem faced by the city in the 1960's. The designs of the vortex intakes and air regulating structures, novel at the time, were designed based on scaled model tests (HRS, 1965). In recent years, several systems of vortex intakes and tunnels have been constructed in the urban area for flood prevention. The Hong Kong West Drainage Tunnel (HKWDT) is a notable example.

The core business district of the City of Hong Kong is located at the northern coast of Hong Kong Island while the residential district situated at the hilly slope behind the city. Intensive development and expansion of the community at the upper catchment have increased considerably the quantity of surface runoff, thereby reducing the flood-carrying capacity of the aging drainage system in densely populated, downstream urban areas. The increased runoff aggravates flooding during rainstorms and times of high tide levels. The objective of the HKWDT is to reduce the flooding risk for the low-lying urban area of north-west Hong Kong Island. Fig. 5.11 shows the layout of the HKWDT.

The HKWDT includes 34 intakes to intercept existing drains or streams from the upper catchment of Hong Kong Island (Kumar et al. 2017, Fig. 5.11). Surface runoff intercepted by the intakes, is then conveyed via dropshafts, adit tunnels, and a 10.5-km-long main tunnel (diameter is 6–7 m) to the sea. The tunnel intercepts surface stormwater runoff and discharge up to 240 m^3/s (a design storm of 200-year return period) at the final outlet portal. The length of some dropshafts is up to 180 m (Kumar et al., 2017).

As the catchment is steep and is marked with supercritical flows (speed in the order of 10 m/s) during heavy rainstorms, close to residential areas with high-priced luxury apartment buildings, spiral and

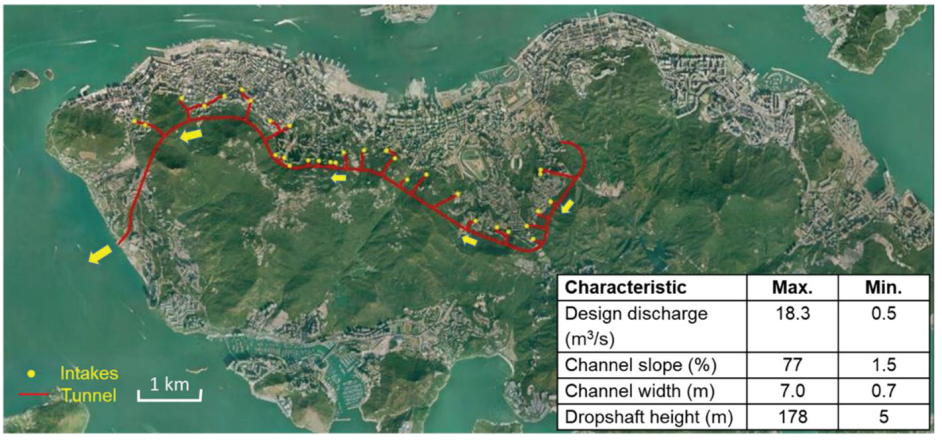

Characteristic	Max.	Min.
Design discharge (m^3/s)	18.3	0.5
Channel slope (%)	77	1.5
Channel width (m)	7.0	0.7
Dropshaft height (m)	178	5

Figure 5.11 | Aerial view of the route of the Hong Kong West Drainage Tunnel.

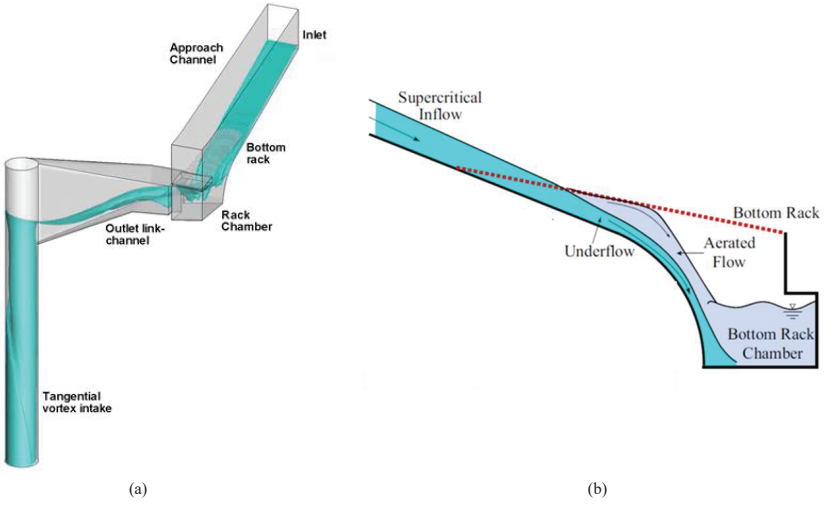

Figure 5.12 | Components of the Hong Kong West Drainage Tunnel: (a) an oblique view of the intake; and (b) an elevation view of the intake's bottom rack and bottom-rack chamber.

tangential vortex intakes were chosen as the most suitable water-interception structures. The vortex intakes were designed using physical and numerical modelling (Lee et al., 2005a; Kumar et al., 2017). The compact, space-saving intake structures divert the supercritical flow smoothly and dissipate the energy, consisting of four key elements: (a) bottom rack; (b) bottom-rack chamber connected to the vortex inlet through a link channel; (c) vortex inlet; and (d) dropshaft (Fig. 5.12a). The bottom rack and

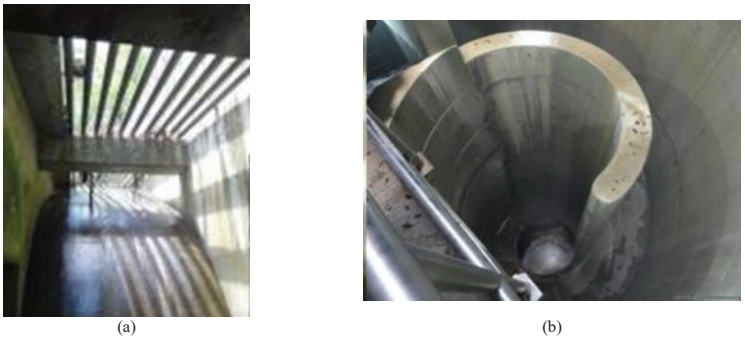

Figure 5.13 | Views of the bottom rack chamber from which water flows to the vortex intake: (a) entrance to bottom rack; and (b) vortex intake to dropshaft.

chamber (Figs. 5.12b and 5.13) help prevent trash and sediment from entering the water-collection tunnel. Further, the tunnel was designed to run as an open channel to avoid the entrapment of air.

A comprehensive physical and numerical model study was carried out to determine the hydraulic behavior of the complex three-dimensional two-phase flow in the intake structure (Lee et al. 2005b; Chan et al. 2018b). Extensive experiments were performed to establish the key performance characteristics of various designs including the following characteristics: (a) the maximum standing wave height in the vortex intake; and b) the minimum air core ratio in the dropshaft ($\lambda > 0.25$). Modeling showed that flow stability and the key performance characteristics strongly depended on the geometry of the bottom rack, link channel and vortex intake. The model tests led to an optimized design of the bottom rack structure connected to a vortex intake (spiral form with warped invert, or tangential form, depending on the interception discharge and site constrain). Intake size was determined from theory and modeling. The size of individual intakes was determined using notions of geometric similarity and application of Froude-number similitude, keeping in mind size of contributing catchment.

Completed in 2012, HKWDT, together with the underground stormwater storage schemes and other drainage-improvement works of Hong Kong City, greatly reduced the risk of flooding in downstream urban areas of the Northern Hong Kong Island. Regular operation, and maintenance of main tunnel and adit tunnels ensure the satisfactory performance of these components of HKWDT.

5.5.2 | London Thames Tideway Tunnel

London's existing combined sewer system was completed in 1875 and is an engineering marvel of the Victorian era. However, the system was designed originally to capture rainwater runoff and sewage

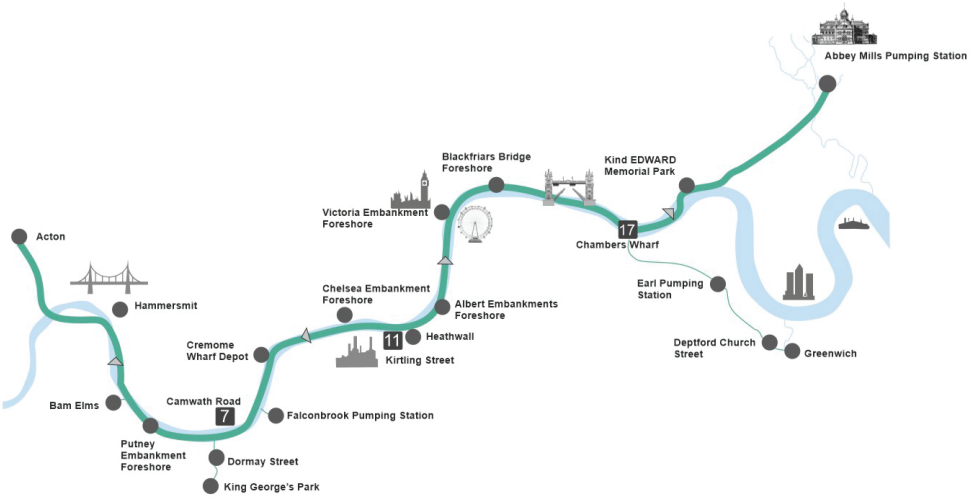

Figure 5.14 | Thames Tideway Tunnel (TTT) route, dropshaft and interception sites (•), along the Thames River, London, UK.

produced by approximately 4 million people. Since the system's construction the population of London has grown to over 9 million people by mid-2020 (Greater London Authority, 2020). Consequently, the system has struggled to cope with this growth. To prevent sewer backups and urban flooding, the system overflows into the tidal River Thames at 57 locations. Overflows occurred with as little as 2 mm of rainfall caused as much as 39 million m^3 of excess untreated wastewater to discharge annually into the River Thames (NAO, 2014). The system needed to be upgraded.

The Tideway Project is a deep tunnel system built along the River Thames, UK, to provide combined sewer overflow (CSO) control. The project features 22 tangential, vortex-intake drop structures designed to convey design flowrates ranging from 2 m^3/s to 40 m^3/s. CSO flows that would otherwise be discharged to the Thames River now are intercepted from the existing sewer network and redirected to the underground Thames Tideway Tunnel (TTT) system. The tunnel includes over 25 kilometers of 7.2-m-diameter tunnel (Fig. 5.14).

The vortex intakes and dropshafts are designed to provide high conveyance capacity though occupying a small footprint at the sites. Due to London's densely populated urban environment, the interception chambers and vortex intake structures are designed in highly constrained arrangements and the vortex intakes are more compact than the widely adopted Jain and Kennedy (1983) guidelines. Also, due to the tidal nature of the River Thames, most of the interception chambers also include flap gates to prevent river water intrusion into TTT during high tide. To accommodate existing infrastructure and multiple inlets successfully, many of the interception chambers were designed in small

footprints relative to their capacity and often feature turns, steps, combining flows, curves, orifices, penstocks, and other non-traditional features that result in highly complex hydraulics and significant design challenges.

The initial designs of the vortex intakes were developed using theory, one-dimensional calculations, CFD modeling, and physical modeling (Plant and Crawford, 2016). The dimensions of the TTT's vortex-intakes stem from research done by Yu and Lee (2009), who experimented with shorter, steeper, and

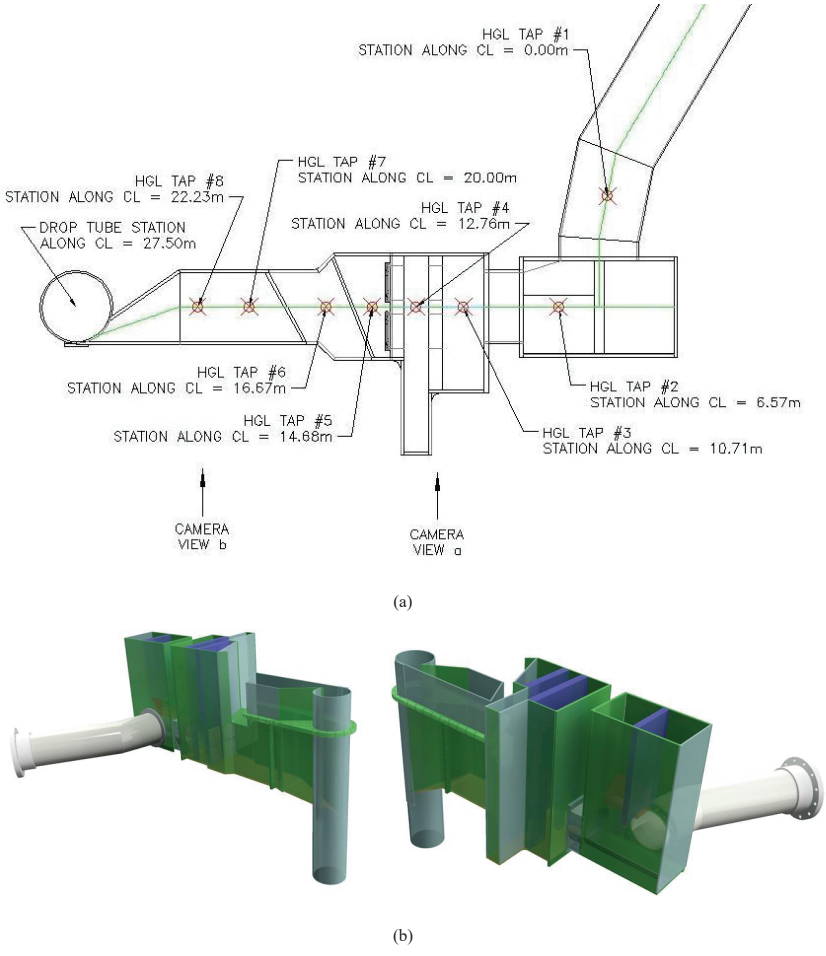

Figure 5.15 | Vortex intakes for the Thames Tideway Tunnel Project: (a) plan view of the physical model plan illustrating tapping locations for water-level measurement, camera positions and annotation identifying hydraulic features (Plant and Crawford, 2016); and (b) two 3D views of the physical model of the flow conduits leading to the vortex intake and dropshaft (Craig et al., 2015).

more compact vortex intakes than traditional designs. CFD modeling was used to develop further and test the initial vortex intake designs and the potential influence of upstream structures. These tests were followed by detailed physical modeling (Craig et al., 2013), which extensively refined then confirmed the designs. The physical models were used to test and adjust designs of the approach channels, interception chambers, flap gates, vortex intakes, dropshafts, and several arrangements of tunnel connection. The physical model focused on confirmation of the upstream water levels, stable flow conditions in the vortex inlet over the operational flow range, conveyance capacity, potential air entrainment issues, flap gate performance, and sediment and debris passage. An example of one of the layouts and design arrangements used for the physical models is depicted in Fig. 5.15.

Currently under construction and scheduled for completion in 2025, TTT will significantly reduce the occurrence of events whereby combined sewer overflows spill into the Thames River. Additionally, TTT is designed to accommodate projected population growth for the next 100 years, and thus will limit pollution from storm overflows and protect the quality of water in the River Thames.

5.6 | Concluding remarks

This chapter discussed the essentials on the designs for three common types of vortex intakes: scroll, tangential, and spiral. Vortex intakes provide stable conditions of water flow in dropshafts, and such intakes form a steady air core that minimizes air entrainment in the dropshaft. The advancement of experimental and computational techniques in the past three decades has greatly improved the understanding of their hydraulics and flow structures, as Chapters 3 and 4 explain further.

Design relationships for determining the appropriate dimensions of vortex-flow intakes are presented. Success examples in water supply, drainage and sewerage systems worldwide have proven their general applicability.

Nevertheless, the prediction of air demand and air transport still relies on the findings from physical model studies and the use of empirical relationships, and is fraught with scale effects that limit applicability for the field scale. Experience is needed to interpret results from physical models. More research is needed for developing theoretical or numerical models on the air-water flow of vortex intakes which could provide robust prediction stemming from physical model and field scale designs. Of necessity, this advance also requires field monitoring of the prototype drop structures to evaluate design performance.

CHAPTER 6

Vortex Formation at Reservoir Intakes

SUSAN J. GASKIN
Civil Engineering, McGill University, Canada. E-mail: *susan.gaskin@mcgill.ca*

ROBERT M. BOES
Laboratory of Hydraulics, Hydrology and Glaciology (VAW), ETH Zurich, Switzerland.
E-mail: *boes@vaw.baug.ethz.ch*

6.1 | Introduction

Water intakes in reservoirs concentrate swirl in the flow and, thereby, are prone to free-surface vortex formation. Notably in reservoirs for hydropower projects, vortices pose a design concern as they consume energy, reduce discharge and efficiency of hydro-machinery, and cause premature wear or damage of turbines. Factors affecting intake vortex formation, particularly submergence, and design considerations to limit their occurrence or mitigate their impact are presented. Free-surface vortices (corner vortices) can also occur at spillways and spillway gates and may reduce discharge.

6.2 | Vortices at hydropower intakes

Free-surface vortices can occur at intakes for hydropower plants with reservoirs or for run-of-the river plants. Swirl or vortices can occur when an approach flow transitions from a free-surface flow in a reservoir or a river channel to a pressure flow within the intake. Reservoirs behind large dams generally have an intake that represents a service outlet for a reservoir with a moderate submergence. In addition, they have low-level, or bottom, outlets for different purposes, such as sediment flushing. These intakes normally have a large submergence, except when reservoir levels are very low.

Vortex formation occurs due to the concentration of low levels of swirl in the reservoir by the outflow, as shown in Fig. 6.1a. The challenge of avoiding free-surface swirl and vortices increases when the reservoir is managed to make use of the full storage capacity or when inflows are reduced causing the drawdown level to be lowered, decreasing the safety margin for avoidance of air-entraining vortices, which occur at critical submergence. Run-of-river plants, which are lower head with much smaller reservoirs, have lower submergence and greater likelihood of flow asymmetries in the approach flow,

(a) (b)

Figure 6.1 | Views of vortices at dam intakes: (a) occurrence of an intake vortex in a reservoir (Yang et al., 2018); and (b) vortex formation due to flow separation around the leading edge of a pier at an intake (Rindels and Gulliver, 1983).

increasing the likelihood of vortex formation. Many modern run-of-river plants have a fixed impoundment level. Small hydropower plants are smaller in scale and budget. For such plants, although vortex formation is more likely owing to upstream river morphology, available funding commonly limits intake optimization studies (USACE, 1979; Fritz, 1984; Fisher and Frankee, 1987).

Vortex formation at a hydropower intake can negatively impact plant performance and longevity due to flow asymmetry or unsteadiness, reduced flow capacity, or entrainment of air or floating debris (Fisher and Franke, 1987; Johnson, 1988). For example, vortices reduce turbine performance due to non-uniform flow conditions or entrained air (Papillon and Sabourin, 2000), reduce flow rate (Pavelyev and Shtarev, 2005), cause local corrosion damage (e.g., of a steel lining, from the presence of air; Möller et al., 2015), cause vibrations leading to premature failure of mechanical components (Jiming et al., 2000), such as turbine-blade cracking (Fisher and Franke, 1987), entrain floating debris or, in cold climates, entrain frazil ice that accumulates on trash racks producing head loss (Jiming et al., 2000; Carriveau et al., 2002). Vortices can also negatively affect plant safety in terms of eruptions of air pockets formed at intermediate shafts, intakes, or surge chambers.

6.3 | Vortex formation, vortex types and hazards

The occurrence of vortices at reservoir intakes, especially hydropower intakes, depends on the flow dynamics upstream of the intake, which depends on the combination of geometry and discharge. Approach flows may vary over time, particularly for run-of-the-river plants, resulting in vortices that are transient and vary in strength and location with time.

6.3.1 | Geometry and approach flow

Free-surface vortices form in open-channel flows due to swirl in the approach flow concentrated by an intake. In the approach flow to a hydropower intake, swirl or vorticity is generated by shear at a boundary (particularly relevant for run-of-river plants), by the geometric configuration of the intake or at boundary discontinuities (Quick, 1970). The configuration of the hydraulic structure at the intake can be a source of vorticity arising from approach-flow asymmetry, velocity gradients (due to the boundary effect), or flow separation behind an obstruction (Durgin and Hecker, 1978). As Fig. 6.1b illustrates, piers holding trash racks can produce flow-separation vortices and are particularly problematic as they are adjacent to the intake opening and strengthen the vortex as they extend over the full depth of flow (Suerich-Gulick et al., 2014a). In multi-turbine installations having parallel intakes, vortices may occur when one or more turbines is not in full operation (Jiming et al., 2000), thereby causing asymmetric flow.

Intakes at reservoirs and hydropower plants can be located on the face of the dam, on the reservoir banks or in the reservoir at a sufficient elevation to avoid entrainment of bottom sediments. Prototype intakes are usually horizontal but can be located vertically downward or inclined from the bed (Yang et al., 2018). Depending on whether the head (water depth) above the intake is low, or high, significantly different flows can be generated, and the associated hydraulic problems are correspondingly different (Hager et al., 2020). At low-head intakes, especially for axisymmetric approach flow conditions, a significant swirl component occurs, with consequence that vortices readily generate. For high-head intakes, intake geometry must be designed so that water pressure remains above local vapor pressure to avoid cavitation damage. As intake submergence is large, air or debris entrainment normally is of less concern.

6.3.2 | Vortex types and hazards

Vortices forming at hydropower intakes (and reservoir intakes generally) are smaller in cross-sectional area than the intake area (typically by up to two orders of magnitude). Moreover, the vortices usually are transient, changing in location and intensity, thereby making them difficult to measure and characterize quantitatively.

Qualitative assessments are used to identify vortex strength based on the size of the surface depression, the behaviour of injected dye and their ability to entrain floating particles or air (Denny, 1956). A commonly used classification system is the Alden Research Laboratory system (Padmanabhan and Hecker, 1984), as described in Fig. 2.3 of Chapter 2. Vortex types VT1 to VT4 contain a forced vortex in their core (where vorticity is concentrated) and a potential (or free) vortex in their outer field,

where vorticity is much lower and is approximated as zero in some models. VT5 is in transition to a free vortex. The air core vortex, VT6, can be assumed to be entirely a free vortex. Weak vortices (VT1-2) have a mild free surface depression, dye injected at the surface forms a visible dye core, while dye injected outside the vortex is diffused by background turbulence. Intermediate strength vortices (VT3-5) have a funnel-shaped depression that does not reach the intake but does entrain floating debris. Strong vortices (VT6) have a funnel shaped free surface depression that reaches all the way down to the intake opening entraining air and (or) debris (Hite and Mih, 1994; Möller et al., 2012).

6.4 | Analytical and semi-analytical vortex models

The original analytical vortex model by Rankine (1876) has been modified to reflect the flow dynamics at horizontal and vertical intakes using empirical constants or best-fit equations (the detailed development is found in Section 2 of Chapter 2). Application of these models to hydropower intakes usually entails combined analytical and computational models. Operation of a prototype intake can result in loss of efficiency or damage when air is entrained, so a good prediction of the point for vortex onset or critical submergence is required. Interpretation of scale model results must consider the effect of the specific geometry and scale effects. A prediction of air entrainment allows the risk of damage to be assessed for given situations.

6.4.1 | Vortex models and developments for hydropower intakes

This section develops the fundamentals presented in Chapter 2 and describes the interpretation, modifications and applications to configurations found at typical hydropower intakes. To recap, Rankine (1876) proposed a model of an axial invariant vortex having a constant vorticity forced vortex inner core surrounded by a free vortex region of zero vorticity and the circulation of the periphery of the forced vortex core.

$$V_\theta(r) = \begin{cases} \dfrac{\Gamma_\infty r}{2\pi r_c^2}, & 0 \le r \le r_c \\ \dfrac{\Gamma_\infty}{2\pi r}, & r_c \le r \le \infty \end{cases}, \quad V_r = 0, V_z = 0 \tag{6.1}$$

$$p_\infty - p = \begin{cases} \dfrac{\rho\omega^2 r^2}{8}, & 0 \le r \le r_c \\ \dfrac{\rho\Gamma_\infty^2}{8\pi^2 r^2}, & r_c \le r \le \infty \end{cases}, \quad V_r = 0, V_z = 0 \tag{6.2}$$

where Γ_∞ is the bulk circulation, assumed to be a constant value far from the vortex center, p_∞, is the pressure at an infinite radius, r_c, is the core radius, ω is the vorticity of the forced core, V_r, V_θ and

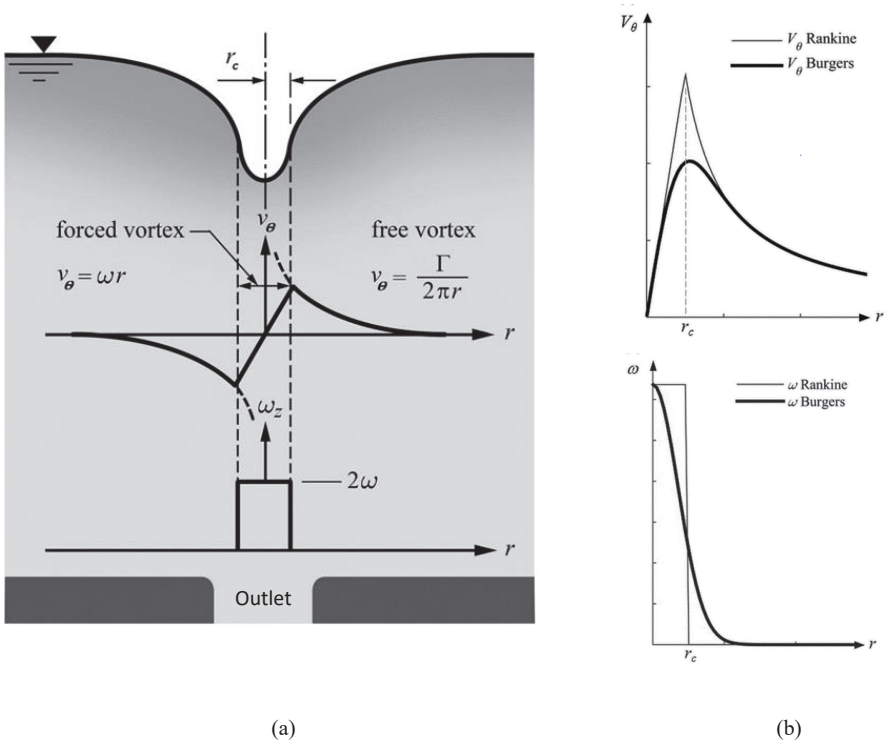

Figure 6.2 | Aspects of a free-surface vortex: (a) Rankine vortex with an inner forced vortex and outer free vortex (adapted from Möller, 2013); and (b) comparison of the azimuthal velocity and vorticity profiles of the Rankine (1876) and Burgers (1948) models.

V_z are the radial, azimuthal and axial velocities in a local cylindrical coordinate system (r, θ, z) with z pointing along the central axis of the vortex (Fig. 6.2a).

In hydropower intakes, the intake flow axially stretches the vorticity in the approach flow concentrating the vorticity into a coherent vortex due to conservation of angular momentum. Axial stretching of the vortex plays a crucial role in vortex stability (Nolan, 2001; Carrriveau, 2006; Carriveau et al., 2009). Axial stretching was incorporated in the Rankine model by Burgers (1948) and Rott (1958) resulting in the streamlines converging towards the vortex axis. Burgers (1948) and Rott (1958) also included diffusion of vorticity, which smoothed the vorticity profile and the azimuthal velocity profile as compared to the Rankine vortex model, as shown in Fig. 6.2b. The inclusion of axial stretching in Burgers' (1948) and Rott's (1958) models results in an increased strength and smaller radius due to conservation of angular momentum. Odgaard (1986) assumes that the axial velocity increases linearly from zero at the free surface to its maximum as the mean outflow velocity.

Experimental results (Odgaard, 1986; Hite and Mih, 1994; Ito et al., 2010) support the use of Burgers' (1948) and Rott's (1958) models for modelling intake vortices. Whereas intake vortices do not capture their full complexity, they form the basis of subsequent models (e.g., Lundgren, 1985; Hite and Mih, 1994; Miles, 1998; Rossi et al., 2004, Andersen et al., 2006; Stepanyants and Yeoh, 2008; Ito et al., 2010; Wang et al., 2011).

The flow structure of free-surface vortices produced in a range of experimental configurations was first observed using injected dye, which clearly delineates the vortex core (e.g., Hecker, 1978; Anwar, 1983). The flow fields formed by free-surface vortices have been measured using particle-image-velocimetry (PIV) at the surface, in plane sections and in 3D. PIV experiments for a steady air-core vortex in a cylindrical tank with bottom outlet (Duinmeijer et al., 2020) validated Burgers' model for estimating the core radius, tangential velocity profile and air core depth ($\pm$10–20%), while particle tracking velocimetry tracked buoyant particles to represent entrained debris (Suerich-Gulick et al., 2014b; Keller et al., 2014; Duinmeijer and Clemens, 2021). PIV experiments of intakes in an open-channel flow with horizontal intakes (Li et al. 2008, Keller et al. 2014) or vertical intakes (Naderi et al., 2019), representing prototype configurations, validated Burgers' model, observing the unsteadiness of the vortex position and strength. In a channel flow, the inflow into the vortex is asymmetric, due to the superposition of the channel velocity and the radial inflow velocity of the vortex, causing a secondary vortex to form, extending horizontally upstream of the air-core vortex (Naderi et al., 2019).

These different studies provide useful insights into the different processes affecting vortex characteristic. However, some phenomena are specific to certain configurations. Variations in flow rate, boundary conditions and geometry complicate the task of identifying the relevant modeling assumptions and processes for prototype configurations.

Analytical models are useful in an industry setting, as CFD still has limitations due to numerical diffusion resulting in the underestimation of vortex formation and strength (see Section 5 of Chapter 2). In an industry setting, initial assessments of an intake for vortex formation risk could be made using a fixed-lid approximation with RANS simulations using the k-ε turbulence model to estimate bulk circulation and the velocity field around the vortex, which then is used with the analytical Rankine model to obtain the geometry, and hence strength, of the vortex (Suerich-Gulick et al., 2014a,b,c). A range of values for its characteristic radius is estimated using

$$r_0 = 2(\nu/a)^{1/2}, \qquad a = \partial V_z/\partial z \tag{6.3}$$

$$a_{est} = \frac{(U_z(\beta s) - U_z(0))}{\beta s} \tag{6.4}$$

where r_0 is the characteristic radius, ν is kinematic viscosity, a is the vertical velocity gradient, V_z is the vertical velocity, β is the ratio of the distance from the free surface to the intake, U is channel velocity. The term βs indicates how far the linear section of the vertical velocity profiles extends from the free surface (in non-dimensional form), and the observed range $0.15 < \beta < 0.85$ is used as the limits (Suerich-Gulick et al., 2014abc). The tip depth, h, and nominal depression slope, $\zeta = h_{n,0}/\mathrm{r}$, are estimated using

$$h_{n,0} = \frac{0.17\Gamma_\infty^2}{\pi^2 r_0^2 g} \tag{6.5}$$

where Γ_∞ is bulk circulation of the vortex, and g is gravity acceleration. Surface-tension effects can be accounted for using the surface-tension correction factor, f_0,

$$f_{0(r_0/l_\sigma)} = \left[\exp(-0.44(r_0/l_\sigma)^2) + 1.9(r_0/l_\sigma)^{1.6}\right]^{-1} \tag{6.6}$$

where l_σ is the characteristic length of the air-water interface (Suerich-Gulick, 2013).

6.4.2 | Critical submergence

Critical submergence, S_c is of prime importance for intake design, and is widely used as a parameter to determine an incipient state for which no air is entrained by intake vortices. According to several studies (e.g., Gordon, 1970; Gulliver et al., 1986; Knauss, 1987), S_c is a function of intake Froude number, $\mathrm{Fr}_D = V/\sqrt{(gD)}$.

Knauss (1987) suggests that critical relative submergence is $S_c/D = 2V/\sqrt{(gD)} + 0.5$ for $\mathrm{Fr}_D > 0.5$. Gordon (1970) indicates that $S_c/D = \xi V/\sqrt{gD} + 0.5$, with $\xi = 1.702$ for symmetrical approach flow, and $\xi = 2.269$ for lateral approach flow. The formula suggested by Knauss applies to intakes with ideal approach conditions that do not require the use of special devices for vortex suppression. With a pre-factor of $\xi = 2$, Knauss' formula is slightly more conservative than Gordon's formula for symmetrical approach flows. Note that submergence, S, is taken relative to the center-axis of an intake's cross-section at constant pipe or penstock diameter (D) or conduit cross-section (D by b), as Fig. 6.3 indicates.

Möller et al. (2015) studied air entrainment rates due to intake vortices using a large-scale, laboratory model and proposed a new approach to determine the critical intake submergence, S_c, based on an air-allowance criterion, relating critical submergence to a minimum air-entrainment rate of $\beta = Q_a/Q_w = 1 \times 10^{-5}$. Their findings resulted in an approximation of the critical submergence

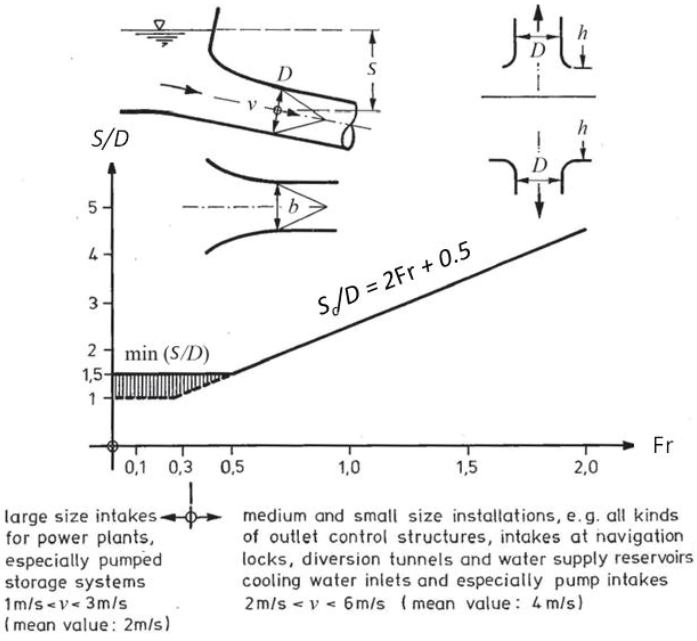

Figure 6.3 | Recommended minimum relative submergence S/D for intakes in ideal approach-flow conditions and without use of special devices for vortex suppression. Also shown are vertical intakes (up and down). (From Knauss, 1987).

as $S_c/D = -2.5(V/\sqrt{[gD]})^{-0.45} + 5.3$ for $0.26 \leq \mathrm{Fr}_D = \mathrm{F}_D \leq 1.2$; note that Fr in Figure 6.3 is based on diameter D. Fig. 6.4 compares critical relative intake submergence, S_c, of the laboratory data to their equation and those of Knauss (1987) and Gordon (1970).

6.4.3 | Effects of geometry on critical submergence

Vortex activity and hence critical submergence is affected by geometric configuration (Denny, 1956; Quick, 1962b; Anwar, 1968a; Quick, 1970; Gulliver et al., 1986; Rutschmann et al., 1987; Hite, 1991; Hite and Mih, 1994; Nakayama and Jones, 1998; Tastan and Yildirim, 2018) or different approach flow profiles (de Siervi et al. 1982, Ansar and Nakato 2001, Yang et al. 2014). Submergence criteria using potential flow models have been developed incorporating the characteristic geometric parameters of intake pipe diameter, shape and wall clearance (Yildirim and Kocabaş, 1998; Yildirim et al., 2000; Yildirim and Kocabaş, 2002; Yildirim, 2004; Tastan and Yildirim, 2010;Yildirim et al., 2012), the number and orientation of intakes (Yildirim et al., 2011; 2012; Khanarmuei et al., 2019; Hashid and Ahmad, 2022) and for different flow configurations (Yildirim and Kocabaş, 1995, 1998). Statistical methods and machine learning techniques have also been tested and continue to be developed (Kocabaş and Unal, 2010; Kocabaş et al., 2013).

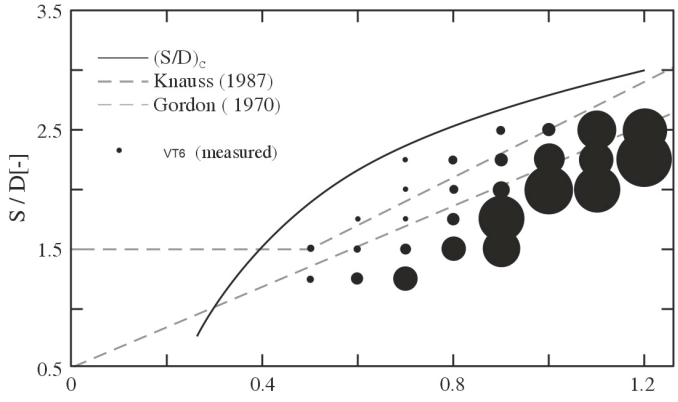

Figure 6.4 | Critical relative intake submergence, S_c, (solid line) as defined for a mean air entrainment rate of VT6 phases, $\beta_{VT6} = 1 \times 10^{-5}$ (see Eq. (6.8)) and approximation of critical submergence (solid line) in comparison with Knauss (1987) and Gordon (1970) (symmetrical approach flow) (adapted from Möller et al., 2015).

6.4.4 | Effects of surface tension, viscosity, and turbulence on critical submergence

The observations from hydraulic models, used to identify the occurrence of free-surface vortices, are subject to scale effects when translated to the full-scale prototype (see Chapter 3). Froude similarity is implemented in scale models. Consequentially, the Weber number (quantifying the effect of surface tension) and the Reynolds number (quantifying the effect of viscosity) do not match when the model and prototype use water and the experiments are performed at the Earth's surface (i.e., the viscosity, surface tension and density of water and acceleration due to gravity are the same). The resulting scale effects lead to uncertainty in the interpretation of model results to the prototype (Heller, 2011).

The impact of scale effects is usually minimized by meeting minimum Weber and Reynolds numbers (see Chapter 3). Surface tension effects are determined by the shape and the scale of the laboratory vortex and have a greater effect on a dimple vortex than on a funnel vortex at scales comparable to the characteristic length of the air-water interface (l_σ) as shown in Figure 6.5 (Suerich-Gulick et al., 2014c). A dimple vortex is a VT1-2 vortex with a milder slope and a funnel vortex is a VT3-5 vortex with $\zeta \geq 5$, where $\zeta = h_0/r_0$, h_0 is the maximum dimple depth and r_0 is the characteristic radius. The scale effect can be estimated using a correction factor (Suerich-Gulick et al., 2014c). The use of a factor suggests that empirical, surface-tension, scaling laws developed from the onset of air entrainment (i.e., deep funnel vortices) should not be directly applied to scale models of hydropower plants in which only dimple vortices form (Suerich-Gulick et al, 2014a). Scale effects due to viscosity and turbulence have so far been difficult to predict or explain, with the proposed model unable to reproduce independence

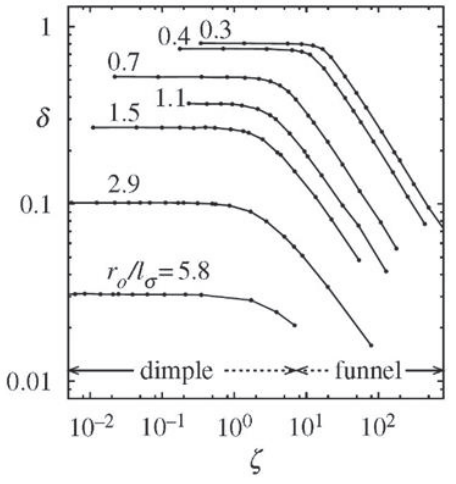

Figure 6.5 | Relative surface tension effect, δ, on vortex depth as a function of the depression scale, r_σ / l_σ, and nominal slope, ζ, where l_σ is the air-water interface characteristic length and r_0 is the characteristic vortex radius (adapted from Suerich-Gulick et al., 2014c).

from Reynolds number, although a decreasing sensitivity to Froude number is shown (Suerich-Gulick et al., 2014c). As a rule-of-thumb (Möller et al., 2010), vortices observed in typical small-scale models are considered, for the prototype, to be the same as two type classes above (e.g., a VT3 in the scale model would likely be a VT5 in prototype).

6.4.5 | Entrainment of air or debris

Air entrainment by vortices is a concern for hydropower intakes as such entrainment reduces turbine efficiency, results in unsteady flow, and reduces flow discharge (Möller et al., 2015). Small amounts of air can decrease turbine efficiency with efficiency loss varying as the square root of the air/water ratio with greater losses occurring for lower heads (Denny and Young, 1957; Papillon et al., 2000). For example, for similar flow conditions, at a head of 30.5 m, efficiency loss increased from 1% to 2.5% for an air/water ratio increasing from 0.5% to 1.5%, whereas at a head of 7.2 m, efficiency loss increased from 3% to 5% for an air/water ratio increasing from 0.5% to 1.5% (Papillon et al., 2000). Entrained air causes unsteady flow producing harmful vibrations or abnormal pressure surges (Zhou et al., 2002, 2013a, b).

Early research roughly quantified air entrainment rates in pumps with estimates varying by an order of magnitude with values of β of up to 10%. Maximum values of volumetric air concentration rates (or void fraction), $C_a = \beta/(\beta + 1)$, were presented graphically as a function of the submergence Froude

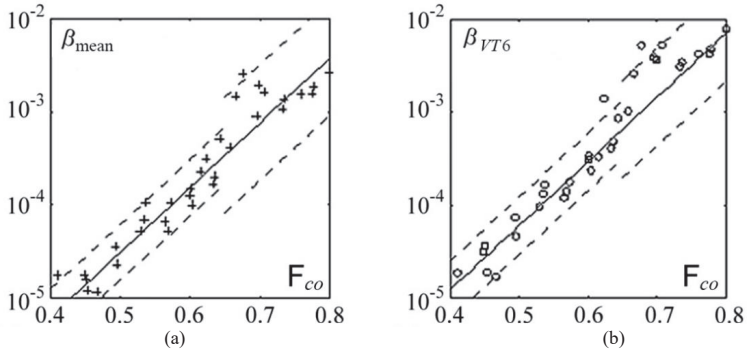

Figure 6.6 | Air entrainment rates, β, versus Fr_{co} with 95% prediction band. Subdivision at $Fr_{co} = F_{co} = 0.66$ accounts for varying prediction widths: (a) mean air entrainment rate, (b) mean air entrainment rate of VT6 phases (adapted from Möller al., 2015).

number, $Fr_s = Fr_{co} = v_D/\sqrt{gS}$, where v_D is the cross-sectionally averaged velocity at the intake and S the intake submergence, with most values below $C_a = 1\%$ (Padmanabhan 1984). Careful quantitative experiments were conducted by Möller et al. (2015) using a sophisticated de-aeration system. The data analysis of 34 experimental runs resulted in a parameter fit describing the air entrainment rates at horizontal intakes (e.g. hydropower intakes). Fig. 6.6 shows that β strongly correlates with F_{co}. A regression analysis, where β_{mean} is the overall mean air entrainment rate, β_{VT6} is the mean air entrainment rate of *VT*6 phases, and $Fr_{co} = F_{co}$ is the combined or submergence Froude number, resulted in

$$\beta_{\text{mean}} = 1.04 \times 10^{-8} \exp(16\, Fr_{co}) \tag{6.7}$$

$$\beta_{VT6} = 2.00 \times 10^{-8} \exp(16\, Fr_{co}) \tag{6.8}$$

The boundaries are given by $Fr_{co} = 0.36$ to 0.8, because the air-entrainment rate at $Fr_{co} = 0.36$ was below the measurement limit of $\beta = 1 \times 10^{-5}$. Approximately, $\beta_{VT6} \approx 2\beta_{\text{mean}}$, indicating thereby that air entraining VT6 vortices are unsteady.

6.5 | Mitigation measures

Mitigation measures entail reducing substantially or eliminating the risk of (or range of conditions under which) vortex formation occurs. Measures include modifying the approach flow or installing a device to break swirl in the flow at the intake entrance. Alternatively, in some situations, weak vortex formation can be tolerated, and the impacts of air entraining vortices reduced by implementing

measures for de-aerating the flow downstream of the intake (Wickenhäuser and Minor, 2007; Wickenhäuser, 2008). Such situations normally involve medium- to high-head hydropower plants in which there is sufficient flow length in which to implement the flow measures like placing a de-aeration dome above the tunnel soffit to collect and remove air pockets.

Run-of-river hydropower plants with low intake submergence and often complex approach flows are more vulnerable to the risk of free-surface vortex formation. The risk can be reduced by straightening the approach flow, using submerged vanes to re-direct approach flows to reduce swirl or modifying the gates and racks to reduce flow separation (Gulliver et al., 1986; Rutschmann et al., 1987; Yang et al., 2018). Structural devices such as anti-vortex plates or vertical vanes can be installed at the intake structure to disrupt swirl at the intake (Borghei and Kabiri-Samani, 2010; Naderi, 2013; Naderi and Gaskin, 2018). Recently, a hydraulic based, anti-vortex method using a momentum water jet to disrupt the vortex at the intake was investigated and showed promise (Taherahamsi et al., 2018). These mitigation measures, however, can involve substantial civil works to be implemented. The merits of individual measures need to be assessed for each site of a hydropower plant.

Fig. 6.7 illustrates an example of modifying and straightening a flow to a run-of-river hydropower plant proposed to be retrofitted to an existing navigation dam on the Mississippi River (Ettema et al., 1996). A physical model was used to determine the required geometry of flow straightening vanes

Figure 6.7 | A view showing a trial set of flow-guidance vanes used for flow straightening at the entrance of a prospective, run-of-river hydropower plant. (Ettema et al., 1996).

used to ensure a suitably uniform and free of swirl approach flow. One layout of five guide vanes (panels 9.2 m high) placed in the approach flow to the powerhouse is shown in Fig. 6.7. Swirl to the sides of the approach flow were deliberately developed to give fish (and boaters) the opportunity to escape the flow into the turbines. In the end, the power facility did not proceed owing to several factors, including cost of straightening the approach flow.

The basic goal of most structural mitigation measures is the extension of the vortex tube between the reservoir level and the intake. This goal is achieved in various ways, for example by cantilevering structures at the intake itself. Fig. 6.8 shows a selection of four general concepts tested for an existing reservoir intake in The Swiss Alps with drawdown level at 1720 m asl, at which intake vortices occur close to the trash rack at the left side of the intake. Concepts (b) and (d) of Fig. 6.8 proved to be efficiently avoiding air-entraining vortices for an intake discharge of 80 m^3/s, whereas an adapted concept (d) with extension of the roof slab beyond the rear of the intake even suppressed vortices for intake flows of 100 m^3/s.

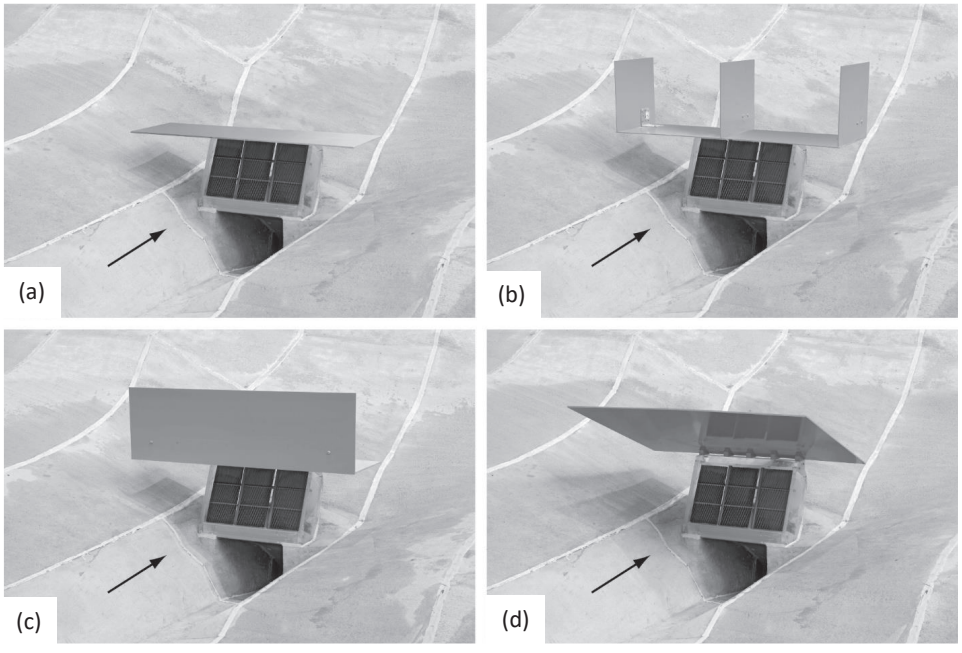

Figure 6.8 | Views showing a trial set of intake vortex suppression methods by cantilevered structures on top of an existing intake (view in flow direction): (a) horizontal cantilever slab; (b) horizontal cantilever slab with three vertical walls parallel to the axis of the intake structure; (c) L-shaped roof slab; and (d) pitched roof slab at an angle of 22° to the horizontal, perpendicular to the trash rack plane, extending up to the reservoir drawdown level (from Möller et al., 2010).

6.6 | Spillways

Spillways provide a means of controlling water levels in reservoirs and outflow from reservoirs. Gated spillways are free-surface flows, which can develop unwanted swirl and vortices at the intake side reducing their discharge capacity, as shown in Fig. 6.9. Gated spillways often are susceptible to vortex formation because of the relatively low submergence of a gate. Additionally, the operation of one or several gates in a series of gates may introduce flow swirl and, thus, vortex formation, which may decrease the flow capacity of the open gates. The critical submergence criteria shown in Fig. 6.3 applies also to spillway gates and should be used in gate design and operation.

Corner vortices of types VT1 to VT6 (Hecker, 1984) develop upstream of sluice gates with underflow due to stagnation flow, causing shockwaves downstream of the gate section (Fig. 6.9). For inviscid flows the vortex is typically of type VT5 and may vary from VT4 to VT6 provided the relative gate opening $A = a/h_o$ is above 0.15, with a = gate opening and h_o = approach flow depth (Fig. 6.9). For $A < 0.15$, the vortex type decreases sharply towards zero. Roth and Hager (1999) propose an anti-vortex device to reduce shock waves by about 50%. The device can be simply added to existing gates. The authors also give limit gate opening values as a function of channel width for Froude similarity.

At low-level outlets of reservoir dams, shockwaves forming downstream of the gate may lead to a complete filling of the tunnel cross-section, possibly resulting in slug flow and flow pulsations, to be avoided for operational safety reasons. Pagliara et al. (2023) performed physical model tests to

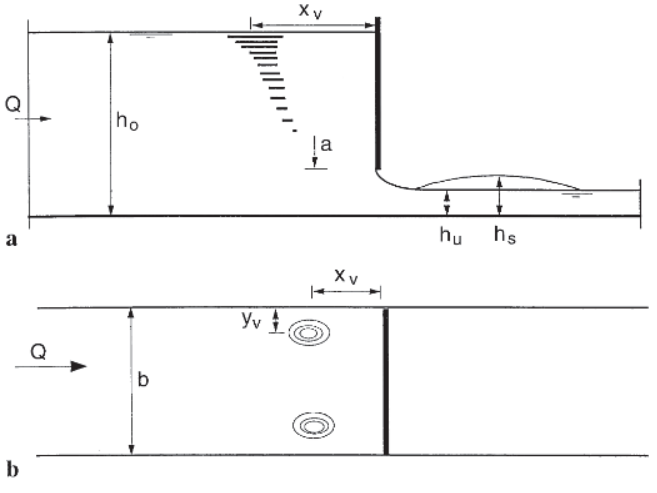

Figure 6.9 | Definition sketch of corner vortices with a) section and b) plan view (adapted from Roth and Hager, 1999).

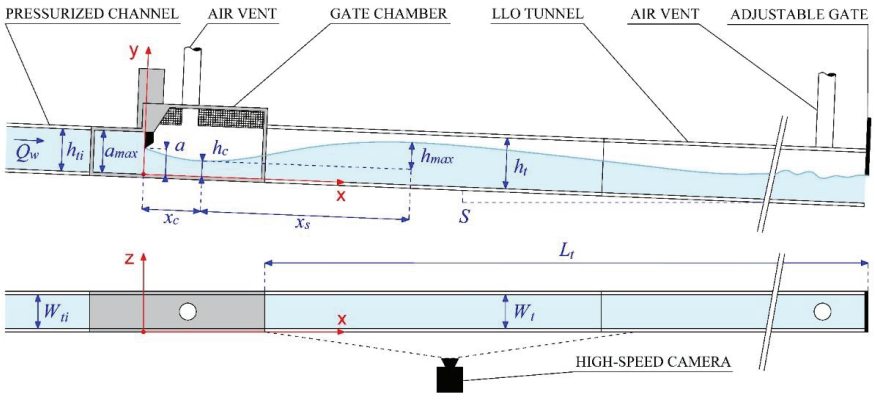

Figure 6.10 | Definition sketch of experimental apparatus along with the main parameters with longitudinal section (top) and plan view (bottom) (from Pagliara et al., 2023).

investigate the effects of relative gate opening A, energy head H, and contraction Froude number Fr_c on the geometrical features of shockwaves occurring downstream of high-head sluice gates; Fr_c. is Froude number at the contraction flow depth, h_c. The maximum wave height $h_{\max}$ measured above the contraction flow depth and its corresponding longitudinal position, x_s, measured downstream of the contraction position, x_c, were obtained by an image analysis of 15 side-view pictures for each tested condition (Fig. 6.10). Empirical equations for predicting $h_{\max}/h_c$ and x_s/h_c as a function of F_c only were derived, to be used for design purposes, e.g., to estimate the minimum required tunnel height in the range $9 < \mathrm{Fr}_c < 41$; Eqs. (6.9) and (6.10), respectively:

$$\frac{h_{\max}}{h_c} = 0.082\,\mathrm{Fr}_c - 0.260 \tag{6.9}$$

$$\frac{x_s}{h_c} = 13.50\frac{h_{\max}}{h_c} \tag{6.10}$$

Results from the model tests were validated against prototype observations at the middle outlet of Luzzone Dam (Hohermuth, 2019), showing a good agreement. Moreover, results were compared to data obtained by Roth and Hager (1999) for sluice gates with underflow to extend the application range of these prediction equations to $\mathrm{F}_c \geq 3$. Accounting for differences in methodology, the two datasets agree well (Fig. 6.11), and the prediction equations are still valid with the introduction of a 20% increasing factor computed on the total shockwave height ($h_{\max} + h_c$). Note that these results are only applicable to gate chambers characterized by either no-expansion from the gate section to the downstream tunnel in plan, or a gradual one (i.e., expansion not leading to flow separation), whereas they do not apply to abrupt expansions after the gate.

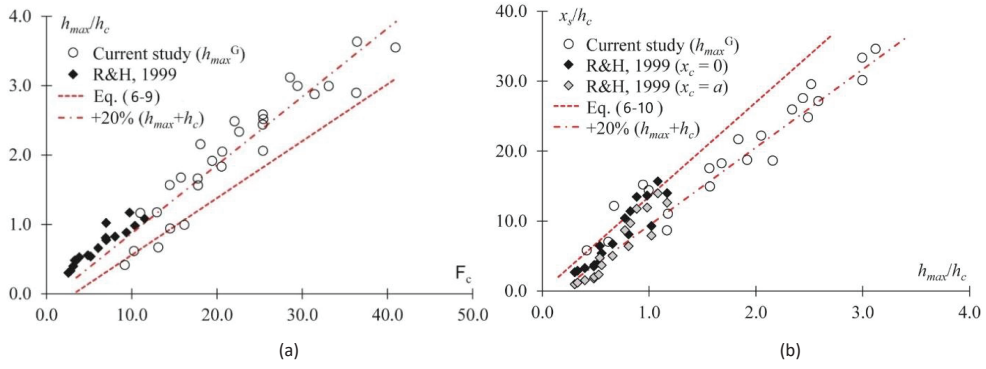

Figure 6.11 | Comparison of shock wave heights at low-level outlets with those downstream of sluice gate investigated by Roth & Hager (1999), i.e., "R&H", for the global maximum (h^G_{max}) data elaboration method: (a) h_{max}/h_c vs F_c; and (b) x_s/h_c vs h_{max}/h_c with the prediction equations (Eq. 6.9) and (Eq. 6.10), respectively; black diamonds: $x_c = 0$; grey diamonds: $x_c = a$ (adapted from Pagliara et al., 2023).

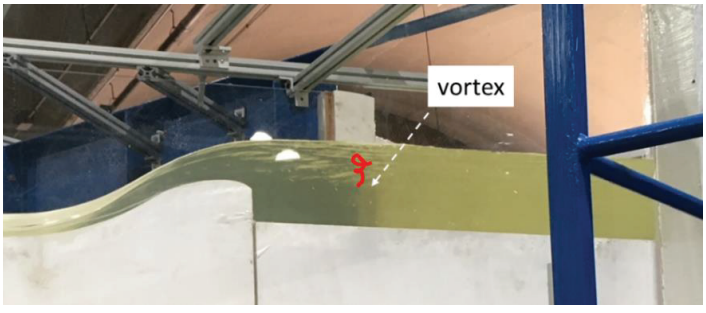

Figure 6.12 | Vortex formation caused by approach-flow separation from an abutment consumed energy for flow down a spillway but did not affect uniformity of flow over an ogee crest: an elevation view showing the location of the vortex at the top of the spillway (Thornton et al., 2021).

An interesting case of vortex formation occurred at gates of a dam in California (Thornton et al., 2021). Vortex formation upstream of the spillway's ogee crest is shown in Fig. 6.12, which illustrates vortex formation (VT2) developed when flow separated from the circular abutment guiding flow to the crest. The vortex was sufficiently far upstream of the crest that it did not adversely affect uniformity of flow over the crest, but the vortex resulted in energy loss. An important consideration to ensure spillway capacity for spillway intakes is to ensure that flow remains uniformly distributed over the spillway crest. The choice of intake location is governed by local features of terrain and dam disposition, as shown by the examples in Figs. 6.7 through 6.12.

CHAPTER 7

Vortex Formation at Pump Intakes

TROY C. LYONS
University of Iowa, IIHR. E-mail: *troy-lyons@uiowa.edu*

SEAN MULLIGAN
VorTech Water Solutions Ltd, Galway, Ireland. E-mail: *sean.mulligan@vortechws.com*

ROBERT ETTEMA
Civil & Environmental Engineering Dept., Colorado State University, USA.
E-mail: *Robert.Ettema@colostate.edu*

7.1 | Introduction

The flow field in a pump intake should not be marked by swirl or presence of vortices. Such flow features consume energy and, therefore, require increased pump energy to deliver a given discharge and may increase wear of parts of the pump. This chapter briefly describes how design of intakes for vertical pumps largely concerns eliminating swirl and vortices. Knauss (1987) extensively discusses problems connected to unwanted swirl and vortices at vertical-pump intakes.

Many water-use facilities need pump intakes. Fig. 7.1 depicts the main layout features of a typical pump intake. As early studies remark (e.g., Denny 1956; Gordon 1970; Reddy and Pickford, 1972), pump-intake design and operation usually entail overcoming problematic flow-related concerns to ensure satisfactory performance of the vertical pumps that they house. The intake draws water from a water body (e.g., a river, lake, or cooling-tower basin). The water is first screened to separate liquid water from debris and ice (or to keep out biota) then passes into one or more pump bays (for individual pumps), whence a vertical pump withdraws the flow.

There are many variations of the generic intake layout illustrated in Fig. 7.1. The variations adapt the pump bays to local site conditions, design of the debris-screening system, and pump arrangement within an intake. For example, water may enter a pump intake after having first passed through a simple trash rack, a series of cylindrical wedge-wire screens, a gate, or other geometric transitions, where it then flows to pump bays (or sumps) at individual pumps.

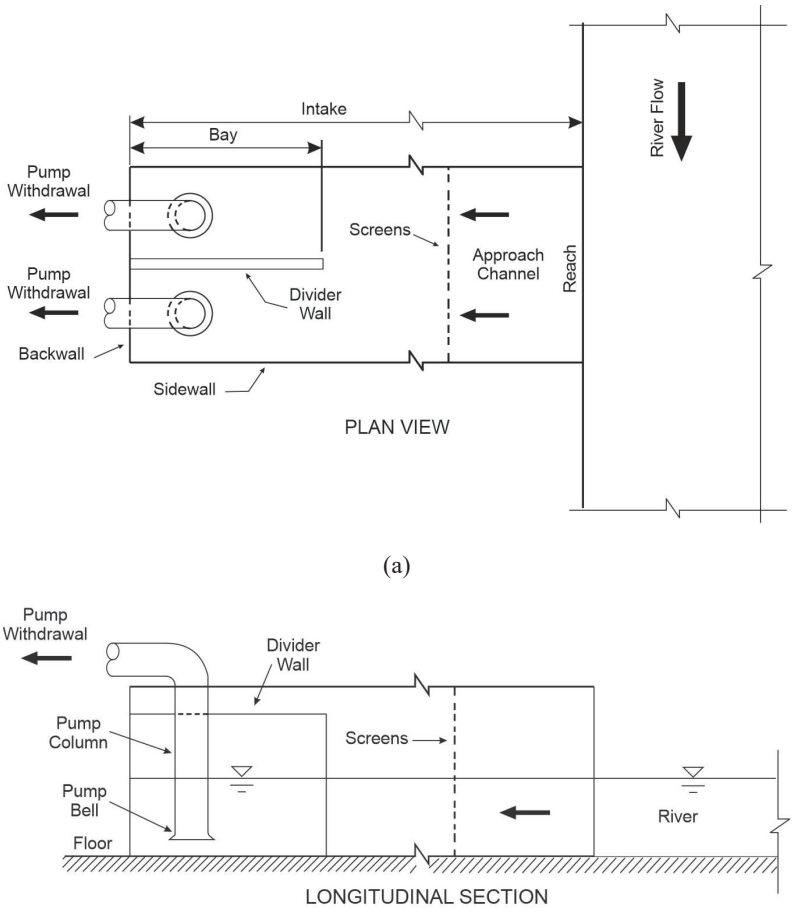

Figure 7.1 | General features of a pump intake: (a) plan view; and (b) longitudinal section.

Ideally, the flow entering a pump bay and approaching a pump column should be uniformly distributed (laterally and vertically), steady, and should not form vortices or provide a continuous source of vorticity. These conditions comprise the main design concerns for pump intakes. In practice, however, it is not possible to eliminate all flow non-uniformity or vortices. Moreover, the presence of side and back walls, plus other structural features, modifies flow distribution. Consequently, the design task is to define acceptable limits for these and other parameters, and to use various corrective devices that ensure suitable pump performance. Knauss (1987), ANSIHI (1998), Ettema et al. (1998), USACE (1995) and Jones et al. (2008), for example, give layout recommendations for pump intakes. Claxon et al. (1999) usefully comments on ANSI/HI (1998).

7.2 | Typical flow problems

The following flow problems typically occur at pump intakes:

- Free-surface vortices, if strong enough, may draw air from the free surface into the pump, causing unbalanced loading of the impeller, periodic vibration, and reduction in pump capacity.
- Subsurface vortices, originating from the floor, backwall or sidewalls, and in the case of a pressurized sump, from the ceiling, may enter the pump and cause vibration and cavitation.
- Circulation of the flow entering the pump may alter the angle of attack of the impeller blades, thereby potentially affecting pump efficiency and causing cavitation.
- Uneven distribution of flow at the pump throat may result in unbalanced loading of the impeller.

These problems are discussed quite extensively in the literature on pump intakes (e.g., Tullis 1979; Sweeney et al. 1982; Knauss 1985; Padmanabhan 1987; Hecker 1987a, b; Melville et al. 1994; Ettema et al. 1998 Jones et al. 2008) and usually are attributable to the following causes:

- Flow conditions in the flow field external to an intake.
- Uneven distribution of flow within an intake.
- A stagnation region forms inside the intake, just downstream of the upstream corner of the diversion.
- Large-scale turbulence generated in the flow within an intake.
- Vorticity generated by flow past pier noses, screen supports and other structural members within an intake.
- Vorticity generated at fluid shear zones formed at discontinuous flow boundaries in the vicinity of the pump (e.g., the corners of a rectangular sump).
- Vorticity generated in the boundary layer at the sump walls and floor.
- Vorticity generated by flow past the pump column.
- Significant unsteadiness of flow through the pump throat.

7.3 | External flow field

Flow features such as streamline curvature and flow separation at an intake, and possibly crossflow currents at an intake face, may produce adverse flow conditions at a pump intake. To design intakes and appropriate flow-control measures, it is important to understand these flow conditions.

Consider the 90-degree rectangular diversion on a fixed bed channel carrying steady discharges in the main channel and in the diversion, such as Fig. 7.2 shows for a pump intake located in a

Figure 7.2 | A large, pump intake adjoining a bank of the Chattahoochie River, Georgia The arrow indicates flow direction in the river.

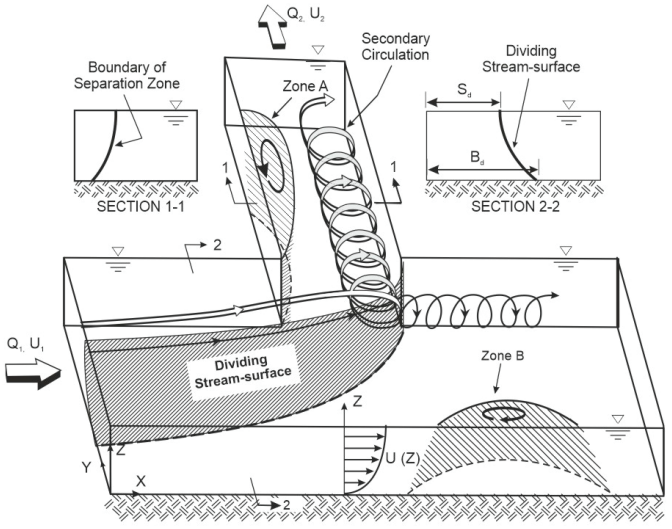

Figure 7.3 | Flow features of a 90° rectangular diversion (Ettema et al., 1998).

riverbank. Fig. 7.3 indicates the discharges (Q_1, main channel discharge; Q_2, discharge diverted into the intake), their commensurate unit discharges (discharge per unit width of flow, q_1 and q_d, respectively) and average velocities (u_1 and u_2, respectively) and angle at which flow is diverted into the

intake, θ. Though Fig. 7.3 is a simplification of the flow field along a riverbank (e.g., the effects of bedforms and vegetation are not included), the flow fields reveal several prominent flow features:

- A stagnation region forms in the river, just downstream of the downstream corner of the diversion.
- A dividing streamline in the river delineates the flow entering the diversion relative to the flow continuing downstream.
- If the intake is set back from the river, and has a forebay, a separation zone may form along the upstream wall of the forebay.

The presence of dunes can make the flow patterns in Fig. 7.3 more irregular, though the main flow features remain the same (e.g., discharge pumped from the intake). Laboratory experiments give quantitative values for the flow features in Fig. 7.3 (e.g., Neary and Odgaard 1993; Barkdoll et al. 1997; Neary et al. 1999; Hsu et al. 2002; Herrero et al. 2015). Neary and Odgaard (1993), for example, proposed relationships developed from laboratory investigations for the width of the surface and bottom dividing streamlines (when $0.2 < u_2/u_1 < 1.0$) for the rough bed channel (Darcy-Weisbach friction factor, $f = 0.05$). The relationships are useful when designing techniques for skimming drifting ice and debris conveyed with the flow (Kubit and Ettema 2001), or bed sediment transport toward the pump-intake (Ettema et al. 1998; Barkdoll et al. 1999).

7.4 | Flow field within pump intakes

The flow field within a pump intake can be marked by non-uniformity of the flow to individual pumps leading potentially to vortex formation. The following specific vortices are of concern for flow fields:

- Surface vortices.
- Subsurface vortices
  - floor-attached vortices
  - backwall-attached vortices
  - sidewall-attached vortices.

The term “-attached” is used for subsurface vortices, because they are wall-bounded at one end by a wall of the intake. Their other end extends into the pump column and ultimately is chopped by the pump impeller. Constantinescu and Patel (1998), for example, gave a detailed diagnostic description of vortex behavior, as determined by means of numerical simulation.

Intakes at dams and hydropower plants can be located on the face of the dam, on the reservoir banks or in the reservoir at a sufficient elevation to avoid entrainment of bottom sediments. Prototype intakes are usually horizontal but can be located vertically downward or inclined from the bed (Yang et al. 2018).

Depending on whether the water depth (head) on the intake is relatively low or high, significantly different flows can be generated, and the associated hydraulic problems are correspondingly different (Hager et al. 2020). At low-head intakes, especially for axisymmetric approach flow conditions, vortices occur, and significant swirl components develop within intakes. For high-head intakes, intake geometry must be designed so that water pressure remains above local vapor pressure, and therefore cavitation damage does not develop. Also, for high-head intakes intake submergence is large, and therefore air or debris entrainment usually is not of concern.

7.4.1 | Water-surface vortices

When describing water-surface vortices, it is helpful to characterize or classify their strengths. Several methods have been proposed to classify the type of vortex that may occur within a pump intake. One of the most popular methods is the system proposed by Alden Research Laboratory (ARL). This classification system is based on the identification of distinct flow features indicative of a gradation of vortex strength. For surface vortices, the basic idea is that stronger vortices are needed to ingest more buoyant material, the material varying from neutral density (dye), to floating trash, to air. The ARL classification system for types of surface vortices (VT) is shown in Fig. 2.3 (Chapter 2). VT3 surface vortices produce a dye core and define the transition from general swirl (VT2) to concentrated vorticity from the free surface to the inlet VT4. Also, VT3 vortices involve minimal depression of the water surface. Vortex types above VT3, are stronger vortices; namely, VT4 (capable of ingesting floating trash but not air; VT5 (capable of ingesting air bubbles); and VT6 for which a full air core exists from the free surface to the inlet. Fig. 7.4 depicts a surface vortex (VT5) that ingests air within a laboratoryscale pump intake.

7.4.2 | Subsurface vortices

Subsurface vortices typically emanate from the floor and walls of a bay. They are visible only when identified using dye tracers injected near their location, or when the pressure at their core is so low that they develop a core of air and water vapor. Consequently, they usually are very difficult to detect in a full-scale pump intake. Figs. 7.5a–c respectively depict backwall-, floor-, and sidewall-attached vortices identified in laboratory models of pump intakes.

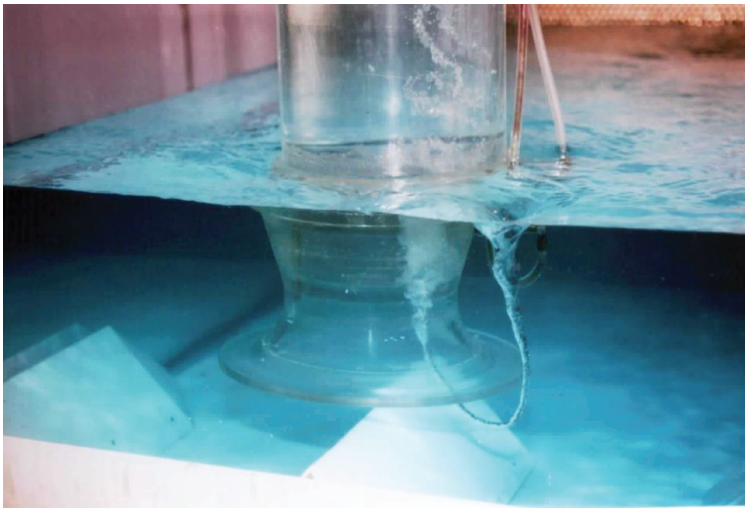

Figure 7.4 | A surface vortex (VT5) entraining air into a pump column. The intake for the pump is fitted with floor and corner splitters. (IIHR, University of Iowa).

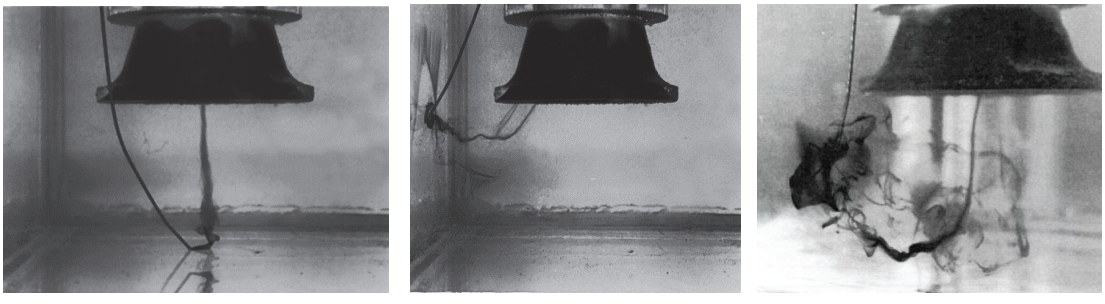

(a) (b) (c)

Figure 7.5 | Subsurface vortices illuminated using dye: (a) floor attached; (b) backwall attached; and (c) sidewall attached. (IIHR, University of Iowa).

As with surface vortices, classifying the range of strengths of subsurface vortices with the ARL classification system is useful. Type 1 (VT1) subsurface vortices are weak swirls while VT2 and VT3 have a coherent core as shown in Figs. 7.5a–c. VT3 vortices have a relatively strong core, and they cause low pressures at the core, sufficient to release dissolved air and water vapor as bubbles in the water.

Vortices may occur intermittently in pump intakes, forming, moving, collapsing then reforming. Some persist for long periods, notably floor-attached vortices beneath a pump bell or an air-entraining

surface vortex. In evaluating the significance and type of an intermittent vortex, it may be useful to monitor the relative period over which it forms. Measurements of the time of occurrence of vortex types can be plotted as a cumulative frequency plot (vortex type versus frequency of vortex type less than or equal to the given type) or a persistence plot.

7.4.3 | Vortex formation sensitivities

Most previous studies of pump-intake flows indicate the importance of non-uniformity of the approach flow. The effect of circulation in the approach flow on free-surface and subsurface vortices is frequently mentioned in the literature but is seldom quantified with the detail given here.

Based on studies of air-entraining vortices at horizontal pump-column intakes, Quick (1970) concluded that formation of such vortices was influenced by the vorticity and unsteadiness in the approach flow as well as the intake geometry. He found that the level of swirl in the approach flow is approximately equal to the circulation in the pump-column intake. Knauss (1987) studied the influence of circulation in the approach flow on the critical submergence and found a significant increase in the strength of vortices when the swirl in the incoming flow (roughly defined as the ratio of the transverse to the longitudinal velocity component) was increased. He proposed an empirical relation between the critical submergence, circulation in the approach flow, and pump-column diameter. Similar relations were obtained by Daggett and Keulegan (1972) and Jain et al. (1978) for free-surface vortices in a cylindrical tank with a bottom orifice. Quite different methods were adopted for inducing swirl. For example, Denny (1956) allowed the flow to enter through part of the channel width, while Tagamori (1980) used guide vanes to create the swirl. The experiments by Amphlett (1978) and Tagamori (1980) were used to determine the constant in Knauss' correlation. Several analytical relations to determine the critical submergence, like the ones based on empirical data, were proposed in the literature. They face the same shortcomings as their empirical counterparts. Hecker (1987) found that subsurface vortices are more likely to form, or grow in intensity, when the ratio of the intake-pump-column velocity to the approach flow velocity is increased, or the circulation in the approach flow is increased, or the distance to the lateral walls is decreased. The location of the pump column relative to the sidewalls and approach flow non-uniformity also influences the intensity of swirl angle inside the pump column. This feature of the flow is of major importance in pump-intake design. Rajendran and Patel (1998) and subsequent studies (e.g., Gessler et al. 2017) use numerical and laboratory models that illuminate how the geometry of an intake affects the intake's flow field.

The principal conclusion from these studies is that vortices in pump intakes depend on swirl in the approach flow (i.e., non-uniformity of approach flow).

7.5 | Considerations in the design of pump intakes

In practical terms, satisfactory design of pump intakes requires the appropriate selection of geometric factors for a prescribed pump discharge. Fig. 7.6 is the layout recommended by USACE (1995). The layout is given in terms of bell diameter, D:

- Bay shape (typically rectangular in plan).
- Distance between intake entrance and pump column ($5.75D$).

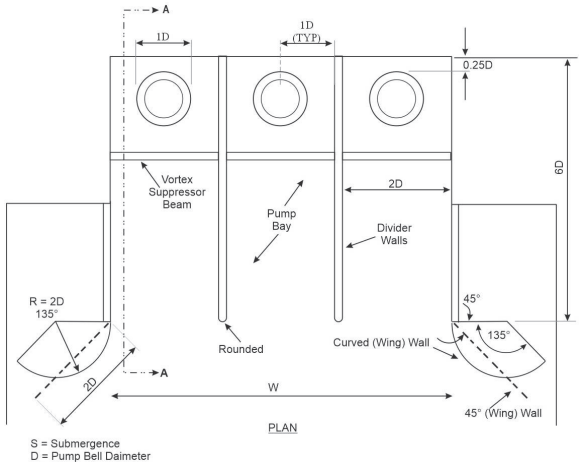

(a)

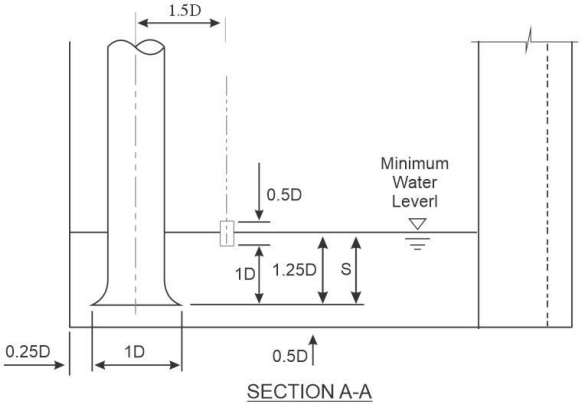

(b)

Figure 7.6 | Pump-intake layout (multi-pump) recommended by the U.S. Army Corps of Engineers (USACE, 1995): (a) plan view; and (b) elevation Section A-A. Also, shown here is a curtainwall (vortex-suppression beam), $1.0D$ above the bell rim. The wall is shown as $0.5D$ high, but height varies with expected values of flow depth in the intake.

- Pump-bell submergence ($S = 1.25D$).
- Floor clearance to the pump bell ($0.5D$).
- Sidewall clearance to the pump bell ($1.0D$).
- Backwall clearance to the pump-bell rim ($0.25D$).

Additionally, the following corrective measures are commonly required for pump-intakes to ensure a pump's performance:

- Reduce approach flow velocity (by increasing flow area).
- Reduce effects of cross flow at bay entrance (by use of a flow-guide or turning vanes).
- Eliminate flow separation (by streamlining the flow using guide walls, fairing of the flow boundaries, streamlining of piers).
- Improve uniformity of the approach-flow distribution to the pump (by introduction of head loss devices, such as surface beams and curtain walls, and a transverse array of vertical baffle bars).
- Eliminate sources of vorticity, and thereby unacceptable subsurface vortices, around a pump column (by use of splitters and fillets).
- Separate pump interaction in multi-pump bays (by flow separation walls or splitters).

Brief elaborations ensue regarding the functioning of the various corrective devices. Also mentioned is the use of a "suction scoop" for situations when approach flows to a pump are comparatively shallow. Readers interested in the design of pump intakes are referred to Knauss (1987) Padmanabhan (1987), USACE (1995), ANSIHI (1998), Ettema et al. (1998), and Jones et al. (2008) The designs aim to make the flow to each pump intake free such that the flow field to the pump acts like flow in an inviscid-flow sink.

7.5.1 | Additional design considerations

Many pump intakes usually are subject to crossflow currents that cause regions of flow-separation at the entrance to a pump intake. In turn, flow separation produces non-uniform distributions of the approach flow into a pump intake. Typically, higher velocities develop along one sidewall and lower velocities (commonly reverse flows) along the other sidewall. This distribution within the usual rectangular-shaped pump bay is a strong source of flow vorticity, which exacerbates vortex formation near the pump column. Such crossflow problems also arise within intakes fitted with drum screens for debris removal and within intakes with multiple pumps in a bay; in the latter case, cross currents may occur when some, but not all, of the pumps are operating.

Corrective fixes to cope with undesirable non-uniformity of flow include baffle bars, perforated plates, flow-turning vanes, etc. These fixes consume flow energy (local energy losses). Rows of properly designed baffle bars placed just downstream from the intake entrance can successfully rectify non-uniform pump-approach distributions. However, many existing intakes do not have adequate space to be fitted with them. Perforated plates, on the other hand, do not require any substantial space and can effectively be used to rectify non-uniform flow distributions. However, perforated plates are susceptible to clogging and may create challenges in debris-laden flows.

Extensive laboratory tests show that a simple, robust layout for flow-turning vanes may be used successfully for virtually all intake structures or their pump bays (Kruetten and Nakato 1998). The vanes are readily incorporated into the trash-rack designs commonly used at the face of riverside water intakes or can be placed at the pump-bay entrance within intakes. The severe test case involved a flow velocity ratio of 5.3 (crossflow velocity in main channel/flow velocity into intake bay). This ratio is an upper value for intakes sited along rivers.

7.5.2 | Approach-flow uniformity

Non-uniform distribution of approach flow is a significant source of flow vorticity, which in turn results in the development and strengthening of vortices in the vicinity of the pump column at the back of the pump bay. Several options exist for making the approach flow acceptably uniform:

- Use turning vanes or wing walls (as shown in Fig. 7.6).
- Install baffle bars (Fig. 7.7 shows an example).
- Place a curtainwall or vortex-suppression beam (as shown in Fig. 7.6).

The latter two devices create flow resistance, and thereby increase flow depth and reduce flow velocity upstream of their location. Because the flow resistance is greatest where the flow velocity is greatest (resistance varies with the velocity squared), these fixes force the flow to redistribute from regions of higher velocity to regions of lower velocity. A design concern, however, is that the fixes overly constrict the flow such that the upstream flow level becomes unacceptably high or the flow downstream of the fixes is too rapid (i.e., is supercritical).

7.5.3 | Baffle bars

Laboratory tests and subsequent field experience show that an effective layout of baffle bars is achievable as shown in Fig. 7.7 (e.g., Muste and Ettema, 1996). Various alternate structural elements may

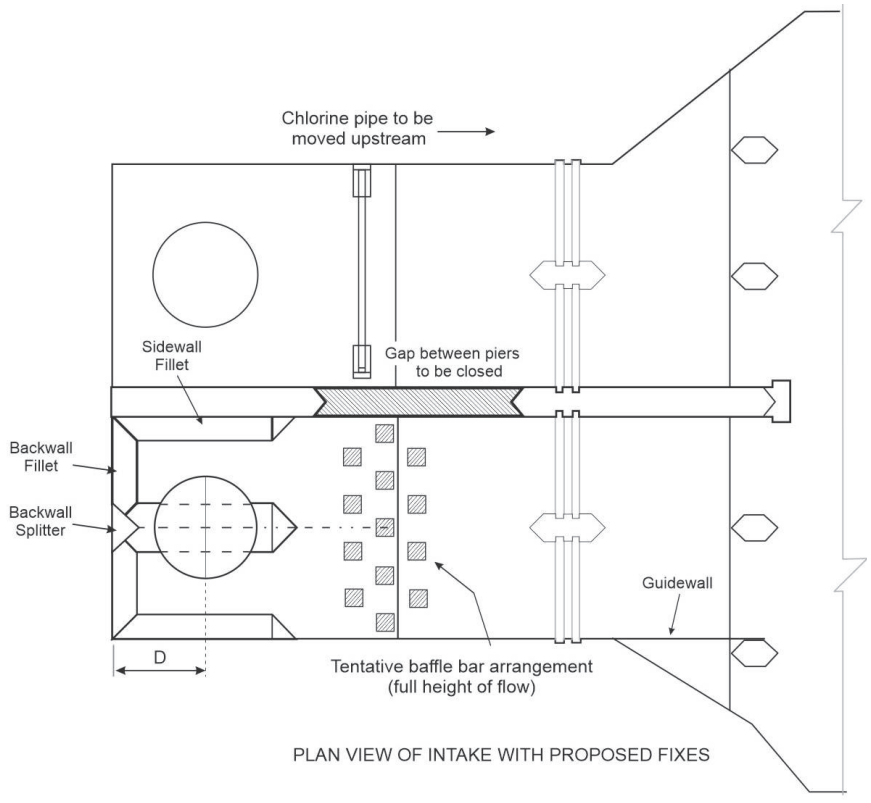

(a)

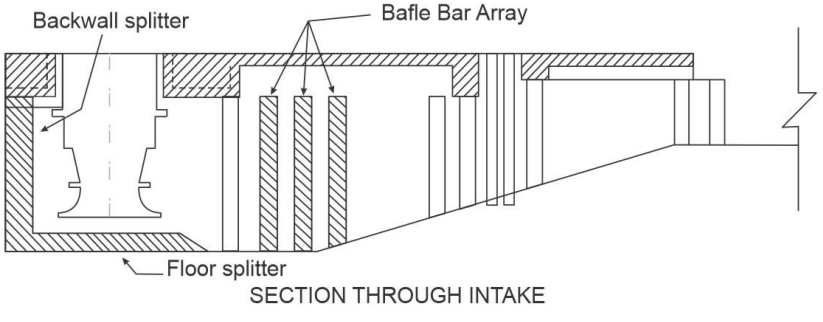

(b)

Figure 7.7 | Example of baffle-bars placed in a pump-intake used for a cooling tower basin: (a) plan view; and (b) vertical section. The baffle bars ensure that the flow within the intake has an acceptable minimum level of swirl and is free of surface vortices at each pump.

be used for the bars. However, H-column sections are more effective in improving flow uniformity because of the greater drag force on those sections and, therefore, greater flow resistance created by them.

7.5.4 | Curtain wall

Curtain walls, or surface beams, also serve to retard the flow, and improve a flow's uniformity. Curtain-wall location and opening (bottom of wall to intake floor) within an intake varies from intake to intake. The bottom elevation of the curtain wall is usually below the low-water elevation expected for an intake. A typical configuration is depicted in Fig. 7.7. Though no formal design guide of curtain walls has been developed and design depends on expected water levels, the indicated location and size dimensions (Fig. 7.6) are typically adopted and have proven effective (e.g., Melville et al. 1994).

7.5.5 | Flow separation

Because many water intakes comprise the composite design effort of several engineering disciplines (e.g., civil, mechanical, electrical) and their sub-specialties, it often happens that the flow approach to a pump bay is not as hydrodynamically smooth as needed. Sundry columns and posts may protrude into the flow. Walls may not be symmetrically located about a bay. The flow may issue abruptly into the bay from a pipe connecting it to the river or some alternate water source (e.g., lake, cooling tower basin). These examples of flow separation usually result in non-uniformity of approach flow into the pump bay and production of flow vorticity; both of which have adverse effects on vortex formation at the pump bell. Consequently, flow separation usually must be avoided.

The main fix for eliminating flow separation is to modify the intake geometry by means of flow-turning vanes (discussed above), flow-guidance walls, fairings, and in-fill fillets. These fixes are intended to lead the flow more-or-less smoothly into the pump bay. The use of guide walls and improved fairing of walls for a multi-pump bay is illustrated in Fig. 7.6.

In some cases, when it is not possible to modify the intake geometry or to fit effective flow-guidance devices, such as vanes, a curtain wall or an array of baffle bars may be used to improve flow uniformity and reduce flow vorticity.

7.5.6 | Elimination of water-surface vortices

Increasing pump-bell submergence may eliminate water-surface vortices if submergence can be increased for a particular bay. For large pump installations, increasing submergence usually is not an economical solution and artificial means of vortex suppression are needed. Several methods exist.

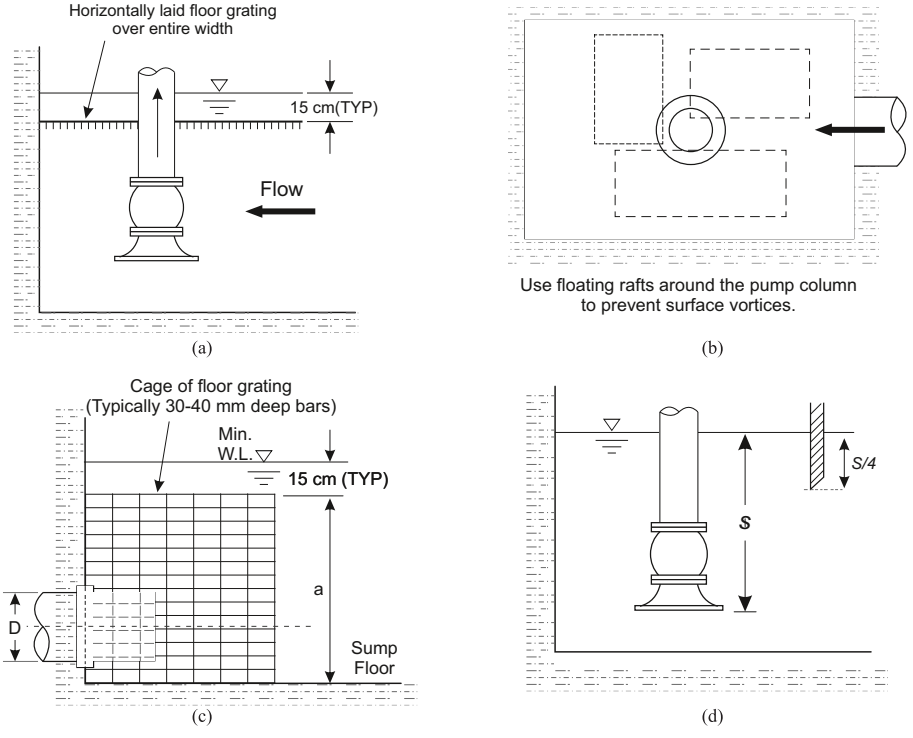

Figure 7.8 | Typical surface-vortex suppression devices: (a) horizontal grating; (b) floating rafts; (c) grating cage; and (d) curtainwall. (Modified from Padmanabhan, 1987).

They all act to lengthen flow path to a pump. Padmanabhan (1987) provides a useful diagram (Fig. 7.8) of commonly used vortex suppressors:

- A horizontal grating about 100 to 150 mm below the water level at which strong vortices are expected (usually the minimum water level).
- Floating rafts around a pump column (rarely used, though).
- A grating cage submerged just below the minimum water level.
- In cases where the approach non-uniformity contributes to strong vortex formation, a curtain wall (as mentioned in the preceding section) or surface beam extending across and into the water surface in the approach channel.

The depth and spacing of the bars in the horizontal grating are important parameters. Padmanabhan (1987) recommends bar depths of 40 to 60 mm and bar spacing of about 25 mm, as Fig. 7.10 indicates.

Tullis (1979) points out the importance of considering the influence of proposed corrective measures on other potential hydraulic problems. For example, an upstream curtain wall can alleviate surface vortex formation, but inadvertently strengthen subsurface vortices.

7.5.7 | Elimination of subsurface vortices

Subsurface vortices usually are the most difficult hydraulic problem to treat. Because flow circulation at or near to the pump suction bell strongly influence them, corrections seek to reduce such circulation. To be mentioned is that flow patterns are affected by floor and wall clearances from the bell.

Padmanabhan (1987) gives a useful diagram (Fig. 7.9) showing several commonly used methods to control subsurface vortices:

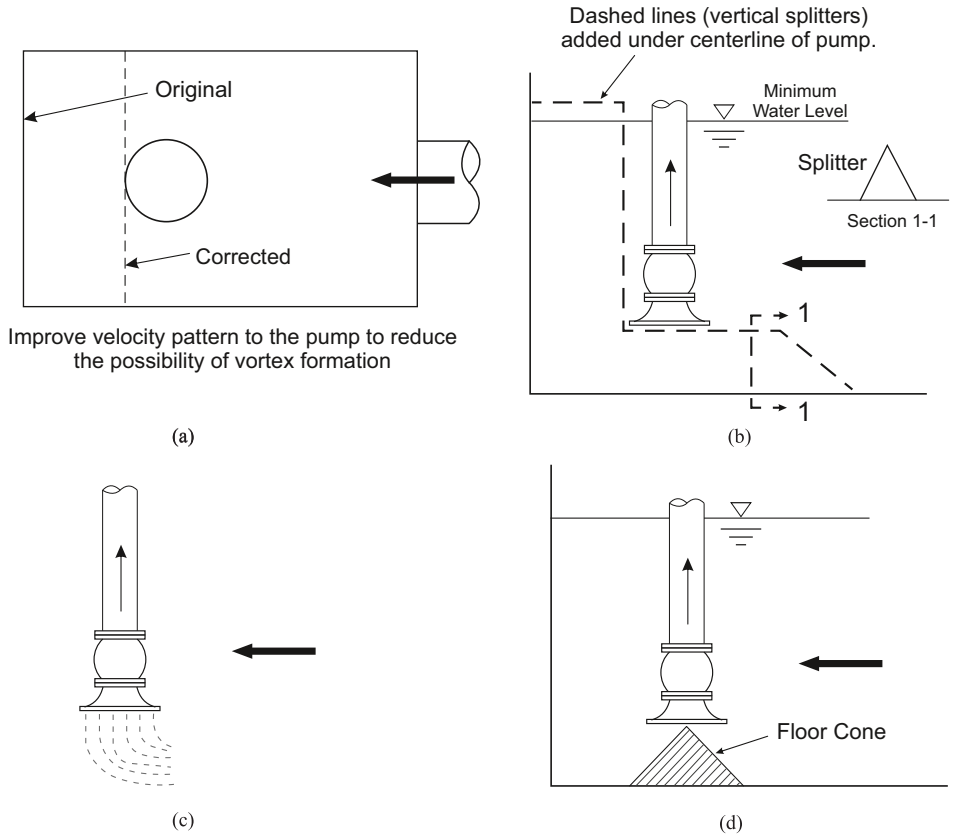

Figure 7.9 | Typical subsurface-vortex suppression devices: (a) increase clearance from backwall; (b) floor and wall splitters; (c) turning vanes fastened to pump bell; and (d) a floor cone. (Source: modified from Padmanabhan, 1987).

- Changes in wall and floor clearances.
- Vertical flow splitters on the backwall behind the pump column.
- Horizontal floor splitter on the axis of longitudinal symmetry.
- Installation of fillets in the corners of the sump to fill zones of flow separation and/or stagnation.
- Turning vanes on the floor to improve alignment of flow into the pump bell (making it impossible for a vortex to form on the floor).
- A floor cone beneath the pump bell.

Turning vanes and cone are sometimes used, though concerns arise owing to clogging by debris. Tullis (1979) states that although floor cones can eliminate floor-attached vortices, they may intensify other problems. Laboratory tests have given the same disappointing result (e.g., Nakato and Yoon 1992; Ettema et al. 1998). For example, a floor cone may increase the strength of sidewall- and backwall-attached vortex. Tullis also mentions the use of floor attached protrusions (like small chute blocks)

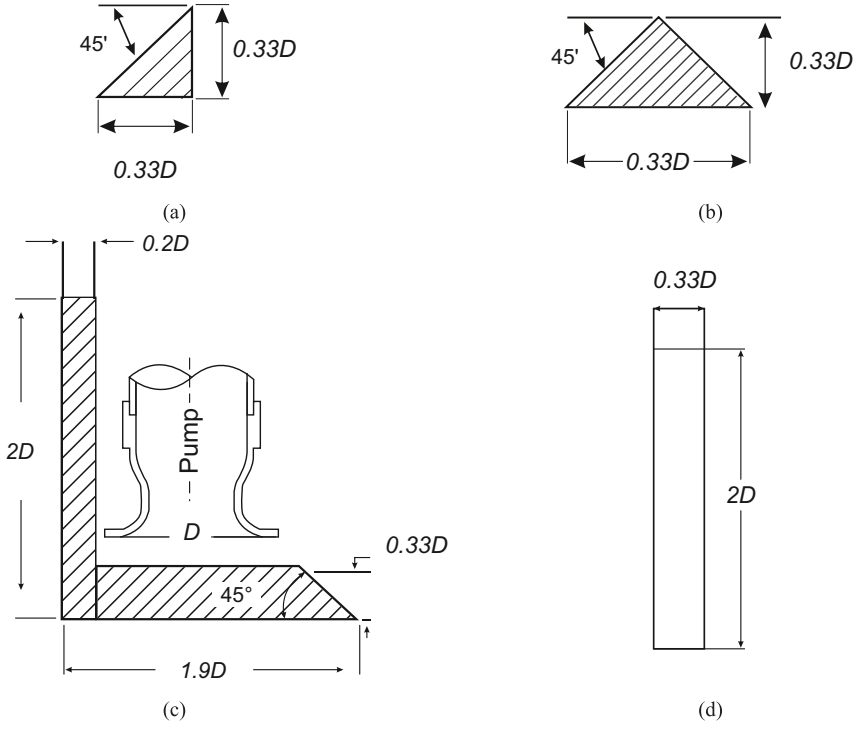

Figure 7.10 | Recommended dimensions of flow splitters: (a) cross-section of corner splitter; (b) cross section of back wall splitter; (c) elevation of floor and backwall splitters; and (d) front elevation of sidewall and backwall splitters. (Ettema et al., 1998).

to break up floor-attached vortices. The devices can cause vibration and cavitation. Padmanabhan (1987) notes that some subsurface vortex suppression devices may partially mitigate problems associated with swirl and uneven flow distribution to a pump.

Splitters and fillets are virtually mandatory for pump bays. Fig. 7.10 indicates a typical layout. Dimensioning may vary with intake geometry. Laboratory tests suggest that floor splitters need to be about $0.35D$ to $0.38D$ in height to function correctly (e.g., Nakato and Yoon, 1992; Ettema et al. 1998); (Fig. 7.6).

7.5.8 | Suction scoop for shallow flows

Flow problems may arise at pump intakes drawing water from rivers whose flow is greatly diminished during the drier periods of the year, or lakes whose water level is greatly lowered. During those shallow-flow conditions, undesirable flow features, notably diverse vortices, may form and adversely affect pump-intake performance. Also, under these flow conditions, other flow-improvement devices (as mentioned above) used in pump intakes may be ineffective.

A suction-scoop, or inverted draft tube, can eliminate many flow problems produced by shallow flow to pump sumps. In other words, a pump may have to operate with a submergence, S, less than specified for the pump. However, these situations entail radically reshaping a pump intake (or a bay within

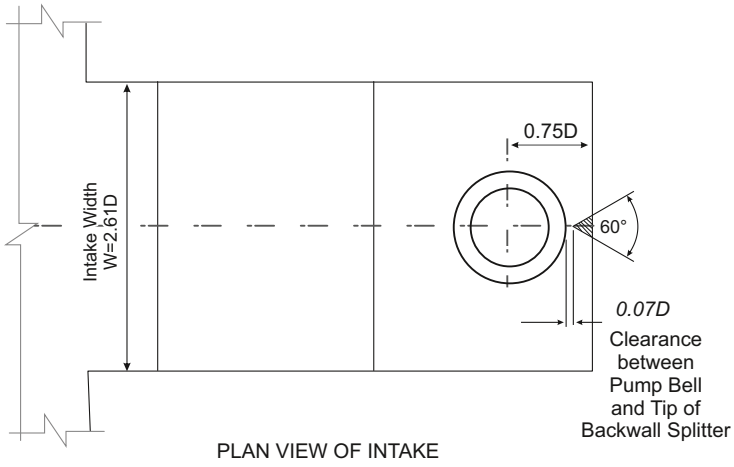

Figure 7.11 | A suction scoop (or inverted draft tube) used for a pump in shallow flows: (a) plan view; and (b) vertical section. (Kreutten and Nakato, 1998).

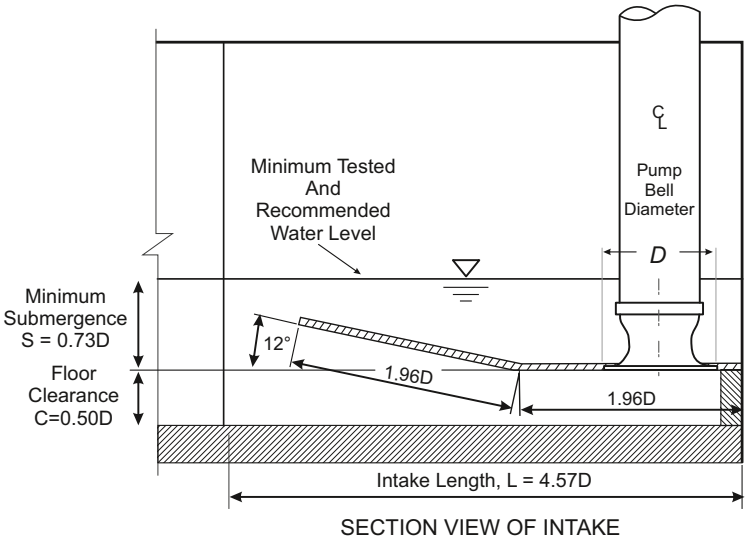

(b)

Figure 7.11 | (Continued)

an intake). The name "suction scoop" derives from the device's resemblance of a draft tube, intended to gradually decelerate the flow at the exit from a medium-head turbine. The scoop eliminates the free surface in the vicinity of the pump's suction bell, lengthens the flow path, gradually accelerates the flow, and directs the flow into a pump's suction inlet. Fig. 7.11 shows the recommended scoop layout normalized using pump bell diameter, *D*.

CHAPTER 8

Concluding Remarks

ROBERT ETTEMA
Civil & Environmental Engineering Dept., Colorado State University, USA.
E-mail: *Robert.Ettema@colostate.edu*

DAVID Z. ZHU
Civil & Environmental Engineering Dept., University of Alberta, Canada. E-mail: *dzhu@ualberta.ca*

8.1 | Introduction

Swirling flows and their consequent formation of vortices have been treated as veritable enemies of flow intakes. But vortex-flow intakes purposely turn this apparent enemy into an ally. Indeed, some features of swirl and vortex formation are desired for certain types of hydraulic structures and in certain flow situations.

Swirl and vortex generation increase flow resistance locally or along the length of a flow conduit. One reference characterizes eddies formed by swirling flows and vortices as the "root of the resistance evil" (Rouse 1963). This reference also goes on to mention that swirl and vortex generation are intrinsically common in a huge range of flows, whose energy flow resistance transforms then diffuses (e.g., flows associated with weather patterns, through to flows within the capillaries of porous media). Swirling flows and vortices add components of flow orthogonal to the primary (or required) direction of flow. Flow components orthogonal to the design direction of flow consume large amounts of flow energy, energy usually treated as lost to flow along the design direction of flow. Designers of intakes seeking to minimize energy loss try to avoid or significantly reduce components of flow orthogonal to the design direction of flow; and thereby greatly reduce swirl and vortex generation. Increased flow resistance usually means increased size of flow intake or conduit, which of course translates to greater cost. A common stratagem used by designers is to eliminate, or at least control swirl and vortex generation, by means of streamlining flow boundaries and, for intakes, ensuring ample submergence of flow. Many books and journal articles go on to describe the fate of energy spent forming swirls and vortices (e.g., just to list a few books, Richardson, 1922; Hinze, 1959; Daily and Harleman, 1966; Reynolds, 1975; Munson et al., 2013).

Moreover, vortices with air cores are viewed (e.g., Knauss 1987) as potentially indicating approach-flow problems for a variety of hydraulic structures or hydraulic machines, because such vortices reduce water-flow area entering an intake, produce unacceptable flow distribution within an intake, and possibly cause undesired vibration loads exerted against structural elements of an intake or machine within an intake (notably, turbines and pumps), all of which reduce design performance of hydraulic structures or machines. Swirl and vortices need not entrain air to reduce performance, as non-uniform flow distribution may lead to under-operation and undue wear. However, interpretation of Hecker (1987, in Knauss 1987) suggests that the occurrence of an air core in a vortex is more an indicator of unacceptable swirl than the air core itself being problematic: the quantity of air involved is relatively small (2% or less by volume rate according to Padmanabhan 1984).

Chapter 2 explains the fundamentals of swirling flows and vortices. As that chapter and Chapter 1 mention, other textbooks elaborate the fundamentals (e.g., the references cited above). Then, Chapters 2 and 3 discuss physical and numerical hydraulic modeling, respectively, methods commonly used to assist in the design of intakes.

8.2 | Vortex-flow intakes

Designers of vortex-flow intakes use to advantage the principal feature of swirl and vortex formation – energy dissipation – when devising water-conveyance systems in situations that require flow to drop abruptly by means of a dropshaft from a higher to a much lower elevation. In these situations, as Chapter 5 explains, energy dissipation, space limitation, air entrainment, and cost are paramount considerations; energy dissipation is required, and space may be limited. With a stable air core formed by the swirling flow in a dropshaft, the amount of air entrained into the dropshaft can be significantly reduced. Typically, though not always, these situations are in urban settings requiring rapid drainage, subsequent storage, and water-quality treatment of runoff, water flow consequent to stormy weather. Storage sometimes is constrained to underground reservoirs or to situations where available land for reservoirs is severely limited. Approach flow to vortex-flow intakes generally is via a relatively narrow open channel that ensures straight flow into such intakes.

This monograph serves as an update of the valuable earlier monograph edited by Knauss (1987) and shows how designers use swirl and vortex generation to convey flows in drainage-flow situations. These days, the use of vortex flow intakes for dropshafts is growing rapidly, as this monograph indicates. The use of such intakes has grown substantially since Knauss (1987) and will continue to grow in the foreseeable future. Contemporary drivers are development of urbanization and concern for the well-being of the natural environment.

8.3 | Hydropower and pump intakes

Intakes drawing water to hydropower turbines or to pumps must be designed to conserve as much as possible of approach-flow energy. For turbines, design seeks to harvest mechanical energy from a given flow and head. For pumps, design seeks to add to a flow the least amount of mechanical energy as feasible. In both cases, design aims to minimize loss of approach-flow energy. Swirl and vortex generation can be undesired consumers of flow energy, as Chapters 6 and 7 explain for hydropower and pump intakes, respectively.

Chapter 6 is broadened to include intakes to both submerged outlets and ogee crests on spillways, as the approach entrance to a spillway crest is a form of intake. Usually, the approach must be free of swirl and consequent vortices to ensure that the unit discharge (discharge per unit width) of approach flow is distributed uniformly over the crest. This consideration is important for developing the stage-discharge relationship for the crest and making sure that flow passes efficiently down the spillway. In many cases, close attention is given to the approach to the ogee crest and to the shape of the abutments flanking the crest.

However, as Hecker stated in the concluding chapter of Knauss (1987), it is important "…to remember that a vortex itself usually is not the issue, but rather the downstream flow characteristics it produces." The key phrase in Hecker's statement, which pertained to vortices at hydropower and pump intakes, is "downstream flow characteristics". Distance downstream has significance. If the distance is large, energy loss at the intake is minor compared to energy loss caused by flow resistance along the conduit conveying flow plus local losses of energy associated by bends, valves, and other appurtenances. Also, provided swirling flow and vortices are sufficiently upstream as not to adversely affect flow uniformity across the throat of a pump column, flow to a turbine, or uniformity of flow distribution on the crest of a spillway, swirling flow and vortices are without consequence. To be sure, the preceding sentence holds so long as vortex formation does not incur unwanted loss of energy or need for additional energy.

8.4 | Final remarks

The IAHR monograph *Swirling Flow Problems at Intakes* (Knauss 1987) remains useful. Knauss' monograph comprises chapters written by people typically at the forefront of their chapter's topic, and thus the monograph contains much ageless wisdom about intakes. The present monograph updates Knauss (1987) to the time the monograph was published. Updates include the positive aspects of vortex-flow intakes purposefully designed to replicate the descending, spiraling flow of vortices. And

updates especially include the development and application of numerical hydraulic models to the design of vortex-flow intakes. As time progresses, numerical models are becoming increasingly used to aid design of intakes of all types.

Some processes (e.g., air ingestion and removal, certain aspects of turbulence, and splash) still are somewhat beyond the numerical models readily available to designers of intakes, and for the moment resort frequently must be made to physical hydraulic models. The present monograph also contains updates regarding physical modeling. However, Knauss (1987) remains handy in this regard.

Flow swirl and vortex formation are flow features that have fascinated people and continue to fascinate people, though the word “vortex” evokes several negative thoughts (e.g., whirlpool or tornado). This monograph shows when hydraulic structures deliberately form vortical flows and when hydraulic structures must minimize or avoid such flows.

References

1 Ackers, P. and Crump, E.S. (1960). The vortex drop. Proc. of Institute of Civil Engineers, Part I, 16(4), 433–442.

2 Adams, G.N. and Gilmore, D.C. (1972). Some observations of vortex core structure. Can. Aeronaut. Space J. Jun, 159–162.

3 Ahn, S.H., Xiao, Y., Wang, Z., Zhou, X. and Luo, Y. (2017). Numerical prediction on the effect of free surface vortex on intake flow characteristics for tidal power station, Renewable Energy, 101, 617–628.

4 Amphlett, M.B. (1978). Air-Entraining Vortices at a Vertically inverted Intake. Hydraulics Research Station Wallingford, Report No. Od/17, UK.

5 Amphlett, M.B. (1979). Discussion of vortex formation at vertical pipe intakes. J. Hydraulics Div., 105(HY10), 1328–1330.

6 Andersen, A., Bohr, T., Stenum, B., Rasmussen and J.J., Lautrup, B. (2006). The bathtub vortex in a rotating container. J. Fluid Mech., 556, 121–146.

7 Anh, T.N. and Hosoda, T. (2005). Steady free surface profile of flows with air-core vortex at vertical intake. In Proc. 31st IAHR Cong., Seoul, S. Korea.

8 Ansar, M., Nakato, T. and Constantinescu, G. (2002). Numerical simulations of inviscid three-dimensional flows at single-and dual-pump intakes, J. of Hydraulic Research, 40(4), 461–470.

9 ANSI/HI (1998). Pump Intake Design. ANSI/HI 9.8–1998. Hydraulic Institute, Parsippany, NJ.

10 Anwar, H. (1965). Flow in a free vortex. Water Power, 4, 153–161.

11 Anwar, H. O. (1968). Prevention of vortices at intakes. Water Power, 20(10): 393–401.

12 Anwar, H.O. (1983). The non-dimensional parameters of free-surface vortices measured for horizontal and vertically inverted intakes. Houille Blanche 1, 11–25.

13 Anwar, H.O. and Amphlett, M.B. (1980). Vortices at vertically inverted intake. J. Hydraulic Research, 18(2), 123–134.

14 Anwar, H.O., Weller, J.A. and Amphlett, M.B. (1978). Similitude of free vortices. J. of Hydraulic Research, Vol. 16(2), 95–105.

15 ASCE. (2000). Hydraulic modeling: concepts and practice (R. Ettema Ed.). Reston, VA: American Society of Civil Engineers Press.

16 Ash, R.L. and Khorrami, M.R. (1995). Vortex stability. In S.I. Green (Ed), Fluid Vortices, 317–369, Kluwer, Dordrecht, NL.

17 Atkinson, E. (1994a). Vortex-tube sediment extractors. I: trapping efficiency. J. of Hydraulic Engineering, 120(10), 1110–1125.

18 Atkinson, E. (1994b). Vortex-tube sediment extractors. II: design. J. of Hydraulic Engineering, 120(10), 1126–1138.

19 Azarpira, M., Zarrati, A., and Farrokhzad, P. (2021). Comparison between the Lagrangian and Eulerian Approach in Simulation of Free Surface Air-Core Vortices. Water 13(5), 726.

20 Azarpira, M., Zarrati, A.R., Farokhzad, P. and Shakibaeinia, A. (2022). Air-core vortex formation in a draining reservoir using smoothed-particle hydrodynamics (SPH). Physics of Fluids, 34(3), p.037101.

21 | Barkdoll, B., Ettema, R. and Odgaard, A.J., (1999). Sediment control at lateral diversions: limits and enhancements to vane use. J. of Hydraulic Engineering, 125(8), 855–861.

22 | Barrows, H.K. (1943). Water power engineering. McGraw-Hill, New York, NY.

23 | Bart, A., Macherel, T., De Cesare, G., Mulligan, S. and Essyad, K. (2020). Vortex siphon–from 1: 1 scale physical model to SPH simulation and prototype. In Advances in Hydroinformatics, 795–807. Springer, Singapore.

24 | Bauer, D. I. and Nakato, T. (1997). Subsurface vortex suppression in water intakes with multiple-pump sumps. Report 231, Iowa Institute of Hydraulic Research, University of Iowa, IA.

25 | Beninati, M.L. and Marshall, J.S. (2005a). An experimental study of the effect of free-stream turbulence on a trailing vortex. Exp. in Fluids 38, 244–257.

26 | Beninati, M.L. and Marshall, J.S. (2005b). External turbulence interaction with a columnar vortex. J. Fluid Mech. 540, 221–245.

27 | Benjamin, T.B. (1962). Theory of vortex breakdown phenomenon. J. Fluid Mech. 14(4), 593–629.

28 | Bhat, V.I.K. and Prakash, G. (2008). Life cycle analysis of run-of-river small hydro power plants in India. Open Renew. Energ. J. 1, 11–16.

29 | Binnie, A. (1964). Some experiments on the bath-tub vortex. J. of Mechanical Engineering Science, 6(3), 256–257.

30 | Binnie, A. and Davidson, J. (1949). The flow under gravity of a swirling liquid through an orifice-plate, Proceedings of the Royal Society of London. Series A, Mathematical and Physical Sciences, 443–457.

31 | Binnie, A.M., and Hookings, G.A. (1948). Laboratory experiments on whirlpools. Proc. of the Royal Soc. of London, Series A, 194(1038), 398–415.

32 | Blaisdell, F.W. (1982). Discussion of model-prototype comparisons of free surface vortices. J. Hydraulics Div., 108(11), 1409–1412.

33 | Bøhling, L., Andersen, A. and Fabre, D. (2010). Structure of a steady drain-hole vortex in a viscous fluid. J. Fluid Mech. 656, 177–188.

34 | Borghei, S.M. and Kabiri-Samani, A.R. (2010). Effect of anti-vortex plates on critical submergence at a vertical intake, Scientica Iranica Trans. A Civ. Eng. 17(2):89–95.

35 | Boes, R.M. (2022). Personal Communication relating Laboratory Experience.

36 | Bradshaw, P. (1973). Effects of streamline curvature on turbulent flow. AGARD_AG-169, London, UK.

37 | Brocard, D. N., Beauchamp, C.H. and Hecker, G.E. (1983). Analytic predictions of circulation and vortices at intakes. Final report. Worcester Polytechnic Inst., Holden, MA, USA.

38 | Brocard, D.S., Gan, J, Koh, L.Y., Tan, T.W., Cox, W. I., Schellhase, T., Woo, L.L., Lo, S.H., Cheng, S., Loh, S. H. and Perumal, V. (2019). Deep tunnel sewerage system phase 2 – hydraulics. Water Practice & Technology, 14(2), 409–422.

39 | Brooks, N.H. and Blackmer, W.H. (1962). Vortex energy dissipator for San Diego Ocean Outfall – Laboratory investigation. Rep. No. KH-R-5. California Institute of Technology, Pasadena. CA.

40 | Burgers, J.M. (1948). A mathematical model illustrating the theory of turbulence. Adv. in Appl. Mech. 1, 171–199.

41 | Camino, G.A., Zhu, D.Z. and Rajaratnam, N. (2015). Flow observations in tall plunging flow dropshafts, ASCE J. of Hydraulic Engineering, 141(1): 06014020

42 | Carriveau, R. (2006). The hydraulic vortex: an autocatakinetic system. Intl. J. General Systems 35(6), 707–726.

43 | Carriveau, R., Baddour, R.E. and Kopp, G.A. (2002). The entrainment envelope of dye-core vortices at submerged hydraulic intakes. Can. J. Civ. Eng. 29, 400–408.

44 | Carriveau, R., Kopp, G.A. and Baddour, R.E. (2009). Free-surface stretching-sustained intake vortices. J. Hydr. Res. 47(4), 486–491.

45 | Carty, A., O'Neill, C., Nash, S., Clifford, E. and Mulligan, S. (2019). Hydrodynamic modelling approaches to assess mechanisms affecting the structural performance and maintenance of vortex drops shaft structures. Journal of Structural Integrity and Maintenance, 4(3), 162–178.

46 | Chan, S.N. (2022). Insights from three-dimensional computational fluid dynamics modelling of a scroll vortex intake. Journal of Hydraulic Research, 60(3), 408–422.

47 | Chan, S.N., Guo, J.H. and Lee, J.H.W. (2022). Physical and numerical modeling of swirling flow in a scroll vortex intake. Journal of Hydro-environment Research, 40, 64–76.

48 | Chan, S.N., Qiao, Q.S. and Lee, J.H.W. (2018a). On the three-dimensional flow of a stable tangential vortex intake. J. of Hydro-environment Research, 21, 29–42.

49 | Chan, S.N., Wong, K.C. and Lee, J.H.W. (2018b). Hydraulics of air-water flow in a supercritical bottom rack intake. J. of Hydro-Environment Research, 21, 60–75.

50 | Chang, E. (1977). Review of literature on the formation and modelling of vortices in rectangular pump sumps. Technical Rep. TN1414, British Hydromechanics Research Association (BHRA), Cranfield, UK.

51 | Chang, E. and Prosser, M.J. (1987). Basic results of theoretical and experimental work. In J. Knauss (Ed), Swirling flow problems at intakes, 39–55, A.A. Balkema, Rotterdam, NL.

52 | Chang, F. and Dhir, V.K. (1995). Mechanisms of heat transfer enhancement and slow decay of swirl in tubes using tangential injection. Intl. J. of Heat and Mass transfer, 16(2), 78–87.

53 | Chen, Y., Wu, C., Wang, B. and Du, M. (2012). Three-dimensional numerical simulation of vertical vortex at hydraulic intake, Procedia Engineering, 28, 55–60.

54 | Chuang, W. L., Hsiao, S. C., and Hwang, K. S. (2014). Numerical and experimental study of pump sump flows, Math. Probl. Eng., 735416.

55 | Cilliers, J.J. (2000). Hydrocyclones for particle size separation. Encyclopedia of Separation Science, Academic Press, Manchester, UK.

56 | Claxton, J., Hecker, G.E. and Sdano, A. (1999). The new Hydraulic Institute pump intake design standard. Texas A&M University, Houston TX.

57 | Cong, J., Chan, S. N. and Lee, J. H.W. (2017). Geyser formation by release of entrapped air from horizontal pipe into vertical shaft. J. Hydraulic Engineering, 143(9): 04017039.

58 | Constantinescu, G. and Patel, V.C. (1998a). Numerical simulation of flow in pump bays using near-wall turbulence models. Report No. 394, Iowa Institute of Hydraulic Research, The University of Iowa, Iowa City, IA.

59 | Constantinescu, G., and Patel, V.C. (1998b). Numerical model for simulation of pump-intake flow and vortices. J. of Hydraulic Engineering, 124(2), 123–134.

60 | Constantinescu, G., and Patel, V.C. (2000). Role of turbulence model in prediction of pump-bay vortices. J. of Hydraulic Engineering, 126(5), 387–391.

61 | Constantinescu, S. G. and Patel, V.C. (1997). Numerical simulation of flow in pump bays using near-wall turbulence models. Iowa Inst. of Hydraulic Research, University of Iowa, Iowa City, IA, USA.

62 | Cotel, A. J. and Breidenthal, R. E. (1999). Turbulence inside a vortex. Physics of Fluids, 11(10), 3026/4/.

63 | Craig, A., Lyons, T.C. and Firoozfar, A. (2013). Hydraulic model studies for Thames Tideway Tunnel: Ranelagh CSO (CS14X) Interception Chamber. Limited Distribution Report No. 384., Iowa Inst. of Hydroscience & Engineering, University of Iowa, Iowa City, IA.

64 | Craig, A.J., Simonson, A.J. and Lyons, T.C. (2015). Hydraulic model studies for vortex generator head-discharge models. Limited Distribution Report No. 400, Iowa Inst. of Hydroscience & Engineering, University of Iowa, Iowa City, IA.

65 | Crispino, G., Pfister, M. and Gisonni, C. (2019). Hydraulic design aspects for supercritical flow in vortex drop shafts. Urban Water J., 16(3), 225–234.

66 | Cristofano, L., Nobili, M. and Caruso, G. (2014). Numerical evaluation of gas core length in free surface vortices. J. of Physics: Conference Series: IOP Publishing, 547, 012030.

67 | Crow, S.C. (1970). Stability theory for a pair of trailing vortices. AIAA J. 8, 2172–2179.

68 | Daggett, L.L. and Keulegan, G.H. (1974). Similitude conditions in free-surface vortex formations. U.S. Army Waterways Experiment Station, Hydraulics laboratory, Vicksburg, MS.

69 | Dai Z., Chou W.-H., Faeth D.M. (1998). Drop formation due to turbulent primary breakup at the free surface of plane liquid wall jets. Physics of Fluids 10(5): 1147–1157.

70 | Daily J.W. and Harleman, D.R.F. (1966). Fluid dynamics. Addison-Wesley Pub. Co., Reading Massachusetts, USA.

71 | De Siervi, F., Viguier, H. C., Greitzer, E. M. and Tan, C. S. (1982). Mechanisms of inlet-vortex formation. Journal of Fluid Mechanics, 124, 173–207.

72 | Del Giudice, G., Gisonni, C. and Rasulo, G. (2010). Design of a scroll vortex inlet for supercritical approach flow. J. of Hydraulic Engineering, 136(10), 837–841.

73 | Denny, D. F., and Young, G. A. J. (1957). The prevention of vortices and swirl at intakes. Proc., 7th IAHR Congress, Lisbon, Portugal.

74 | Denny, D.F. (1956). An Experimental Study of Air-Entraining Vortices in Pump Sumps. J. of the Inst. of Mech. Engineers 170(2), London, UK, 106–123.

75 | Domfeh, M.K., Gyamfi, S., Amo-Boateng, M., Andoh, R., Ofosu, E. A. and Tabor, G. (2020). Numerical simulation of an air-core vortex at a hydraulic intake using OpenFOAM, Scientific African, 8: e00389.

76 | Drioli, C. (1947). Su un particolare tipo di imbocco per pozzi di scarico. L'Energia Elettrica, 24(10), 447–452 (in Italian).

77 | Drioli, C. (1969). Esperienze su installazioni con pozzo di scarico a vortice. L'Energia Elettrica, 46(6), 399–409 (in Italian).

78 | Duinmeijer, A. and Clemens, F. (2021). An experimental study on the motion of buoyant particles in the free-surface vortex flow. J.l of Hydraulic Research, 59(6), 947–962.

79 | Duinmeijer, A., Oldenziel, G. and Clemens, F. (2021). Experimental study on the 3D flow field of a free-surface vortex using stereo PIV, J. of Hydraulic Research, 58(1): 105–119.

80 | Durgin, W. W. and Hecker, G. E. (1978). The modeling of vortices at intake structures. Proc. of the ASCE, IAHR, and ASME Joint Symposium on Design and Operation of Fluid Machinery, 381–391.

81 | Dyakowski, T. and Williams, R.A., (1993). Modelling turbulent flow within a small-diameter hydrocyclone. Chemical Engineering Science, 48(6), 1143–1152.

82 | Echavez, G., McCann, E. (2002). An experimental study on the free surface vertical vortex. Exp. in Fluids 33(3), 414–421.

83 | Eguchi, Y., Yamamoto, K., Funada, T., Tanaka, N., Moriya, S., Tanimoto, K., Ogura, K., Suzuki, T., Maekawa, I. (1994). Gas entrainment in the IHX vessel of top-entry loop-type LMFBR. Nucl. Eng. Des. 146, 373–381.

84 Einstein, H.A., Li, H. (1951). Steady vortex flow in a real fluid. In Proc. Heat Trans. and Fluid Mech. Inst., 33–43, Stanford University, Palo Alto, US.

85 Ervine, D.A. and Kolkman, P.A. (1980), Air entrainment and transport in closed conduit hydraulic structures, Delft Hydraulics Laboratory.

86 Ettema, R., Jain, S.C., Nakato, T. and Schaefer, J. (1996). "Hydropower development at Lock and Dam 14, Mississippi River," Limited Distribution Report No. 241, Iowa Institute of Hydraulic Research, The University of Iowa, Iowa City, Iowa.

87 Ettema, R., Nakato, T. and Patel, V.C. (1998). Flow in water-intake pump bays: a guide for utility engineers. EPRI Report TR-110948, Palo Alto, CA.

88 Ezure, T., Kimura, N., Hayashi, K. and Kamide, H. (2008). Transient behavior of gas entrainment caused by surface vortex. Heat Transfer. Eng. 29(8), 659–666.

89 Felder, S. and Pfister, M. (2017). Comparative analyses of phase detective intrusive probes in high-velocity air-water flows. Intl. J. of Multiphase Flow, 90, 88–101.

90 Felder, S., Hohermuth, B., Pfister, M. and Boes, R.M. (2019). Which phase detection intrusive probe to use is a high-velocity air-water flows? E-proc. 38th IAHR Congress, Panama City, Panama, 5683–692.

91 Fernandes J. and Jonatas, R. (2019). Experimental flow characterization in a spiral vortex drop shaft. Water Science and Technology, 80(2), 274–281.

92 Fischer, H. B. (1979). Mixing in inland and coastal waters. New York: Academic Press.

93 Fisher, Jr, R. and Franke, G. (1987). The impact of inlet flow characteristics on low head hydro projects. Proc. Intl. Conf. on Hydropower, 1671–1680, Portland, OR.

94 Fisher, R.K. and Franke, G.F. (1988). The impact of inlet flow characteristics on low-head hydro projects. ASCE, Proc. Waterpower '87, New York, NY.

95 Fritz, J.J. (1984). Small and mini hydropower systems. McGraw-Hill, New York, NY.

96 Galuška, J. (2017). Simulation of intake vortices, Galuška, Jiří. Brno University of Technolog, Thesis, Brno, Czech Republic.

97 Gardarsson S.M., Gunnarsson A., Tomasson G.G., and Pfister M. (2015). Karahnjukar Dam spillway: Comparison of operational data and results from hydraulic modelling. Proc. HYDRO 2015 Conf., Paper 22.05, Bordeaux, France.

98 Gessler, D., Johansson, A. and Hall, B. (2017). Computational fluid dynamics vs. physical modeling for pump intake design. Water Online.

99 Godde D. (1994). Experimentelle untersuchung zur anströmung von rohrturbinen: ein beitrag zur optimierung des turbineneinlaufs ("Experimental investigation of bulb turbine approach flow: a contribution to optimized turbine intakes"). Bericht Nr. 75, der Versuchsanstalt Obernach und des Lehrstuhls für Wasserbau und Wassermengen-wirtschaft der TU München, Germany (in German).

100 Gordon, J.L. (1970). Vortices at intakes. Water Power, April (4), 137–138.

101 Greater London Authority (2020). 2020 Mid-year estimates. retrieved from https://data.london.gov.uk/dataset/londons-population

102 Green, S. I. (1995). Fluid vortices – Fluid mechanics and its applications, Kluwer Academic Publishers, Netherlands.

103 Gulliver, J.S. (1988). Discussion of "Free-surface air core vortex", by A.J. Odgaard. J. Hydraulics Div., 114(4), 447–449.

104 Gulliver, J.S. and Arndt, R.E.A. (1991). Hydropower engineering handbook. McGraw-Hill, New York, NY.

105 | Gulliver, J.S., Rindels, A.J., and Lindblom, K.C. (1986). Designing intakes to avoid free-surface vortices. Int. Water Power Dam Constr. 38(9), 24–28.

106 | Guo, J.-H. (2012). Velocity field measurement of a scroll vortex intake flow. M. Phil Thesis. The University of Hong Kong, Hong Kong.

107 | Guo, Z., Chen, F., Wu, P. and Qian, Z. (2017). Three-dimensional simulation of air entrainment in a sump pump. J. of Hydraulic Engineering, 143(9).

108 | Hager, W.H. (1985). Head-discharge relation for vortex shaft. J. of Hydraulic Engineering, 111(6), 1015–1020.

109 | Hager, W.H. (1990). Vortex drop inlet for supercritical approaching flow. J. of Hydraulic Engineering, 116(8), 1048–1054.

110 | Hager, W.H. (2010). Wastewater hydraulics: theory and practice. Springer, Heidelberg, Germany.

111 | Hager, W.H., Schleiss, A.J., Boes, R.M., and Pfister, M. (2020). Hydraulic engineering of dams. Taylor & Francis, London, https://doi.org/10.1201/9780203771433.

112 | Hashid, M. and Ahmad, Z. (2022). Critical submergence for horizontal dual water intakes under perpendicular uniform approach flow. J. of Hydraulic Engineering, 148(10), 04022020.

113 | Hay, N. and West, P.D. (1975). Heat transfer in free swirling flow in a pipe. ASME, J. of Heat Transfer, 97(3), 411–416.

114 | Hebaus, G.G. (1979). Discussion of vortex formation at vertical pipe intakes. J. Hydraul. Div. ASCE 105(HY10), 1330–1332.

115 | Hecker, G. (1981). Model-prototype comparison of free surface vortices. J. Hydraulics Div., 107(HY10), 1243–1259.

116 | Hecker, G.E. (1984). Scale effects in modeling vortices. Proc. of IAHR/DVWK Symposium of Scale Effects in Modelling Hydraulic Structures, Technische Academie Esslingen, Paper 6.1, Germany.

117 | Hecker, G.E. (1987). Fundamentals of vortex intake flow, (pp. 13–38). Swirling flow problems at intakes, IAHR Hydraulic Structures Design Manual 1, Taylor & Francis: Balkema, Rotterdam, NL.

118 | Hecker, G.E. (1987a). Fundamentals of vortex intake flow. Chap. 2, Swirling flow problems at intakes, IAHR Hydraulic Structures Design Manual, Balkema, Rotterdam, NL.

119 | Hecker, G.E. (1987b). Conclusions. Chap.8, Swirling flow problems at intakes, IAHR Hydraulic Structures Design Manual, Balkema, Rotterdam, NL.

120 | Heller, V. (2011). Scale effects in physical hydraulic engineering models. J. of Hydraulic Research, 49(3), 293–306.

121 | Helmholtz, H. (1867). On integrals of the hydrodynamical equations, which express vortex motion. Phil. Mag. S. 4 33(226), 485–512.

122 | Herrero, A. Bateman, A. and Medina, V. (2015). Water flow and sediment transport in a 90° channel diversion: an experimental study. J. of Hydraulic Research, Vol. 53(2), 1–11.

123 | Hinze, J. (975). Turbulence. McGraw-Hill Inc., New York, NY, USA.

124 | Hirt, C.W. (1992). Volume-fraction techniques: Powerful tools for flow modeling, Flow Sci. Rep. FSI-92–00, 2.

125 | Hirt, C.W. (2003). Modeling turbulent entrainment of air at a free surface. FSI-03-TN61-R. Flow Science Inc, Santa Fe, NM, USA.

126 | Hirt, C. W. and Nichols, B. D. (1981). Volume of fluid (VOF) method for the dynamics of free boundaries. Journal of Computational Physics, 39(1), 201–225. Hirt, C.W., 2003. Modeling turbulent entrainment of air at a free surface. FSI-03-TN61-R. Flow Science Inc, Santa Fe, NM, USA.

127 | Hite, J.E. (1991). Vortex formation and flow separation at hydraulic intakes. Ph.D. thesis, Washington State University, Pullman, US.

128 Hite, J.E. and Mih, W.C. (1994). Velocity of air-core vortices at hydraulic intakes. J. of Hydraulic Engineering, 120(3), 284–297.

129 Hohermuth, B. (2019). Aeration and two-phase flow characteristics of low-level outlets. VAW-Mitteilung 253 (R. Boes, ed.), Laboratory of Hydraulics, Hydrology and Glaciology (VAW), ETH Zurich, Switzerland.

130 Hohermuth, B., Boes, R.M. and Felder, S. (2021). High-velocity air-water flow measurements in a prototype tunnel chute: scaling of void fraction and interfacial velocity. J. of Hydraulic Engineering, 147(11): 04021044.

131 Hohermuth, B., Schmocker, L. and Boes, R.M. (2020). Air demand of low-level outlets for large dams. J. of Hydraulic Engineering, 146(8): 04020055, 10.1061/(ASCE)HY.1943–7900.0001775.

132 Hohermuth, B., Kramer, M., Felder, S. and Valero, D. (2021). Velocity bias in intrusive gas-liquid measurements. Nature Communications, 12, Article 4123.

133 Holstad, M.S. (2020). A Tale of Three Projects: Vortex manholes design, operation and improvement. Proc. of the Water Environment Federation. doi. 10.2175/193864718825157458

134 HRS (1965). Plover cove water supply scheme, Hong Kong: Report on hydraulic model investigation of a typical dropshaft and de-aeration chamber. Report No. EX 264, Ministry of Technology, Hydraulics Research Station (HRS), Wallingford, Berkshire, England.

135 Ito, K., Kunugi, T., Ohshima, H. and Kawamura, T. (2009). Formulations and validations of a high-precision volume-of-fluid algorithm on nonorthogonal meshes for numerical simulations of gas entrainment phenomena. J. Nucl. Sci. Technol., 46: 366–373.

136 Ito, K., Sakai, T., Eguchi, Y., Monji, H., Ohshima, H., Uchibori, A. and Xu, Y. (2010). Improvement of gas entrainment prediction method—introduction of Surface Tension Effect, J. of Nuclear Science and Technology, 47(9), 771–778.

137 Jacquin, L., Fabre, D., Sipp, D. and Coustols, E. (2005). Unsteadiness, instability and turbulence in trailing vortices. C. R. Physique 6, 399–414.

138 Jacquin, L. and Pantano, C. (2002). On the persistence of trailing vortices. J. Fluid Mech. 471, 159–168.

139 Jain, A.K., Raju, K.G.R. and Garde, R.J. (1978). Vortex formation at vertical pipe intakes. J. Hydraulics Div. ASCE 104(HY10), 1429–1445.

140 Jain, S.C. (1984). Tangential vortex-inlet. J. of Hydraulic Engineering, 110(12), 1693–1699.

141 Jain, S.C. (1988). Air transport in vortex-flow drop shafts. J. of Hydraulic Engineering, 114(12), 1485–1497.

142 Jain, S.C., and Ettema, R. (1987). Swirling flow problems at intakes. in Vortex Intakes, IAHR hydraulic structures design manual 1, Knauss, J. (Ed), Balkema, Rotterdam, NL, 125–137.

143 Jain, S.C. and Kennedy, J.F. (1983). Vortex-flow drop structures for the Milwaukee Metropolitan Sewerage District Inline Storage System. Rept. No. 264, Iowa Institute of Hydraulic Research, Univ of Iowa, Iowa City, IA.

144 Jiming, M., Yuanbo, L. and Jitang, H. (2000). Minimum submergence before double-entrance pressure intakes. J. Hydraulic. Engineering, 126(8), 628–631.

145 Johnson, P.L. (1988). Hydro-power intake design considerations. J. Hydraulic Eng., ASCE, 114(6), 651–661.

146 Jones, G.M., Sanks, R.L, Tchobanoglous, G. and Bosserman, B.E. (Eds) (2008). Pumping station design. Elsevier, Amsterdam, NL.

147 Kalinske, A.A. (1941). Hydraulics of vertical drains and overflow pipes. Investigations of the Iowa Institute of Hydraulic Research 1939–1940, Edited by J.W. Howe, Iowa Institute of Hydraulic Research, The University of Iowa, Iowa City, IA.

148 | Kellenberger H. (1988). Wirbelfallschachte in der Kanalisationstechnik (Vortex drop shafts in sewer systems), VAW-Mitteilung 98 (D. Vischer, ed.). Laboratory of Hydraulics, Hydrology and Glaciology (VAW), ETH Zurich, Switzerland (in German).

149 | Keller, J., Möller, G. and Boes, R.M. (2014). PIV measurements of air-core intake vortices. Flow Measurement and Instrumentation, 40, 74–81.

150 | Khanarmuei, M., Rahimzadeh, and H. Sarkardeh, H. (2019). Effect of dual intake direction on critical submergence and vortex strength. J. of Hydraulic Research, 57(2), 272–279.

151 | Kimura, N., Ezure, T., Tobita, A. and Kamide, H. (2008). Experimental study on gas entrainment at free surface in reactor vessel of a compact sodium-cooled fast reactor. J. Hydraulic Eng., 45(10), 1053–1062.

152 | Klimenko, A.Y. (2007). Do we find hurricanes on other planets? Proc. 16th Australasian Fluid Mech. Conf., Gold Coast, Australia.

153 | Knauss, J. (1987). Swirling flow problems at intakes. IAHR, Hydraulic Structures Design Manual 1, Balkema, Rotterdam, The Netherlands.

154 | Kobus, H. (1984). Local air entrainment and detrainment. Universität Stuttgart, Federal Republic of Germany.

155 | Kocaba¸s, F. and Yıldırım, N. (2002). Effect of circulation on critical submergence of an intake pipe. J. Hydraulic Research, 40(6), 741–752.

156 | Kocabas, F. and Unal, S. (2010). Compared techniques for the critical submergence of an intake in water flow. Advances in Engineering Software, 41(5), 802–809.

157 | Kocabaş, F., Ünal, B., Ünal, S., Fedakar, H. I. and Gemici, E. (2013). Fuzzy genetic approach for modeling of the critical submergence of an intake. Neural Computing and Applications, 23(1), 73–82.

158 | Kramer, M., Hohermuth, B.. Valero, D. and Felder, S. (2020). Best practices for velocity estimates in highly aerated flows with dual-tip detection probes. Intl. J. of Multiphase Flow, 126, Article 103228.

159 | Kreith, F. and Soniu, O.K. (1965). The decay of turbulent swirl in a pipe. J. of Fluid Mechanics, 22, 257–271.

160 | Kruetten, M. and Nakato, T. (1998). Cross-flow control for pump bays, IIHR Report, Iowa Institute of Hydraulic Research, The University of Iowa, Iowa City, IA.

161 | Kubit, O. and Ettema, R. (2001). Debris and ice-skimming booms at riverside diversions. J. of Hydraulic Engineering, 127(6), 489–499.

162 | Kumar, A, Wong, C.T.L. and Tai, R. (2017). Hydraulic design of Hong Kong West Drainage Tunnel. Proc. of the 37th IAHR World Congress, Aug 13–18, 2017, Kuala Lumpur, Malaysia.

163 | Lamb, H. (1932). Hydrodynamics. Cambridge University Press.

164 | Laushey, L.M. and Mavis, F. (1953). Air entrained by water flowing down vertical shafts. Proc. Minnesota International Hydraulic Convention, Minneapolis, MN.

165 | Lee, J.H.W., Chan, H.C. Yu, D.Y. and Choi, K.W. (2005a). Physical hydraulic model tests for Hong Kong West Drainage Tunnel in Northern Hong Kong Island – Intake Structure. Croucher Laboratory of Environmental Hydraulics, The University of Hong Kong, Hong Kong.

166 | Lee, J.H.W., Yu, D., Chan, H.C., Gore, L. and Ackers, J. (2005b), Bottom rack intake for supercritical storm flow diversion on steep urban catchment. Proc. IAHR World Congress 2005, Seoul, Korea.

167 | Lee, J.H.W., Yu, D.Y. and Choi, K.W. (2006). Physical hydraulic model tests for Lai Chi Kok transfer scheme intake structure. Croucher Laboratory of Environmental Hydraulics, The University of Hong Kong.

168 Levi, E. (1972). Experiments on unstable vortices. J. Eng. Mech. Div. 98(3), 539–559.

169 Lewellen, W.S. (1962). A solution for three-dimensional vortex flows with strong circulation. J. Fluid Mech. 14(Part 3), 420–432.

170 Li, H.F., Chen, H.X., Ma, Z. and Zhou, Y. (2008). Experimental and numerical investigation of free surface vortex. J. of hydrodynamics, 20(4), 485–491.

171 Li, S., Lai, Y., Weber, L., Silva, J.M. and Patel, V.C. (2004). Validation of a three-dimensional numerical model for water-pump intakes, J. of Hydraulic Research, 42(3), 282–292.

172 Lu, L.G., Cao, Z. G. and Zhou, J.R. (1997). The optimum hydraulic design of pump intakes. Shui Li Xue Bao, 3(1), 16–25.

173 Lugt, H. J. (1983). Vortex flow in nature and technology. New York, Wiley-Interscience, New York, NY.

174 Lundgren, T.S. (1985). The vortical flow above the drain-hole in a rotating vessel. J. Fluid Mech. 155, 381–412.

175 Lyons, T.C. (2021). Air demand in deep drop structures. Doctoral Thesis, The University of Iowa, Iowa City, IA.

176 Ma, Y.Y., Zhu, D.Z. and Rajaratnam, N. (2016). Air entrainment in a tall plunging flow dropshaft, J. of Hydraulic Engineering, 142(10): 04016038.

177 Mahmoudi-Rad, M. and Najafzadeh M. (2021). Air entrainment mechanism in the vortex structure: experimental study. J. of Irrigation and Drainage Engineering, 147(5), 04021007.

178 Markland, E. and Pope, J.A. (2003). Flow field, turbulence and critical condition at a horizontal water intake. Proc. IME J. Power Energy 217, 53–62.

179 Martiemianov, S. and Okulov, V.L. (2004). On heat transfer enhancement in swirl pipe flows. Intl. J. of Heat and Mass Transfer, 47, 2379–2393.

180 Meier, J. (2003). Leistungsfähiger sandabzug für moderne entsander in neu- und umbauprojekten (Efficient sand removal for modern desanders in new and retrofit projects). Wasser, Energie, Luft, 95(7/8), 205–206 [in German].

181 Melville, B.W., Ettema, R. and Nakato, T. (1994). Review of flow problems at water intake pump sumps. EPRI Report TR-103474, Palo Alto, CA.

182 Menter, F. R. (1994). Two-equation eddy-viscosity turbulence models for engineering applications, AIAA Journal, 32(8), 1598–1605.

183 Merzari, E., Ninokata, H.,Wang, S. and Baglietto, E. (2009). Numerical simulation of free-surface vortices. Nucl. Technol., 165, 313–320.

184 Miles, J. (1998). A note on the Burgers-Rott vortex with a free surface. Z. Angew. Math. Phys. 49, 162–165.

185 Möller G., Detert, M. and Boes, R.M. (2015). Vortex-induced air entrainment rate at intakes. J. of Hydraulic Engineering, 141(11), http://dx.doi.org/10.1061/(ASCE)HY.1943–7900.0001036.

186 Möller, G. (2013). Vortex-induced air entrainment rates at intakes. VAW-Mitteilung 220 (R. Boes, ed.), Laboratory of Hydraulics, Hydrology and Glaciology (VAW), ETH Zurich, Switzerland, https://ethz.ch/content/dam/ethz/special-interest/baug/vaw/vaw-dam/documents/das-institut/mitteilungen/2010–2019/220.

187 Möller, G., Detert, M. and Boes, R.M. (2012). Air entrainment due to vortices – state-of-the-art. Proc. 2nd IAHR Europe Cong., paper B16.

188 Möller, G., Pinotti, M. and Boes, R. (2010). "Einlaufwirbeluntersuchung am Kraftwerk Handeck 2 – Kritische Überdeckungshöhe und Wirbelunterdückungsmassnahmen" ('Investigation of intake vortices at the Handeck 2 hydropower plant – critical submergence and vortex suppression methods'). Report 124, Lehrstuhl und Versuchsanstalt für Wasserbau und Wasserwirtschaft, TU München, Germany: 407–416.

189 | Mortara, M. (1948). Sprial flow increases capacity of vertical discharge shaft. Civil Engineering, American Society of Civil Engineers, Dec., 50–51.

190 | Mulligan, S. (2015). Experimental and numerical analysis of three-dimensional free-surface turbulent vortex flows with strong circulation. Rept., Institute of Technology Sligo, Ireland.

191 | Mulligan, S., Casserly, J. and Sherlock, R. (2016). Effects of geometry on strong free-surface vortices in subcritical approach flows. J. of Hydraulic Engineering, 142(11), 04016051.

192 | Mulligan, S., De Cesare, G., Casserly, J. and Sherlock, R., (2018). Understanding turbulent free-surface vortex flows using a Taylor-Couette flow analogy. Scientific Reports, 8(1), pp.1–14.

193 | Mulligan, S., Creedon, L., Casserly, J. and Sherlock, R. (2019a). An improved model for the tangential velocity distribution in strong free-surface vortices: and experimental and theoretical study. J. of Hydraulic Research, 57(4):547–560.

194 | Mulligan, S., Plant, J., Nash, S. and Eoghan, C. (2019b). Vortex drop shaft structures: state-of-art and future trends. Proc. 38th IAHR World Congress, Panama City, Panama, doi:10.3850/38WC092019–1813.

195 | Munson, B.R., Okiishi, T.H., Huebsch. W.W. and Rothmayer, A.R. (2013). Fundamentals of fluid mechanics. John Wiley & Sons, Hoboken, N.J., USA.

196 | Muntean, S., Buntiæ, I., Ruprecht, A. and Susan-Resiga, R. (2005). A numerical investigation of the 3D swirling flow in a pipe with constant diameter. Part 2: Turbulent computation. Scientific Bulletin of the "Politehnica" Univerity of Timisoara, Transactions on Mechanics, 50(64), 87–96.

197 | Muste, M. and Ettema, R. (1996). Hydraulic model study of cooling tower pump sump for Salt City Energy Center. Limited. Distn. Rept. No. 245, Iowa Institute of Hydraulic Research, The University of Iowa, Iowa City, IA.

198 | Muste, M., Aberle., J. Admiraal, D., Ettema, R., Garcia, M.H., Lyn, D., Nikora, V. and Rennie, C. (Eds.), (2017). Experimental hydraulics: methods, instrumentation, data processing and management. IAHR Book, Two Vol., CRC Press, Boca Raton, FL.

199 | Naderi, V. and Gaskin, S.J. (2018). An experimental study of the performance of an ogee-shaped vertical intake: geometrical parameters of cross-vane vortex inhibitor. Proc. 7th Intl. Symposium on Hydraulic Structure, Aachen Germany, 15–18 May, 2018.11.

200 | Naderi, V., Farsadizadeh, D., Hosseinzadeh-Dalir, A. and Arvanaghi, H. (2014). Effect of using vertical plates on vertical intake on discharge coefficient, Arabian J. for Science and Engineering, 39(12): 8627–8633.

201 | Naderi, V., Farsadizadeh, D., Lin, C. and Gaskin, S. (2019). A 3D study of an air-core vortex using HSPIV and flow visualization. Arab J. Sci. Eng., 44, 8573–8584.

202 | Nakato, T. and Yoon, B. (1992). A Model study of the proposed St. Louis County Water Company's water intake near River Mile 37 on the Missouri River. Limited Distn. Report No. 187, Iowa Institute of Hydraulic Research, The University of Iowa, Iowa City, IA.

203 | Nakayama, A. and Hisasue, N. (2010). Large eddy simulation of vortex flow in intake channel of hydropower facility, J. of Hydraulic Research, 48(4), 415–427.

204 | Nakayama, A. and Jones, J. R. (1999). Correlation for formation of inlet vortex. AIAA journal, 37(4), 508–510.

205 | National Audit Office (NAO). (2014). Thames Tideway Tunnel: early review of potential risks to value for money.

206 | Neary, V. Sotiropoulos, F. and Odgaard, A.J. (1999). Three-dimensional numerical model of lateral-intake inflows. J. of Hydraulic Engineering, 125(2), 126–140.

207 | Neary, V.S. and Odgaard, A.J. (1993). Three-dimensional flow structure at open-channel diversions. J. of the Hydraulics Division, Vol. 119(11), 1223–1230.

208 Nolan, D.S. (2001). The stabilizing effects of axial stretching on turbulent vortex dynamics. Phys. Fluids 13(6), 1724–1738.

209 Odgaard, A.J. (1986). Free-surface air core vortex. J. Hydraulic Engineering, 112(7), 610–620.

210 Ogihara, K. and Kudou, T. (1996). Theoretical analysis of air-entrained flow in vertical drop shafts of the channel in urban drainage systems. Paper presented at the Proc., 27th Congress of IAHR, Water Resources Division.

211 Okamura, T., Kamemoto, K. and Matsui, J. (2007). CFD prediction and model experiment on suction vortices in pump sump. Proc. of the 9th Asian International Conference on Fluid Machinery. Jeju, Korea.

212 Oseen, C. W. (1912). Über die Wirbelbewegung in einer reibenden Flûssigkeit (On vortex motion in a fricitional fluid'). Ark. Mat. Astro. Fys., 7, 14–26 (in German).

213 Padmanabhan, M. (1984). Air ingestion due to free surface vortices. J. of Hydraulic Engineering, 110(12), 1855–1859.

214 Padmanabhan, M. (1987). Design recommendations: pump sumps. Section 6.2, Swirling Flow Problems at Intakes, IAHR Hydraulic Structures Design Manual., Balkema, Rotterdam.

215 Padmanabhan, M. and Hecker, G.E. (1984). Scale effects in pump sump models. J. Hydraulic Eng., 110(11), 1540–1556.

216 Pagliara, S., Hohermuth, B. and Boes, R.M. (2023). Air-water flow patterns and shockwave formation in low-level outlets. J. Hydraulic Engineering, 149(6), https://ascelibrary.org/doi/abs/10.1061/JHEND8.HYENG-13357.

217 Pan, Q., Zhao, R., Wang, X., Shi, W and Zhang, D. (2019). LES study of transient behaviour and turbulent characteristics of free-surface and floor-attached vortices in pump sump. J. of Hydraulic Research, 57(5), 733–743.

218 Pan, S. and Shao, Y. (1984). Scale effects in modeling air demand by a ramp slot. Proc. Symposium on Scale Effects in Modelling Hydraulic Structures, 4(7), 1–5.

219 Papillon, B., Kirejczyk J. and Sabourin, M. (2000). Atmospheric air admission in hydroturbines. In Proc. Hydrovision2000, Charlotte, N.C.

220 Pavelyev, A. and Shtarev, A. (2005). Effect of sinkhole position symmetry on the formation of nonstationary vortex funnels. Fluid Dynamics 40(5), 829–834.

221 Petitjeans, P. (2003). Stretching of a vortical structure: filaments of vorticity. Europhysics News 34(1), 20–23.

222 Pfister, M. and Chanson, H. (2014). Two-phase air-water flows: scale effects in physical modeling. J. of Hydrodynamics, Ser. B, 26(2), 291–298.

223 Pfister, M. and Chanson H. (2012). Discussion of "Scale effects in physical hydraulic engineering models". J. Hydraulic Research, 50 (2): 244–246.

224 Pfister, M., Crispino, G., Fuchsmann, T., Ribi, J.M. and Gisonni, C. (2018). Multiple inflow branches at supercritical-type vortex drop shaft. J. Hydraulic Engineering, 144(11), 05018008.

225 Pfister, M. and Hager, W.H. (2010a). Chute aerators I: Air transport characteristics. J. of Hydraulic Engineering, 136(6): 352–359.

226 Pfister, M. and Hager, W.H. (2010b). Chute aerators II: Hydraulic design. J. of Hydraulic Engineering, 136(6): 360–367.

227 Pica, M. (1970). Scaricatori a vortice. L'Energia Elettrica, 47(4), 1–18 (in Italian).

228 Pinto N.L. de S, Neidert, S. H. and Ota, J.J. (1982a). Aeration at high velocity flows. Water Power and Dam Constr., Vol. 34(2&3), 34–38 and 42–44.

229 Pinto, N.L. de S. and Neidert, S.H. (1982b). Model prototype conformity in aerated spillway flow. Proc. International Conference on Hydraulic Modeling of Civil Engineering Structures, BHRA, Cranfield, England, Paper E6, 273–284.

230 Plant, J. and Crawford, D. (2016). Pushing the limits of tangential vortex intakes: is higher capacity and flow measurement possible in a smaller footprint? Proc. of the Water Environment Federation, 2016(12), 4108–4136.

231 | Plant, J., Crawford, D. and Nielsen, K. (2016). Design standards for in-shaft vertical deaeration and energy dissipation for deep storage-conveyance tunnels. Proc. of WEFTEC 2016, New Orleans, Water Environment Federation.

232 | Prosser, M.J. (1977). The hydraulic design of pump sumps and intakes. BHRA/Construction Industry Research and Information Association, London, UK.

233 | Putra, R.A. and Lucas, D. (2020). Modeling of the free-surface vortex-driven bubble entrainment into water, Water 12, 709.

234 | Qian, Z., Wu, P., Guo, Z., and Huai, W. (2016). Numerical simulation of air entrainment and suppression in pump sump. Science China Technological Sciences, 59(12), 1847–1855.

235 | Quick, M.C. (1961). A study of the free spiral vortex. University of Bristol, Bristol, UK.

236 | Quick, M.C. (1962). Scale relationships between geometrically similar free spiral vortices. Civil Engineering and Public Works Reviews, 57(10), 1423–1436.

237 | Quick, M.C. (1970). Efficiency of air-entraining vortex formation at water intake. J. of the Hydraulics Division, 96(7), 1403–1416.

238 | Rabe, B.K., Najafabadi, S.H.G., and Sarkardeh, H. (2017). Numerical simulation of air-core vortex at intake. Current Science, 113(1), 141–147.

239 | Rachelly, C., Albayrak, I., Boes, R.M., Weitbrecht, V. (2022). Bed-load diversion with a vortex tube system. Proc. of the 39th IAHR World Congress Granada, Spain, 5900–5909.

240 | Rajaratnam, N., Mainali, A. and Hsung, C.Y. (1997). Observations on flow in vertical dropshafts in urban drainage systems. J. Environ. Eng., 123(5), 486–491.

241 | Rajendran, V. and Patel, V.C. (1998). Experimental investigation of vortices in a pump bay using non-measurement techniques. IIHR Report No. 396, Iowa Institute of Hydraulic Research, The University of Iowa, Iowa City, IA.

242 | Rajendran, V., Constantinescu, S. and Patel, V.C. (1999). Experimental validation of numerical model of flow in pump-intake bays, J. of hydraulic Engineering, 125(11), 1119–1125.

243 | Rajendran, V.P. and Patel, V.C. (2000). Measurement of vortices in model pump-intake bay by PIV. J. Hydraulic Engineering, 126(5), 322–334.

244 | Rankine,W.J.M. (1876). A Manual of applied mechanics. 9th Ed., C. Griffin & Co., London, UK.

245 | Rao, S., Diwanji, V. and Srivastava, Y. (1997). Discussion of “Critical submergence for intakes in open channel flow”. J. Hydraulic Engineering, 123(6), 588–589.

246 | Reddy, Y.R. and Pickford, J.A. (1972). Vortices at intakes in conventional sumps. Water Power 24(3), 108–109.

247 | Reynolds, A.J. (1974). Turbulent flows in engineering. John Wiley & Sons, Hoboken, N.J., USA.

248 | Richardson, L.F. (1922). Weather prediction by numerical process. Cambridge Univ. Press, Cambridge, U.K.

249 | Rindels, A.J. and Gulliver, S. (1983). An experimental study of critical submergence to avoid free-surface vortices at vertical intakes. Project Report No. 224, St. Anthony Falls Hydraulics Laboratory, University of MN.

250 | Rosenhead, L. (1930). The spread of vorticity in the wake behind a cylinder. Proc. of the Royal Society of London. Series A, containing papers of a mathematical and physical character, 127(8),590–612.

251 | Rossi, M., Bottausci, F., Maurel, A. and Petitjeans, P. (2004). A nonuniformly stretched vortex. Phys. Rev. Lett. 92(5), 054504/1–4.

252 | Roth, A. and Hager, W. H. (1999). Underflow of standard sluice gate. Experiments in Fluids, 27(4), 339–350.

253 | Rott, N. (1958). On the viscous core of a line vortex. Z. Angew. Math. Phys. 9b, 543–553.

254 Rouse, H. (1963). On the role of eddies in fluid motion. American Scientist, 51(3), 265–308.

255 Rutschmann, P., Volkart, P. and Vischer, D. (1987). Design recommendations – intake structures. In. Knauss, (Ed), Swirling flow problems at intakes, 91–100, A.A. Balkema, Rotterdam, NL.

256 Saffman, P.S. (1992). Vortex dynamics. Cambridge University Press, Cambridge, UK.

257 Sakai, T., Eguchi, Y., Monji, H., Ito, K. and Ohshima, H. (2008). Proposal of design criteria for gas entrainment from vortex dimples based on a computational fluid dynamics method. Heat Transfer Engineering, 29(8), 731–739.

258 Schäfer, F. and Hellman, D.H. (2005). Optimization of approach flow conditions of vertical pumping systems by physical model investigation. Proc of ASME FEDSM2005, Houston, TX,

259 Schmidt, P.W. and Ghosh, A. (2019). United States Patent No. 10,458,446 B1., Washington, D.C.

260 Scorer, R. (1967). Local instability in curved flow, IMA J. of Applied Mathematics, 3(3), 250–265.

261 Shi, X.M., Yang, F., Dai, R., Chen, T.J. and Wu, Y.L. (2012). Simulation of free-surface vortex produced by a rotating cylindrical wall below a static barrel. Proc. Conf. Ser. Earth Environ. Sci., 15, 052034.

262 Shur, M.L., Strelets, M.K., Travin, A.K. and Spalart, P.R. (2000). Turbulence modeling in rotating and curved channels: assessing the Spalart-Shur correction. AIAA Journal, 38(5), 784–792.

263 Sielbold, F. Ligrani, P. and Weigand, B. (2022). Flow and heat transfer in swirl pipes – A Review. Intl. J. of Heat and Mass transfer, 187, 122455.

264 Škerlavaj, A., Lipej, A., Ravnik, J. and Škerget, L. (2010). Turbulence model comparison for a surface vortex simulation. Iop Conf. Ser. Earth Environ. Sci., 12, 012034.

265 Škerlavaj, A., Škerget, L., Ravnik, J. and Lipej, A. (2011). Choice of a turbulence model for pump intakes, Proceedings of the Institution of Mechanical Engineers, Part A: J. of Power and Energy, 0957650911403870.

266 Škerlavaj, A., Škerget, L., Ravnik, J. and Lipej, A. (2014). Predicting Free-Surface Vortices with Single-Phase Simulations, Engineering Applications of Computational Fluid Mechanics, 8(2), 193–210.

267 Spalart, P. and Shur, M. (1997). On the sensitization of turbulence models to rotation and curvature, Aerospace Science and Technology, 1(5), 297–302.

268 Spalart, P.R. (1998). Airplane trailing vortices. Annual Rev. Fluid Mech. 30, 107–138.

269 Steenbergen, W. and Voskamp, J. (1998). The rate of decay of swirl in turbulent pipe flow. Flow Measurement and Instrumentation, 9, 67–78.

270 Stepanyants, Y. and Yeoh, G. (2008). Stationary bathtub vortices and a critical regime of liquid discharge. J. Fluid Mech. 604, 77–98.

271 Stephens, D. and Mohanarangam, K. (2010). Turbulence model analysis of flow inside a hydrocyclone, Progress in Computational Fluid Dynamics, an International J., 10(5–6), 366–373.

272 Stevens, J.C, and Kolf, R.C. (1957). Vortex flow through horizontal orifices. ASCE Trans. Paper No. 3004, 871–883.

273 Suerich-Gulick, F. (2013). Axial stretching, viscosity, surface tension and turbulence in free surface vortices at low-head hydropower intakes, Ph.D. Thesis, McGill University, Montreal, Canada.

274 Suerich-Gulick, F., Gaskin, S., Villeneuve, M., Holder, G. and Parkinson, E. (2006). Experimental and numerical analysis of free surface vortices at a hydropower intake. Proc. of the 7th International Conference on Hydroscience and Engineering, 1–11.

275 Suerich-Gulick, F., Gaskin, S.J., Villeneuve, M. and Parkinson, E. (2014a). Characteristic of free surface vortices at low-head hydropower intakes. J. of Hydraulic Engineering, 140(3): 291–299.

276 | Suerich-Gulick, F., Gaskin, S.J., Villeneuve, M. and Parkinson, E. (2014b). Free surface intake vortices: theoretical model and measurements. J. of Hydraulic Research. 52(4): 502–512.

277 | Suerich-Gulick, F., Gaskin, S.J., Villeneuve, M. and Parkinson, E. (2014c). Free surface intake vortices: scale effects due to viscosity and surface tension. J. of Hydraulic Research. 52(4): 513–522.

278 | Sungur, A. (2018). Numerical investigation of vortex formation at asymmetric horizontal intakes. Rept. Middle East Technical University, Turkey.

279 | Svartovsky, L. and Thew, M.T. (1992). Hydrocyclones: applications and analysis. Springer Science+Business, Dordect, NL.

280 | Sweeney, C.E., Elder, R.A. and Hay, D. (1982). Pump sump design experience: summary. J. of the Hydraulics Div., Vol. 108 (3), 361–377.

281 | Tagomori, M. (1980). Flow Pattern and Air Intake Vortex in an Intake Sump, Part 2 - Influence of Inflow Conditions. Ebara Seisakusho Central Laboratory, Japan, published in Turbomachinery Vol 8–10, translation (Dec. 1992) by Y. Tahara, Iowa Institute of Hydraulic Research, the University of Iowa, Iowa City, IA.

282 | Tahershamsi, A., Rahimzadeh, H., Monshizadeh, M. and Sarkardeh, H. (2018). A new approach on anti-vortex devices at water intakes including a submerged water jet. Eur. Phys. J. Plus 133, 143.

283 | Tang, X.L., Wang, F.J., Li, Y.J., Cong, G.H., Shi, X.Y., Wu, Y.L. and Qi, L.Y. (2011). Numerical investigations of vortex flows and vortex suppression schemes in a large pumping-station sump. P I Mech Eng C-J Mec 225(6), 1459–1480.

284 | Taştan, K. andYildirim, N. (2010). Effects of dimensionless parameters on air-entraining vortices. J. of Hydraulic Research, 48(1), 57–64.

285 | Taştan, K. and Yıldırım, N. (2018). Effects of intake geometry on the occurrence of a free-surface vortex. J. of Hydraulic Engineering, 144(4), 04018009.

286 | Thomson, W.T. (1869). On vortex motion. Trans. Roy. Soc. Edinb., 25, 217–260.

287 | Thornton, C.I., Ettema, R., Ellis, J. Volt, C. and Hogan, T. (2021). Los Vaqueros Reservoir expansion: hydraulic model study of spillway and sluice. Hydraulics Lab., Colorado State University, Fort Collins, CO.

288 | Tiwari, P., Xia, Z. and Han, X. (2020). Comparison of VLES and LES turbulence modeling for swirling flow. J. of Applied Fluid Mechanics, 13(4), 1107–1116.

289 | Toda, K. and Inoue, K. (1999). Hydraulic design of intake structures of deeply located underground storage systems. Water Science and Technology, 39(9), 137–144.

290 | Tokyay, T. and Constantinescu, S. (2005). Coherent structures in pump intake flows: A Large Eddy Simulation study. Proc. 31st International Association Hydraulic Research Congress, Seoul, Korea.

291 | Tokyay, T., and Constantinescu, S. (2006). Validation of a large-eddy simulation model to simulate flow in pump intakes of realistic geometry. J. of Hydraulic Engineering, 132(12), 1303–1315.

292 | Toyokura, T. and Akaike, S. (1970). Vortex phenomenon in a water tank. Bulletin of the Japan Soc. of Mech. Eng., 13(57), 373–381.

293 | Trefethen, L.M., Bilger, R., Fink, P., Luxton, R. and Tanner, R. (1965). The bath-tub vortex in the southern hemisphere. Nature 207, 1084 – 1085.

294 | Trivellato, F. and Ferrari, W. (1997). A finite difference model for intake vortices. Proc. 3rd Int. Congress on Hydraulic Engineering, Holguin, Cuba.

295 | Trivellato, F., Bertolazzi, E. and Firmani, B. (1999). Finite volume modelling of free surface draining vortices, J. of Computational and Applied Mathematics, 103(1), 175–185.

296 | Tullis, J.P. (1979). Modelling in design of pumping pits. J. of the Hydraulics Div., 105(9), 1053–1063.

297 | USACE (1979). Feasibility studies for small scale hydropower additions: a guide manual. U.S. Army Corps of Engineers, Hydrologic Engineering Center, Davis, CA.

298 | USACE (1995). General principles of pumping station design layout. EM No. 110–2-3120, U.S. Army Corps of Engineers, Washington D.C.

299 | Vatistas, G. H., Kozel, V. and Mih, W. C. (1991). A simpler model for concentrated vortices. Experiments in Fluids, 11(1), 73–76.

300 | Vatistas, G.H. and Li, P.M. (1988). A similar profile for the tangential velocity in vortex chambers. Exp. in Fluids 6, 135–137.

301 | Viparelli, M. (1950). Su un particolare tipo di imbocco e sull'efflusso con vortice. L'Energia Elettrica, 27(10), 610–624 (in Italian).

302 | Viparelli, M. (1961). Air and water currents in vertical shafts. La Houille Blanche, 47(6), 857–869.

303 | Vischer, D.L. and Hager, W.H. (1995). Vortex drops, energy dissipators: Hydraulic structures design manual. Chapter. 9, A.A. Balkema, Rotterdam, 167–181, NL.

304 | Vischer, D.L. and Hager, W.H. (1998), Dam hydraulics, Wiley, UK.

305 | Voith (1996), in "Hydropower development at Lock & Dam 14, Mississippi River: Hydraulic model studies, part 1 – approach-flow concerns". Limited Distn. Report 241, Iowa Inst. of Hydraulic Research, U. of Iowa, Iowa City, IA.

306 | Walder, S. and Rutschmann, P. (2007). Hybrid modeling of an intake for hydraulic optimization. Proc. 32nd IAHR Congress, Venice, Italy.

307 | Wang, Y., Jiang, C. and Liang, D. (2011). Comparison between empirical formulae of intake vortices J. Hydraulic Research 49(1), 113–116.

308 | Wang, Y.K., Jiang, C.B. and Liang, D.F. (2010). Investigation of air-core vortex at hydraulic intakes. J. of Hydrodynamics, Ser. B 22(5, Supplement 1), 696 – 701.

309 | Water Power and Dam Construction (WP&DC) (2004). Into the vortex. Water Power & Dam Construction, London, UK.

310 | Weiss, G., Brombach, H. and Hohl, E. (2010). Hydraulic model tests on a stormwater vortex drop shaft: Verification of special conditions. NOVATECH 2010.

311 | Whillock, A.T. and Thorn, M.F.C. (1973). Air entrainment in dropshafts. Construction Industry Research and Information Assoc., Technical note 48.

312 | White, A. (1964). Flow of a fluid in an axially rotating pipe. J. Mech. Eng. Sc. 6(1), 47–52.

313 | Wickenhäuser, M. (2008). Zweiphasenströmung in entlüftungssystemen von druckstollen ('Two-phase flow in de-aeration systems of pressurized tunnels') VAW-Mitteilung 205 (H.E. Minor, Ed.), Laboratory of Hydraulics, Hydrology and Glaciology (VAW), ETH Zurich, Switzerland (in German).

314 | Wickenhäuser, M. and Minor, H.-E. (2007). De-aeration by structural means in pressurized flow. Proc., 32nd IAHR Congress, Venice, 1–8.

315 | Wilcox, D. C. (1998). Turbulence modeling for CFD. DCW industries La Canada, CA, USA.

316 | Wood, I. R. (1991). Air entrainment in free surface flows: IAHR Hydraulic Structure Design Manual 4. Rotterdam, Netherlands: A.A. Balkema.

317 | Wright, S. J., J. W. Lewis, and J. G. Vasconcelos (2011). Geysering in rapidly filling storm-water tunnels. J. Hydraulic Engineering, 137(1), 112–115.

318 | Wu, P., Munoz, D.H., Constantinescu, G. and Qian, Z. (2020). Two-phase flow DES and URANS simulations of pump-intake bay vortices. J. of Hydraulic Research, 58(1), 120–132.

319 | Yamade, Y., Kato, C., Nagahara, T. and Matsui, J. (2020). Suction vortices in a pump sump—their origin, formation, and dynamics. J. of Fluids Engineering, 142(3): 031110.

320 | Yang, J., Andreasson, P., Högström, C.-M. and Teng, P. (2018). The tale of an intake vortex and its mitigation countermeasure: a case study from Akkats Hydropower Station. Water, 2018, 10, 881.

321 | Yang, J., Liu, T., Bottacin-Busolin, A. andLin, C. (2014). Effects of intake-entrance profiles on free-surface vortices. J. of Hydraulic Research, 52(4), 523–531

322 | Yildirim, N. and Kocabaş, F. (1995). Critical submergence for intakes in open channel flow. J. of Hydraulic Engineering, 121(12), 900–905.

323 | Yildirim, N. and Kocabaş, F. (1998). Critical submergence for intakes in still-water reservoir. J. of Hydraulic Engineering, 124(1), 103–104.

324 | Yildirim, N. and Kocabaş, F. (2002). Prediction of critical submergence for an intake pipe. J. of Hydraulic Research, 40(4), 507–518.

325 | Yildirim, N., Akay, H. and Taştan, K. (2011). Critical submergence for multiple pipe intakes by the potential flow solution. J. of Hydraulic Research, 49(1), 117–121.

326 | Yıldırım, N., Eyüpoôlu, A. S. and Taştan, K. (2012). Critical submergence for dual rectangular intakes. J. of Energy Engineering, 138(4), 237–245.

327 | Yıldırım, N., Kocabaş, F. and Gülcan, S. C. (2000). Flow-boundary effects on critical submergence of intake pipe. J. of Hydraulic Engineering, 126(4), 288–297.

328 | Yıldırım, T. (2020). Experimental and numerical investigation of vortex formation at multiple horizontal intakes Ph.D. Middle East Technical University, Turkey.

329 | Yu, D. and Lee J.H.W. (2009). Hydraulics of tangential vortex intake for urban drainage. J. of Hydraulic Engineering, 135(3), 164–174.

330 | Zeman, O. (1995). The persistence of trailing vortices: a modeling study. Phys. Fluids 7(1), 135–143.

331 | Zhang, W., Zhu, D.Z., Rajaratnam, N., Edwini-Bonsu, S., Fiala, J., and Pelz, W. (2016). Use of air circulation pipes in deep dropshafts for reducing air entrainment into sanitary sewers, J. of Environmental Engineering, 142(4): 04015092.

332 | Zhao, C., Zhu, D.Z., Sun, S. and Liu, Z., (2006). An experimental study of a vortex dropshaft, J. of Hydraulic Engineering, 132(1), 61–68.

333 | Zhou, F., Hicks, F. E. and Steffler, P. M. (2002). “Transient flow in a rapidly filling horizontal pipe containing trapped air.” J. Hydraulic Engineering, 625–634.

334 | Zhou, H., Ji, Q., Liu, W., Ma, H., Lei, Y. and Zhu, K. (2022). Experimental study on erosion-corrosion behavior of liquid-solid swirling flow in pipeline. Materials & Design, 214.

335 | Zhou, L., Liu, D. and Karney, B. (2013a). Investigation on hydraulic transients of two entrapped air pockets in a water pipeline. J. Hydraulic Engineering, 949–959.

336 | Zhou, L., Liu, D., Karney, B. and Wang, P. (2013b). Phenomenon of white mist in water rapidly filling pipeline with entrapped air pocket. J. Hydraulic Engineering, 139(10), 1041–1051.

337 | Zi, D., Xuan, A., Wang, F. and Shen, L. (2020). Undefined numerical study of mechanisms of air-core vortex evolution in an intake flow. Intl. J. of Heat and Fluid Flow, 81, Article 108517.

This IAHR Water Monograph offers a comprehensive overview of the hydraulics of swirling flows commonly encountered in vortex dropshafts, reservoir intakes, and pump intakes. It encompasses significant advancements in our understanding of swirling flows over the past few decades, attributed to the progress in numerical modeling and laboratory measurement technology. The monograph provides valuable guidance for researchers, hydraulic modellers, and engineers engaged in studying and working with swirling flows and vortex intake design.

Can Hua (Ken) Zhao

ABOUT THE AUTHORS

Robert Ettema, Professor, Civil and Environmental Engineering, Colorado State University, Colorado, USA

David Z. Zhu, Professor, Ningbo University, Zhejiang, China and Professor Emeritus of Civil and Environmental Engineering, University of Alberta, Alberta, Canada

Susan J. Gaskin, Professor, Civil Engineering, McGill University, Quebec, Canada

Sean Mulligan, Founder and CEO at VorTech Water Solutions Ltd, Galway, Ireland

Troy C. Lyons, Associate Director and Director of Engineering Services, IIHR—Hydroscience & Engineering, University of Iowa, Iowa, USA

Robert Boes, Professor, Laboratory of Hydraulics, Hydrology and Glaciology (VAW), ETH Zurich, Switzerland

Shu Ning Chan, Research Assistant Professor (former), Department of Civil and Environmental Engineering, The Hong Kong University of Science and Technology, Hong Kong, China

Joseph H. W. Lee, President and Chair Professor, Macau University of Science and Technology, Macao, China

ISBN 978-90-833476-1-5

IAHR Global Secretariat
iahr@iahr.org

Madrid Office
Paseo Bajo Virgen del Puerto, 3
28005 Madrid, SPAIN
T +34 91 335 7908
F +34 91 335 7935

Beijing Office
A-1 Fuxing Road, Haidian District
100038 Beijing, CHINA
T +86 10 6878 1128
F +86 10 6878 1890

IAHR.org